Spring 5-15-2019

Approaches to Understanding the Function of Intrinsic Activity and its Relationship to Task-evoked Activity in the Human Brain

Dohyun Kim
Washington University in St. Louis

WASHINGTON UNIVERSITY IN ST. LOUIS

School of Engineering and Applied Science

Department of Biomedical Engineering

Dissertation Examination Committee:
Maurizio Corbetta, Chair & Advisor
Dennis Barbour
Brendan Juba
Eric C. Leuthardt
Steven Petersen

Approaches to Understanding the Function of Intrinsic Activity and its Relationship to Task-evoked Activity in the Human Brain

by
DOHYUN KIM

A dissertation presented to
The Graduate School
of Washington University in
partial fulfillment of the
requirements for the degree
of Doctor of Philosophy

May 2019
St. Louis, Missouri

Table of Contents

List of Figures

List of Tables

Acknowledgments

When I arrived in Texas as an exchange student in 2007, I didn't know what a wonderful journey of Science started for me. None of my friend and family including myself didn't expect me to live in this country more than a decade. It was an exceptional fortune that I got accepted into the Biomedical Engineering department in Washington University in St. Louis for both the undergraduate and the graduate program. I've met so many talented people in this university and I've learned so much from them.

I would first like to thank my advisors Maurizio Corbetta. When I joined his Lab, I had zero back ground on neuroimaging and had no idea how graceful the hidden nature of intrinsic activity is. He introduced me a groundbreaking idea of task-rest correspondence which became my primary interest for years. I genuinely enjoyed listening him talking about his big picture of combining 1) resting-state activity, 2) cognitive and behavioral task performances, and 3) associated task-evoked activities for both patients and healthy subjects into one unified model. I truly believe he will make his idea come true in future, and I'm very proud that I contributed my work for it.

I would like to thank Gordon L. Shulman. I just can not describe how heavily he influenced me throughout my Ph.D. I was just an engineer who just play with numbers without careful understanding of physiological meanings until I met him. He tried so hard to train me as a scientist who know how to properly design and conduct an experiment and how to correctly analyze and understand data. I could have not finished my experiments correctly without his guidance.

I would also like to thank my thesis committee for great advice and encouragement and, especially, Eric Leuthardt, who advised my rotation project in my first year. Without him I was not able to finish my 1st year fruitfully and would have left the country with empty hands.

I would like to thank the members of the Corbetta Lab – Nick Metcalf, Joseph Giffis, Josh Siegel, Tomer Livne, Lenny Ramsey, Amy Daitch, and Tommaso Volpi as well as the members of the Leuthardt Lab – Nick Szrama, Ravi Chacko, Carl Hacker, Mrinal Pahwa, David Bundy, Joseph Humphries and Andy Daniel for being such a pleasure to work with them.

Finally, there are many friends who have support me throughout my Ph.D. I really appreciate them. Especially, I thank to Sunho Lee and Junwoo Suh who are currently working on their Ph.D. too – wish their projects go smoothly.

My parents deserve the largest credit for supporting me. The amount of love they gave to me cannot be simply counted. All the achievements I made throughout my life were possible because they believed and supported me. I love them so much and hope they live as long and healthy as possible.

DoHyun Kim

Washington University in St. Louis

May 2019

Dedicated to my parents.

ABSTRACT OF THE DISSERTATION

Approaches to Understanding the Function of Intrinsic Activity and its Relationship to Task-evoked Activity in the Human Brain

by

DoHyun Kim

Doctor of Philosophy in Biomedical Engineering

Washington University in St. Louis, 2019

Professor Maurizio Corbetta, Chair

Traditionally neuroscience research has focused on characterizing the topography and patterns of brain activation evoked by specific cognitive or behavioral tasks to understand human brain functions. This activation-based paradigm treated underlying spontaneous brain activity, a.k.a. intrinsic activity, as noise hence irrelevant to cognitive or behavioral functions. This view, however, has been profoundly modified by the discovery that intrinsic activity is not random, but temporally correlated at rest in widely distributed spatiotemporal patterns, so called resting state networks (RSN). Studies of temporal correlation of spontaneous activity among brain regions, or functional connectivity (FC), have yielded important insights into the network organization of the human brain. However, the underlying fundamental relationship between intrinsic and task-evoked brain activity has remained unclear, becoming an increasingly important topic in neuroscience. An emerging view is that neural activity evoked by a task and the associated behavior is influenced and constrained by intrinsic activity. Additionally, intrinsic activity may be shaped in the course of development or adult life by neural activity evoked by a task through a

Hebbian learning process. This thesis aims to reveal correspondences between intrinsic activity and task-evoked activity to better understand the nature and function of intrinsic brain activity. We measured in human visual cortex the blood oxygen level dependent (BOLD) signal with fMRI to analyze the multivoxel activity patterns and FC structures of intrinsic activity, and compare them to those evoked by natural and synthetic visual stimuli.

In chapter 1, we review previous evidence of an association between intrinsic and task-evoked activity across studies using different experimental methods. Two experimental strategies from the literature were adapted to our own experiments. First, from anesthetized animal studies of intrinsic activity in visual cortex, we set out to measure macro-scale multi-voxel patterns of spontaneous activity fluctuations as they relate to visually driven patterns of activity (Chapters 2 and 4). Second, from inter-subject correlation studies of visual activity driven by natural stimuli, we measure relationships between intrinsic and evoked activity, specifically in relation to their topographic similarity at the network level (Chapter 5).

In Chapter 2 to 4, we establish a multivariate-pattern analysis (MVPA) approach to evaluate patterns of intrinsic and task-evoked activity. The main idea is that patterns of activity induced by behaviorally relevant stimuli over long periods of time would be represented in spontaneous activity patterns within the same areas. To test the idea, in Chapter 2, we compare the overall degree of pattern similarities between resting-state activity patterns, frame-by-frame (framewise), and visual-stimulus evoked activity patterns for natural (face, body, scenes, man-made objects) and synthetic (phase and position scrambled) object images during low-level detection task. We found that the variability, not the mean, of pattern similarity was significantly higher for natural than synthetic stimuli in visual occipital regions that preferred particular stimulus categories. Chapter 3 extends the static categorical pattern similarity measure of

Chapter 2 into a temporal correlation measure. We built pattern-based FC matrices for different stimulus categories (e.g. a face specific multivoxel pattern) in regions that preferred particular stimulus categories (e.g. FFA, STG), and showed that the occurrence of a specific categorical pattern generalizes across category specific regions. These pattern-based FCs resemble that of resting-state FC of the same regions supporting that resting state patterns are related to category-specific stimulus-evoked multivoxel activity patterns. In Chapter 4, we repeat the analysis used in Chapter 2 with language stimuli. Language stimuli (alphabetic letters and English words) are interesting as they are learned through intensive training as kids learn to read. Therefore, they represent a non-natural category of stimuli that is, however, highly trained in literate individuals.

The visual stimuli used in Chapter 2 to 4 are designed specifically for a laboratory environment that does not correspond to realistic ecological environments. In Chapter 5, to overcome this limitation, we use the more naturalistic visual experience of movie-watching and compare the whole-brain FC network structure of movie-watching and of resting-state. We show the whole-brain FC structure evoked by movie-watching is partly constrained by the resting network structure.

In conclusion, our experiments show that the link between intrinsic activity and task-evoked activity is not only limited to inter-regional interactions (as in regular resting-state FC), hence potentially reflecting anatomical connectivity or modulations of excitability between cortical regions, but extends to multivoxel patterns that carry information about specific stimulus categories. This result supports the notion that intrinsic activity constrains task-evoked, not only in terms of topography or activation levels, but also in terms of the information states that are represented in cortex.

Chapter 1: General Introduction and Background

1.1 Is Intrinsic activity a simple noise signal?

Traditional neuroscience research has focused on characterizing the topography and the patterns of brain activation evoked by specific cognitive or behavioral tasks to understand human brain functions. Inter-trial variability of task-evoked brain activation is one universal feature observed across different signals (single unit, local field potentials, EEG, fMRI). Since spontaneously fluctuating activities in primary sensory areas were observed in the absence of a stimulus, the origin of inter-trial variability was explained as superimposed spontaneous neuronal background activity on a fixed task-evoked response (Arieli et al. 1995 and 1996). Averaging across trials, therefore, has been a common technique to increase the signal-to-noise of evoked responses, and remove spontaneous activity regarded as background noise. (Aguirre et al. 1998; Tsodyks et al. 1999; Engel et al. 2001; Varela et al. 2001; Schroeder and Lakatos, 2009; Raichle, 2010; Henriksson et al. 2015).

Despite its ubiquity and strength, spontaneous brain activity, also known as intrinsic activity, for many years was not of primary interest to physiologists mainly interested in characterizing evoked responses. Still, even many years ago, there were clues for a potential functional role. For instance, recordings from local field potentials (LFP) and single neurons showed synchronous ongoing activity patterns among neighboring neurons, which is against an assumption of pure stochastic noise (Arieli, et al. 1992; Abeles et al. 1995).

The traditional neurophysiological stance of dealing with intrinsic activity as noise has been profoundly modified by the discovery that intrinsic activity is not random, but is temporally correlated in widely distributed spatiotemporal patterns, even in the absence of a task (i.e. rest),

so called resting state networks (RSN). Since the initial report of Biswal (Biswal et al. 1995), the fMRI literature has shown that the topography of the temporal covariance structure of resting BOLD activity is similar to the topography of various cognitive and behavioral task-evoked responses (Raichle et al. 2001; Fox et al. 2005; Nir et al. 2006; Smith et al. 2009; Power et al. 2010 and 2011; Yeo et al. 2011; Carl D Hacker et al. 2013; Mennes et al. 2013; Cole et a., 2014).

One interpretation of such correspondence is that there is a reciprocal relationship between evoked and spontaneous activity. On the one hand, in the course of development and experience, task states are sculpted into resting state patterns through a Hebbian learning process (Fiser et al. 2004; Albert et al. 2009; Hasson et al. 2009; Lewis et al. 2009; Tambini et al. 2010; Raichle 2011; Petersen and Sporns 2015). On the other hand, spontaneous activity patterns represent a repertoire of neural states replaying a subset of states of specific task neuronal ensembles over time. These patterns may constrain task states by providing spatiotemporal priors that encode common or behaviorally relevant patterns of activity.

In the next sections, I will review previous studies directly comparing either local task-evoked and intrinsic brain activity patterns, or population whole brain task-evoked and intrinsic activity patterns.

1.2 Intrinsic activity to task-evoked activity in animal studies.

The direct comparison of spatial patterns of intrinsic activity and task-evoked activity was initially carried out using optical imaging techniques. The pioneering studies of Grindvald, Arieli, and colleagues used voltage-sensitive dye (VSD) imaging simultaneously with other

electrophysiological methods (e.g. local field potential and electroencephalogram) to understand the nature of the variability of stimulus-evoked responses, in relation to spontaneous activity (Arieli et al. 1995 and 1996). They measured VSD signals in early visual cortex (area 17 and 18) of cats during the presentation of high contrast drifting gradients, and when the eyes were patched. Area 17 and 18 are retinotopically organized and tuned for bars, gratings, and edges. Traditionally, it was thought that the majority of inputs was retinal via the geniculo-calcarine pathway. Arieli and colleagues showed that spontaneous ongoing neuronal activity were not independent random processes, but rather reflected the correlated response of many cortical neurons. Moreover, they showed that the magnitude of the stimulus-evoked response could be predicted from the amplitude of the preceding ongoing activity. In later work (Fiser et al. 2004) it was shown that the mean and variability of stimulus-evoked responses to visual stimuli, especially natural ones, was indistinguishable from the mean and variability of intrinsic activity in primary visual cortex.

Later studies included a direct comparison of the spatial patterns of intrinsic activity vs. task-evoked patterns. Specifically, activity patterns in anaesthetized cat V1 evoked by oriented gratings were spatially matched to patterns of spontaneous activity (Tsodyks et al. 1999; Kenet et al. 2003). In the study of Kenet et al. (2003), VSD signals were used to continuously monitor 30s long periods of activity in cat area 18 either in the presence or absence of full field oriented grating visual stimuli. The distribution of spatial correlation coefficients between ongoing spontaneous activity maps and orientation selective stimulus-driven maps was significantly wider than the spatial correlation coefficient distribution between simulated control maps and orientation maps. Across recordings, in about 20% of time frames the spontaneous activity map matched the orientation map based on a significant correlation threshold of $\rho=0.25$ ($P<0.01$).

A direct comparison of spatial activity patterns for ongoing and stimulus evoked activity in visual cortex has been recently extended to anesthetized monkeys (Omer et al. 2018). Omer and colleagues measured the spatial correlation between activity patterns derived from sets of 10 sec resting state, and difference activity patterns obtained by stimulating with orthogonally oriented gratings (i.e. 0/90 degree pair vs. 45/135 degree pairs). The resulting distribution of correlation coefficients was compared to a null control distribution obtained by flipping the stimulus-evoked pattern. Both real and null distributions were centered on zero, but the real orthogonal orientation distribution showed wider positive and negative tails. Since orthogonally oriented gratings should activate different columns, a straightforward interpretation is that the wider positive/negative distribution reflects this opposing functional organization in cortex. Interestingly, however, Omer et al. found that real and null distributions completely overlapped when the monkey was awake. Still, the authors argued, based on time resolved measures, for a significant match of spatial cortical activity patterns between spontaneous and orientation selective maps, but on a smaller spatial and faster temporal scale.

1.3 Intrinsic activity to task-evoked activity in fMRI literatures.

Human resting-state studies have used fMRI to measure the temporal correlation of the blood oxygenation level dependent (BOLD) signal between brain regions. These studies have shown overall that spontaneous activity in the brain is correlated in space between neighboring voxels and in time between regions that show similar temporal fluctuations of the BOLD signals. Regions that show temporally correlated signals at rest (functional connectivity, FC) define

resting-state networks (RSN) (Fox et al. 2005; He et al. 2008; Nir et al. 2008; Smith et al. 2009; Power et al. 2010 and 2011; Yeo et al. 2011; Gordon et al. 2016).

There is indirect evidence of a functional relationship between spontaneous activity patterns and task-evoked activity.

First, RSNs are topographically matched to the topography of networks recruited by different sensory, motor, and cognitive tasks. The functional characterization of different RSNs as sensory (visual, auditory), motor, or cognitive (e.g. default, dorsal attention, ventral attention, etc.) is based on the spatial correlation of activity in cortex (Biswal et al. 1995; Lowe et al. 1998; Corbetta and Shulman, 2002; Greicius et al. 2003; Fox et al. 2006; Dosenbach et al. 2007; Nelson et al. 2010; Power et al. 2010). Other networks have been named ad-hoc, often ignoring the overlap with previously described networks (e.g. salience vs. ventral attention or cingulo-opercular) (Seeley et al. 2007). Finally, other networks are based on different criteria, partly data-driven like ICA or using task-related definitions, e.g. task positive vs. negative networks (Fox et al. 2005; Golland et al. 2008).

In most case, the spatial overlap between an RSN and task network has been studied in a small number of networks, or small number of conditions (Greicius et al. 2003; Fair et al. 2007; Fox et al. 2007; Buckner et al. 2013; Hermundstad et al. 2013; Mennes et al. 2013). A robust comparison of resting state FC and task-evoked FC was conducted for 265 functional regions with 64 distinct task states and revealed a very high overall topographic similarity of $\rho = 0.90$ (Cole et al. 2014). However, this high degree of similarity should not be overstated. In fact, recent work from our lab has shown that this high similarity depends on residual spontaneous fluctuations that were not properly removed by temporal averaging. The similarity, once residual

fluctuations are removed, is only moderate ($\rho = 0.60\text{-}0.7$), and consistent rest-task differences in connectivity can be identified (Kim et al. 2018).

A stronger link between task and spontaneous activity comes from experiments in which the intensive repetition of a paradigm (hundreds to thousands of trials) induces alterations of FC within/between task-driven circuitries. This has been shown for motor, visual, memory, and neuro-feedback paradigms (Albert et al. 2009; Lewis et al. 2009; Tambini et al. 2010; Harmelech and Malach 2013). These learning-related FC changes indicate a role of task patterns in entraining resting patterns.

Recent work also suggested long-term, experience-dependent influences on FC in visual cortex. FC between different visual areas is increased in ROIs that have overlapping receptive fields (Heinzle et al. 2011; Raemaekers et al. 2014; Wilf et al. 2017) or represent similar eccentricities (Arcaro et al. 2015). These effects could also reflect structural connections.

Wilf et al. (2017), additionally, reported that FC in visual cortex from movie viewing, after removal of intrinsic activity, was more similar to resting FC than FC from iso-eccentricity stimulation, iso-polar stimulation, or predictions based on retinotopic, polar angle or eccentricity distance. These findings, therefore, indicate that resting state activity patterns are not only due to low level visual features, but also reflect behaviorally relevant stimuli as in the viewing of movies.

Finally, models built from resting-state FC predicted task-evoked activity maps – suggesting neural activity evoked by a task is influenced and constrained by intrinsic activity. Models of activity flows over resting-state FC networks were trained, and predicted large-scale cognitive task activation networks. (Cole et al. 2016; Ito et al. 2017). Meanwhile, models trained

using resting-state FC predicted individual differences in novel cognitive task performances or task-evoked activation maps (Baldassarre et al. 2012; Tavor et al. 2016).

While the above reviewed animal literatures and human fMRI literatures showed evidences of the closed-loop relationship between intrinsic activity and task-evoked activity, methodological limitations exist in both experimental methods. Animal studies were conducted within a primary visual area with only low-level visual stimuli presented; therefore, the findings could not be extended to higher-level cognitive or behavioral tasks. In contrast, the fMRI studies comparing FC topographies for intrinsic and task-evoked activity were limited since the FC measurement is based on the temporal correlations of the BOLD signals averaged over time at the level of entire ROIs, or voxel-wise but with no regard to high level stimulus categories. In this thesis we propose a complementary experimental strategy to test the relationship between rest and task-evoked activity. Based on the animal studies, we adapted multivariate-pattern (MVPA) techniques to identify behaviorally relevant activity patterns for specific naturalistic set of stimuli, and then used these patterns to study the spatial patterns of activity at rest.

1.4 Analyzing task-evoked activity patterns in fMRI

Human ventral-occipital temporal cortex (VOTC) is known for containing information about visual stimuli. Several regions in VOTC show stronger activation for specific object categories such as faces (Allison et al. 1994; Kanwisher et al. 1997; Ishai et al. 2000;), body parts (Downing et al. 2001; Grossman and Blake 2002), places (Aguirre et al. 1998a and 1998b; Epstein and Kanwisher 1998; Ishai et al. 2000), tools (Martin et al. 1996; Chao et al. 1999; Beauchamp et al. 2002), and words (Cohen et al. 2000; Hasson et al. 2002; Grossman et al. 2002). A recent review by Grill-Spector and Weiner (2014) thoroughly describes information

contents within the human VOTC in terms of color, eccentricity bias, visual field maps, expertise, and object categories (Grill-Spector and Weiner 2014).

Traditional task-evoked activation studies in fMRI literature were limited in analyzing the magnitude and profile of activation due to both slow temporal and low spatial resolutions. Univariate statistic measurement of task-evoked activations, therefore, was a first step in understanding brain function. With technological developments in fMRI, it was possible to obtain images at higher spatiotemporal resolution that allowed a shift from a univariate to a multivariate statistical framework (Haxby et al. 2001 and 2006; Cox and Savoy 2003; Kriegeskorte et al. 2007 and 2008). Multivariate pattern analysis (MVPA) assumes that information is encoded in patterns of neural activity; therefore, by decoding these patterns it is possible to distinguish different stimuli. MVPA classifications of categorical stimuli (e.g. faces and places) allowed for high accuracy of classification (Haxby et al. 2001, 2006, and 2011; Cox and Savoy 2003). Also, representational similarity analysis (RSA), based on the correlation distance of different multivariate pattern of activation, showed a hierarchical representational space of animate and inanimate stimuli, with sub-spaces for human faces, human bodies, animal faces, animal bodies, natural objects, and artificial objects (Kriegeskorte et al. 2008).

The above studies showed that human VOTC contains a number of category specific regions, and that patterns of activity within these regions code for the preferred stimulus category. By ‘code’ I mean that these patterns can be used for accurate classification of stimulus categorization. It is reasonable to assume that this organization reflects not only genetic factors, but also structural connectivity (Saygin et al. 2011; Osher et al. 2016), as faces are coded in more foveal sub-regions that are in turn connected with each other across multiple regions. Also, to some extent, patterns of task activation underlie individual experience. For instance, the analysis

of visual words is entrained in cortex through training in reading, putatively, through a Hebbian learning process.

1.5 Issues addressed in this thesis, general strategy, and plan of dissertation

Based on this background, we are interested in evaluating the potential role of spontaneous activity in encoding information states. Specifically, we propose that one of the functions of spontaneous activity is to maintain on-line behaviorally relevant information states, and that these states, entrained by thousands of exposures in the course of development and experience, will be statistically related to task evoked patterns. Spontaneous activity states can function as a prior in space (e.g. a manifold) or in time (e.g. a neural trajectory) from which task states can originate. Our strategy is to test this hypothesis by showing that information states, as coded in stimulus-evoked activity for different stimulus categories, are also represented at rest within a cortical region.

In order to control for spurious correlations between task-evoked and rest patterns, we plan two different controls. One, categorical stimuli that activate high-level visual cortex (faces, objects, bodies) will be compared to low level control stimuli (phase and position scrambled stimuli) that will drive earlier visual regions. If resting activity codes for behaviorally relevant patterns, then we shall observe a topographic difference at rest between high- and low-level regions. Two, we also plan to control for stimulus selectivity in resting state patterns by comparing within a region specialized for one category (e.g. FFA for faces) whether resting state

patterns that are more similar to faces are more common that resting patterns that are more similar to another category (e.g. bodies, or scenes).

An important theoretical point is whether the emergence of a particular stimulus state in one area at rest corresponds to an isolated random event, or whether multiple regions show simultaneously the same state. This would be consistent with a distributed information state representing a particular stimulus. For instance, at one point in time, the whole visual cortex may be more likely to code for faces than other stimuli. Accordingly, if resting activity is representing information widely in cortical space over time, then we shall find significant temporal correlation of activity patterns, coding for a specific stimulus category, across multiple visual regions. Also, in this case, activity patterns over time and across regions should be stronger for stimulus preferred than non-preferred categories.

Finally, static pictures do not correspond to realistic ecological stimulation. Hence, we plan to compare rest and task patterns during more natural visual stimulation, as during movie watching. Movie watching is a popular paradigm in neuroimaging and can be used to analyze similarities of activations across subjects (Hasson et al, 2004; Hasson and Malach 2004). Another application is the study of semantic organization, which has been shown to be distributed in cortex (Huth et al. 2012; Stansbury et al. 2013). Additionally, Wilf et al. (Wilf et al. 2017) have shown that in early visual cortex, resting FC patterns are better accounted for by movies than by standard retinotopic stimuli, while Strappini et al. (Strappini et al. 2018) have shown that in higher-level visual cortex, resting FC patterns are better accounted for by movies than by static pictures of objects. To overcome the limitation of laboratory environment conditioned visual stimuli, therefore, we used the more naturalistic visual experience of movie-watching in a separate analysis.

This thesis is organized as follows. Chapter 1 is introductory. In Chapter 2, I first establish an approach to compare multi-vertex resting-state activity pattern and multi-vertex stimuli-evoked activity pattern in laboratory conditions. The visual stimuli used in Chapter 2 are categorical object images that are prevalent in everyday life. Each categorical stimulus exemplar is presented on a grey background and has its corresponding control stimulus, preserving some local or global visual properties. We investigate the relationship between intrinsic and extrinsic activity in terms of an artificial static parameter from spatial correlation coefficient distributions computed across entire resting-state BOLD frames within regions in human visual cortex. The regions of interest (ROIs) used in this chapter include previously reported classical categorical visual regions of face fusiform area (FFA), extrastriate body area (EBA), lateral occipital (LO), parahippocampal place area (PPA), transverse occipital sulcus (TOS).

Chapter 3 describes analyses aimed at identifying stimulus states that are widely represented in cortex. The inter-regional temporal correlation computed from multivoxel similarity timeseries for a category template will be compared across both regions that are more or less specific for that category. We demonstrate a coherent brain resting state representing one stimulus category.

In Chapter 4, we repeat the analysis used in Chapter 2 with language stimuli since alphabetic letters and English words are stimuli that are not ecologically prevalent but are explicitly trained over time.

In Chapter 5, we compared a whole-brain FC structure evoked by movie-watching to a whole-brain resting-state FC structure to overcome the limitation of laboratory conditioned

categorical visual stimulus used in previous chapters. We demonstrate that the whole-brain FC structure evoked by movie-watching is partly constrained by the resting network structure.

1.6 References

Abeles M, Bergman H, Gat I, Meilijson I, Seidemann E, Tishby N, Vaadia E. 1995. Cortical activity flips among quasi-stationary states. Proc Natl Acad Sci USA. 92(19):8616-20

Albert NB, Robertson EM, Miall RC. 2009. The resting human brain and motor learning. Curr Biol. 19(12):1023–1027

Allison T, McCarthy G, Nobre A, Puce A, Belger A. 1994. Human Extrastriate Visual Cortex and the Perception of Faces, Words, Numbers, and Colors. Cereb Cortex. 4(5):544-54.

Arcaro MJ, Honey CJ, Mruczek RE, Kastner S, Hasson U. 2015. Widespread correlation patterns of fMRI signal across visual cortex reflect eccentricity organization. Elife. 19:4

Arieli A. 1992. Novel strategies to unravel mechanisms of cortical function: from macro-to micro-electrophysiological recordings. Information processing in the cortex. 123-138,

Arieli A, Shoham D, Hildesheim R, Grinvald A. 1995. Coherent spatiotemporal patterns of ongoing activity revealed by real-time optical imaging coupled with single-unit recording in the cat visual cortex. J Neurophysiol. 73(5):2072-93.

Arieli A, Sterkin A, Grinvald A, Aertsen A. 1996. Dynamics of ongoing activity: explanation of the large variability in evoked cortical responses. Science. 273:1868-1871.

Aguirre GK, Zarahn E, D'esposito M. 1998. The variability of human, BOLD hemodynamic responses. Neuroimage.8(4):360-9.

Aguirre, GK., Zarahn E., D'Esposito, M. 1998. An area within human ventral cortex sensitive to "building" stimuli: evidence and implications. Neuron 21, 373–383

Aguirre, GK., Zarahn E., D'Esposito, M. 1998. Neural components of topographical representation. Proc Natl Acad Sci USA. 95(3):839-46.

Baldassarre A, Lewis CM, Committeri G, Snyder AZ, Romani GL, Corbetta M. 2012. Individual variability in functional connectivity predicts performance of a perceptual task. Proc Natl Acad Sci USA. 109:3516-3521.

Beauchamp MS, Lee KE, Haxby JV, Martin A. 2002. Parallel Visual Motion Processing Streams for Manipulable Objects and Human Movements. Neuron. 34(1):149-59.

Biswal B, Yetkin FZ, Haughton VM, Hyde JS. 1995. Functional connectivity in the motor cortex of resting human brain using echo-planar MRI. Magnetic resonance in medicine. 34:537-541.

Buckner, R.L., Krienen, F.M., and Yeo, B.T.T. 2013. Opportunities and limitations of intrinsic functional connectivity MRI. Nat. Neurosci. 16, 832–837

Chao LL, Haxby JV, Martin A. 1999. Attribute-based neural substrates in temporal cortex for perceiving and knowing about objects. Nat Neurosci. 2(10):913-9.

Cohen L, Dehaene S, Naccache L, Lehericy S, Dehaene-Lambertz G, Henaff MA, Michel F. 2000. The visual word form area: spatial and temporal characterization of an initial stage of reading in normal subjects and posterior split-brain patients. Brain. 123 (Pt 2):291-307.

Cole MW, Bassett DS, Power JD, Braver TS, Petersen SE. 2014. Intrinsic and task-evoked network architectures of the human brain. Neuron. 83(1):238–251.

Cole MW, Ito T, Bassett DS, Schultz DH. 2016. Activity flow over resting-state networks shapes cognitive task activations. Nat Neurosci. 19(12):1718-1726

Cox DD, Savoy RL. 2003. Functional magnetic resonance imaging (fMRI) "brain reading": Detecting and classifying distributed patterns of fMRI activity in human visual cortex. Neuroimage. 19(2 Pt 1):261-70.

Corbetta M, Shulman GL. 2002. Control of goal-directed and stimulus-driven attention in the brain. Nat Rev Neurosci. 3(3):201-15.

Dosenbach NU, Fair DA, Miezin FM, Cohen AL, Wenger KK, Dosenbach RA, Fox MD, Snyder AZ, Vincent JL, Raichle ME, Schlaggar BL, Petersen SE. 2007. Distinct brain networks for adaptive and stable task control in humans. Proc. Natl. Acad. Sci. USA 104, 11073–11078.

Downing PE, Chan AW, Peelen MV, Dodds CM, Kanwisher N. 2006. Domain specificity in visual cortex. Cereb Cortex. 16:1453-1461.

Engel AK, Fries P, Singer W. 2001. Dynamic predictions: oscillations and synchrony in top-down processing. Nat Rev Neurosci. 2(10):704-16.

Epstein R, Kanwisher N. 1998. A cortical representation of the local visual environment. Nature. 392(6676):598-601.

Fiser J, Chiu C, Weliky M. 2004. Small modulation of ongoing cortical dynamics by sensory input during natural vision. Nature. 431(7009):573–578.

Fox MD, Snyder AZ, Vincent JL, Corbetta M, Van Essen DC, Raichle ME. 2005. The human brain is intrinsically organized into dynamic, anticorrelated functional networks. Proc Natl Acad Sci USA. 102:9673-9678.

Fox MD, Corbetta M, Snyder AZ, Vincent JL, Raichle ME. 2006. Spontaneous neuronal activity distinguishes human dorsal and ventral attention systems. Proc Natl Acad Sci USA. 103:10046-10051.

Fox MD, Snyder AZ, Vincent JL, Raichle ME. 2007. Intrinsic fluctuations within cortical systems account for intertrial variability in human behavior. Neuron. 56:171-184.

Greicius MD, Krasnow B, Reiss AL, Menon V. 2003. Functional connectivity in the resting brain: a network analysis of the default mode hypothesis. Proc Natl Acad Sci USA. 100:253-258.

Grill-Spector K, Weiner KS. 2014. The functional architecture of the ventral temporal cortex and its role in categorization. Nat Rev Neurosci. 15(8):536-48.

Grossman ED, Blake R. 2002. Brain areas active during visual perception of biological motion. Neuron. 35(6):1167-75.

Golland Y, Golland P, Bentin S, Malach R. 2008. Data-driven clustering reveals a fundamental subdivision of the human cortex into two global systems. Neuropsychologia. 46(2):540–553.

Gordon EM, Laumann TO, Adeyemo B, Huckins JF, Kelley WM, Petersen SE. 2016. Generation and Evaluation of a Cortical Area Parcellation from Resting-State Correlations. Cereb Cortex. 26 (1):288-303

Hacker CD, Laumann TO, Szrama NP, Baldassarre A, Snyder AZ, Leuthardt EC, Corbetta M. 2013. Resting state network estimation in individual subjects. Neuroimage. 82:616-633.

Harmelech T, Malach R. 2013. Neurocognitive biases and the patterns of spontaneous correlations in the human cortex. Trends Cogn Sci. 17(12):606–615.

Hasson U, Levy I, Behrmann M, Hendler T, Malach R. 2002. Eccentricity Bias as an Organizing Principle for Human High-Order Object Areas. Neuron. 34(3):479-90.

Hasson U, Nir Y, Levy I, Fuhrmann G, Malach R. 2004. Intersubject synchronization of cortical activity during natural vision. Science. 303(5664):1634–1640.

Hasson U, Nusbaum HC, Small SL. 2009. Task-dependent organization of brain regions active during rest. Proc Natl Acad Sci. 106(26):10841–10846.

Haxby JV, Gobbini MI, Furey ML, Ishai A, Schouten JL, Pietrini P. 2001. Distributed and overlapping representations of faces and objects in ventral temporal cortex. Science. 293:2425-2430.

Haxby JV, Bryan R, Gobbini MI. 2006. The representation of mammalian faces in human cortex. Journal of Vision. 6(86)

Haxby JV, Guntupalli JS, Connolly AC, Halchenko YO, Conroy BR, Gobbini MI, Hanke M, Ramadge PJ. 2011. A Common, High-Dimensional Model of the Representational Space in Human Ventral Temporal Cortex. Neuron. 72(2):404-16.

He BJ, Snyder AZ, Zempel JM, Smyth MD, Raichle ME. 2008. Electrophysiological correlates of the brain's intrinsic large-scale functional architecture. Proc Natl Acad Sci USA. 105:16039-16044.

Heinzle J, Wenzel MA, Haynes JD. 2012. Visuomotor Functional Network Topology Predicts Upcoming Tasks. J. Neurosci. 32(29), 9960–9968.

Henriksson L, Khaligh-Razavi SM, Kay K, Kriegeskorte N. 2015. Visual representations are dominated by intrinsic fluctuations correlated between areas. Neuroimage. 114:275–286.

Hermundstad, A.M., Bassett, D.S., Brown, K.S., Aminoff, E.M., Clewett, D., Freeman, S., Frithsen, A., Johnson, A., Tipper, C.M., Miller, M.B., et al. 2013. Structural foundations of resting-state and task-based functional connectivity in the human brain. Proc. Natl. Acad. Sci. USA 110, 6169–6174

Huth AG, Nishimoto S, Vu AT, Gallant JL. 2012. A continuous semantic space describes the representation of thousands of object and action categories across the human brain. Neuron. 76(6): 1210–1224.

Ishai A, Ungerleider LG, Martin A, Haxby JV. 2000. Distributed representation of objects in the human ventral visual pathway. J Cogn Neurosci. 12 Suppl 2:35-51.

Ito T, Kulkarni KR, Schultz DH, Mill RD, Chen RH, Solomyak LI, Cole MW. 2017. Cognitive task information is transferred between brain regions via resting-state network topology. Nat Commun. 8(1):1027.

Kanwisher N, McDermott J, Chun MM. 1997. The fusiform face area: a module in human extrastriate cortex specialized for face perception. J Neurosci. 17(11):4302-11.

Kenet T, Bibitchkov D, Tsodyks M, Grinvald A, Arieli A. 2003. Spontaneously emerging cortical representations of visual attributes. Nature. 425(6961):954-956.

Kim D, Kay K, Shulman GL, Corbetta M. 2018. A New Modular Brain Organization of the BOLD Signal during Natural Vision. Cereb Cortex. 28(9):3065-3081.

Kriegeskorte N, Goebel R, Bandettini P. 2006. Information-based functional brain mapping. Proc Natl Acad Sci U S A. 103:3863-3868.

Kriegeskorte N, Formisano E, Sorger B, Goebel R. 2007. Individual faces elicit distinct response patterns in human anterior temporal cortex. Proc Natl Acad Sci U S A. 104:20600-20605.

Kriegeskorte N, Mur M, Ruff DA, Kiani R, Bodurka J, Esteky H, Tanaka K, Bandettini PA. 2008. Matching categorical object representations in inferior temporal cortex of man and monkey. Neuron. 60:1126-1141.

Kriegeskorte N, Mur M, Bandettini P. 2008. Representational similarity analysis - connecting the branches of systems neuroscience. Front Syst Neurosci. 2:4.

Lewis CM, Baldassarre A, Committeri G, Romani GL, Corbetta M. 2009. Learning sculpts the spontaneous activity of the resting human brain. Proc Natl Acad Sci. 106(41):17558–17563.

Lowe MJ, Mock BJ, Sorenson JA. 1998. Functional connectivity in single and multislice echoplanar imaging using resting-state fluctuations. Neuroimage. 7(2):119-32.

Nelson, S.M., Cohen, A.L., Power, J.D., Wig, G.S., Miezin, F.M., Wheeler, M.E., Velanova, K., Donaldson, D.I., Phillips, J.S., Schlaggar, B.L., and Petersen, S.E. 2010. A parcellation scheme for human left lateral parietal cortex. Neuron 67, 156–170.

Nir Y, Hasson U, Levy I, Yeshurun Y, Malach R. 2006. Widespread functional connectivity and fMRI fluctuations in human visual cortex in the absence of visual stimulation. Neuroimage. 30:1313-1324.

Martin A, Wiggs CL, Ungerleider LG, Haxby JV. 1996. Neural correlates of category-specific knowledge. Nature. 379(6566):649-52.

Mennes M, Kelly C, Colcombe S, Castellanos FX, Milham MP. 2013. The extrinsic and intrinsic functional architectures of the human brain are not equivalent. Cereb Cortex. 23(1):223–229.

Omer DB, Fekete T, Ulchin Y, Hildesheim R, Grinvald A. 2018. Dynamic Patterns of Spontaneous Ongoing Activity in the Visual Cortex of Anesthetized and Awake Monkeys are Different. Cereb Cortex.

Osher DE, Saxe RR, Koldewyn K, Gabrieli JD, Kanwisher N, Saygin ZM. 2016. Structural

Connectivity Fingerprints Predict Cortical Selectivity for Multiple Visual Categories across Cortex. Cereb Cortex. 26:1668-1683.

Petersen SE, Sporns O. 2015. Brain Networks and Cognitive Architectures. Neuron. 88(1):207–219.

Power, JD, Fair DA, Schlaggar BL, and Petersen SE. 2010. The development of human functional brain networks. Neuron 67, 735–748.

Power JD, Cohen AL, Nelson SM, Wig GS, Barnes KA, Church JA, Vogel AC, Laumann TO, Miezin FM, Schlaggar BL, Petersen SE. 2011. Functional network organization of the human brain. Neuron. 72:665-678.

Smith SM, Fox PT, Miller KL, Glahn DC, Fox PM, Mackay CE, Filippini N, Watkins KE, Toro R, Laird AR, Beckmann CF. 2009. Correspondence of the brain's functional architecture during activation and rest. Proc Natl Acad Sci U S A. 106:13040-13045.

Stansbury DE, Naselaris T, Gallant JL. 2013. Natural Scene Statistics Account for the Representation of Scene Categories in Human Visual Cortex. Neuron. 79(5):1025–1034.

Tambini A, Ketz N, Davachi L. 2010. Enhanced Brain Correlations during Rest Are Related to Memory for Recent Experiences. Neuron. 65(2):280–290.

Tavor I, Parker Jones O, Mars RB, Smith SM, Behrens TE, Jbabdi S. 2016. Task-free MRI predicts individual differences in brain activity during task performance. Science. 352:216-220.

Tsodyks M, Kenet T, Grinvald A, Arieli A. 1999. Linking spontaneous activity of single cortical neurons and the underlying functional architecture. Science. 286:1943-1946.

Raemaekers M, Schellekens W, van Wezel RJ, Petridou N, Kristo G, Ramsey NF. 2014. Patterns of resting state connectivity in human primary visual cortical areas: A 7T fMRI study. Neuroimage. 84:911-921.

Raichle ME, MacLeod AM, Snyder AZ, Powers WJ, Gusnard DA, Shulman GL. 2001. A default mode of brain function. Proc Natl Acad Sci USA, 98(2):676–682

Raichle ME. 2010. Two views of brain function. Trends Cogn Sci. 14:180-190.

Raichle ME. 2011. The restless brain. Brain Connect. 1(1):3-12.

Saygin ZM, Osher DE, Koldewyn K, Reynolds G, Gabrieli JD, Saxe RR. 2011. Anatomical connectivity patterns predict face selectivity in the fusiform gyrus. Nat Neurosci. 2011 Dec 25;15(2):321-7.

Seeley WW., Menon V, Schatzberg AF, Keller J, Glover GH., Kenna H, Reiss AL, Greicius MD. 2007. Dissociable intrinsic connectivity networks for salience processing and executive control. J. Neurosci. 27, 2349–2356

Schroeder CE, Lakatos P. 2009. Low-frequency neuronal oscillations as instruments of sensory selection. Trends Neurosci. 2009 Jan;32(1):9-18.

Strappini F, Wilf M, Karp O, Goldberg H, Harel M, Furman-Haran E, Golan T, Malach R. 2018. Resting-State Activity in High-Order Visual Areas as a Window into Natural Human Brain Activations. Cereb Cortex

Tsodyks M, Kenet T, Grinvald A, Arieli A. 1999. Linking spontaneous activity of single cortical neurons and the underlying functional architecture. Science. 286:1943-1946.

Varela F, Lachaux JP, Rodriguez E, Martinerie J. 2001. The brainweb:phase synchronization and large-scale integration. Nat Rev Neurosci. 2(4):229–239.

Wilf M, Strappini F, Golan T, Hahamy A, Harel M, Malach R. 2017. Spontaneously Emerging Patterns in Human Visual Cortex Reflect Responses to Naturalistic Sensory Stimuli. Cereb Cortex. 27:750-763.

Yeo BT, Krienen FM, Sepulcre J, Sabuncu MR, Lashkari D, Hollinshead M, Roffman JL, Smoller JW, Zollei L, Polimeni JR, Fischl B, Liu H, Buckner RL. 2011. The organization of the human cerebral cortex estimated by intrinsic functional connectivity. J Neurophysiol. 106:1125-1165.

Chapter 2: Categorical object recognition activity and intrinsic activity in visual cortex

2.1 Abstract

The relationship between spontaneous and task-evoked brain activity is an increasingly important topic in neuroscience. Here, we ask if spontaneous multivoxel activity patterns in human visual cortex correspond to patterns evoked by naturalistic (e.g. faces), and non-naturalistic (e.g. phase-scrambled faces) visual stimuli. We determined the regions that preferred particular object categories during localizer scans, combined those regions into 'joint-ROIs', and measured multivoxel patterns in the joint-ROIs for each stimulus class during separate task scans. We then spatially correlated these stimulus-evoked multivoxel patterns to the multivoxel pattern measured in each frame of resting-state scans. The mean correlation coefficient was essentially zero for all regions and stimulus categories, indicating that resting activity patterns were not biased toward a joint-ROI's preferred stimulus. However, the spread of correlation coefficients (positive, negative) was significantly greater for the preferred stimulus. Therefore, spontaneous activity patterns, at specific time points, positively or negatively matched preferred stimulus evoked activity patterns, both within and across regions. We conclude that spontaneous multi-voxel activity patterns are linked to stimulus-evoked patterns in human visual cortex.

2.2 Introduction

The functional role of spontaneous brain activity in human behavior is an increasingly important topic in neuroscience. An emerging view is that the neural activity evoked by a task

and the associated behavior is influenced and constrained by ongoing neural activity (Tsodyks et al. 1999; Fiser et al. 2004; Fox et al. 2007; Cole et al. 2016; Tavor et al. 2016) an idea that contrasts with a long-standing view that spontaneous activity is random, and only important as a mechanism for facilitating forward transmission of information processing (Shadlen and Newsome 1994). Many studies have now shown that spontaneous activity is highly structured in space and time (Biswal et al. 1995; Greicius et al. 2003; Kenet et al. 2003; He et al. 2008; de Pasquale et al. 2010; Power et al. 2011; Yeo et al. 2011). Imaging of neural activity at a scale that extends across many cortical columns has shown that the macro-scale pattern of spontaneous neural activity within a sensory area in an anesthetized animal mirrors the pattern of activity evoked by stimulation of a specific visual feature (Kenet et al. 2003; Omer et al. 2018). Moreover, stimulus-evoked activity can be predicted from the ongoing activity that occurs before or coincident with stimulus onset (Arieli et al. 1996; Tsodyks et al. 1999).

On a more global scale, human imaging studies have shown that widely distributed regions that are co-activated during a task show temporally correlated activity at rest(Biswal et al. 1995; Fox et al. 2005; Smith et al. 2009). For example, human frontal eye field (FEF) and dorsal intraparietal sulcus (IPS) or superior parietal lobule (SPL) are routinely co-activated in tasks that involve oculomotor or visuospatial attentional demands and also show highly correlated activity at rest(Fox et al. 2006). In fact, the blood-oxygenation-level-dependent (BOLD) activity in large groups of regions at rest are highly correlated, forming what are termed resting-state networks (RSNs) that are associated with particular functions (e.g. dorsal attention network) (Power et al. 2011; Yeo et al. 2011). The measurement of interregional correlations at rest, functional connectivity magnetic resonance imaging (fcMRI), has become a primary tool for measuring spontaneous interactions between brain regions. Moreover, a growing body of work is

using fcMRI to understand and assess brain damage and disease (He et al. 2007; Sheline and Raichle 2013; Sharp et al. 2014; Gao and Wu 2016).

The relationship between resting and task-evoked activity in fMRI studies has been conceptualized in terms of the correspondence between resting and task networks defined by inter-regional correlations (Cole et al. 2014; Kim et al. 2018), or between resting networks and patterns of task co-activation (Smith et al. 2009). Also, recent studies have examined whether task activation can be predicted from resting functional connectivity (FC) (Cole et al. 2016; Tavor et al. 2016). Here, we discuss a conceptualization more related to the animal work noted above, which provides novel insight into why rest-task correspondences occur and thus, the function of spontaneous activity. This conceptualization posits that statistical regularities in the external and internal (motor planning, cognitive routines) environment result in similar distributions of the neural states encoding those regularities (Fiser et al. 2010). Resting states in turn reflect these high-information neural states through a Hebbian learning process (Lewis et al. 2009). Studies have shown that performing a task changes FC in subsequent resting epochs (Albert et al. 2009; Hasson et al. 2009; Tambini et al. 2010). Conversely, an individual's pattern of FC at rest predicts their performance on a subsequent task (Baldassarre et al. 2012). Therefore, interactions between resting states and task states form a complete or closed cycle that may reflect the functional significance of spontaneous interactions between regions in everyday life: resting activity affects task-evoked neural activity and behavioral performance, which in turn affects resting FC through a Hebbian process (Fig. 2.1a). According to this conceptualization, resting-state activity provides a useful prior or scaffold of biological states that can be modified for performance of different tasks. A related conceptualization focuses on the 'internal' environment and posits that the spontaneous interactions between regions, as in resting FC, are

due to connectivity patterns that are coded as synaptic efficacies in cortical networks and reflect an individual's cognitive traits or biases (Harmelech and Malach 2013; Strappini et al. 2018).

To evaluate these ideas, however, one must move beyond measures of overall FC between regions and instead test for the presence and connectivity of resting multi-voxel patterns that conform to the neural patterns associated with states of the internal and external environment. Multi-voxel analyses of fMRI task signals have shown that neural states or patterns of local activity during tasks do in fact carry information about stimulus categories, retrieved memories or cognitive processes such as attention (Haxby et al. 2001; Haynes and Rees 2005; Kamitani and Tong 2005; Kriegeskorte et al. 2006; Serences and Boynton 2007; Kriegeskorte et al. 2008; Greenberg et al. 2010; Kuhl and Chun 2014) and can be modulated by learning.

A representational function for resting activity might seem surprising since the brain appears capable of coding a huge, almost unlimited number of states. However, studies of the motor system indicate that the brain partly deals with the large number of possible hand movements through synergies (Schieber and Santello 2004; Santello et al. 2013) that reduce dimensionality. Studies of human hand movements under experimental and naturalistic conditions (Santello et al. 1998; Ingram et al. 2008) have isolated a small number of principal components that code for large amounts of variance and distinguish a variety of movements. Moreover, a recent fMRI study reported that these components map onto multi-voxel patterns of movement-evoked BOLD activity in regions of motor and premotor cortex, SMA, SPL, and anterior IPS (Leo et al. 2016). The existence of these modal axes or synergies increases the plausibility that resting activity might encode these biologically important representations. A similar idea can be extended to other domains. For example, multi-voxel patterns in temporal-occipital cortex vary along general features of object categories such as animacy (Martin et al.

1996; Chao et al. 1999; Kriegeskorte et al. 2008; Sha et al. 2015) or, in literate adults, sensitivity to orthography (Cohen et al. 2000; Dehaene et al. 2004; Binder et al. 2006; Vinckier et al. 2007).

Here we tested the hypothesis that multi-voxel patterns of resting state activity in visual cortex are related to the multi-voxel patterns evoked by naturalistic (e.g. faces) and non-naturalistic (e.g. phase-scrambled faces) visual stimuli. We determined this relationship in high-level regions of visual cortex that show preferences for object categories, and are presumably sensitive to the higher-order features/statistics that define naturalistic objects. We also tested regions in early visual cortex that are more influenced by low-level features. These latter features occur in naturalistic objects but are also present in phase-scrambled and grid-scrambled objects in which the higher-order features/statistics that define natural categories have been removed. Subjects received resting scans, localizer scans, and task scans. Localizer scans determined the tested ROIs and task scans identified the multi-voxel 'representational' patterns evoked by the different object categories. These representational patterns were then correlated with the multi-voxel patterns measured on each frame of resting-scans. The resulting distribution of correlation coefficients indicated the extent to which resting activity patterns matched stimulus-evoked patterns.

We specifically contrasted whether resting state multivoxel patterns 1) corresponded better to multivoxel patterns evoked by some ecological object categories (e.g. faces) than others (e.g. tools) and/or 2) corresponded better to patterns evoked by object categories than corresponding controlled stimuli (e.g. phase-scrambled faces or tools).

2.3 Methods

2.3.1 Participants

The study included 16 healthy young adult volunteers (10 female; age 21 – 35 years-old) with no prior history of neurological or psychiatric disorders. All participants were right-handed native English speakers with normal or corrected-to-normal vision. All participants gave informed consent to take part in the experiment, and the study was approved by the Institutional Review Board (IRB) of Washington University in St. Louis School of Medicine.

2.3.2 Stimuli

Nine categories of color images subtending 8^o x 8^o of visual angle were included in event-related 'task' fMRI scans. Seven categories consisted of images that are often encountered in the environment: human faces, human bodies, mammals, chairs, tools, scenes, and words. Stimuli, excluding the word category, were obtained from Downing et al. 2006 (Downing et al. 2006). Faces, bodies and mammals served as animate categories, and chairs, tools and scenes as inanimate categories (Kriegeskorte et al. 2008). Word stimuli were included for exploratory analyses and results for those stimuli will not be considered in this paper.

Two control stimulus categories were constructed from the above stimuli used in the experiment, excluding the word stimuli. A low-level control consisted of phase-scrambled stimuli that preserved the spatial frequency amplitude spectrum of the intact-stimulus images. An intermediate-level control consisted of grid-scrambled stimuli that included basic visual properties of the intact-stimulus images such as line segments and connectors. For the low-level control condition, 2D phase-scrambled images of the exemplars from the 6 categories were

generated by applying the same set of random phases to each 2-dimensional frequency component of the original image while keeping the magnitude constant (Watson et al. 2016). Exemplars from all six intact-stimulus categories except real word stimuli were 2D phase-scrambled, yielding a total of 144 2D Phase-scrambled stimuli. For the intermediate-level control condition, grid-scrambled images of exemplars from the six intact-stimulus categories were generated by sub-dividing each image into a 10 x 10 grid (each grid is 0.8o x 0.8o) and randomly rearranging the individual grid segments.

Color images of exemplars from seven categories were included in localizer scans: human faces, human bodies, objects (chairs and tools), scenes, words, false font character strings and phase scrambled images. The categories for the localizer scans differed slightly from the categories for the task scans since the former was only used to define the regions of interest (ROIs). ROIs related to the false font and word stimuli will not be considered in this paper. Stimuli were presented using the Psychophysics Toolbox package (Brainard 1997) in MATLAB (The MathWorks). Stimulus images were projected onto a screen and were viewed through a mirror mounted on the head coil. All stimuli were presented centrally on a gray background.

2.3.3 Scanning Procedure

The study consisted of two separate sessions, each conducted on a separate day. In session one, subjects received 3 resting state runs, 2 localizer runs, and 8 task runs. In session 2, subjects received 2 resting state runs, 2 localizer runs, 8 task runs, and 2 post-task resting state runs. One subject had a total of 13 task runs over the two sessions instead of 16 (Fig. 2.1b).

Resting state runs. Participants received a total of 7 resting state scans, each lasting 5 min (300 TRs). During a scan the participant was asked to maintain fixation on a cross that was displayed at the center of the screen during the entire run. Five resting scans (3 for first session and 2 for second session) were conducted before any localizer or task scans to collect stimulus-free intrinsic activities. For the second session only, two additional 5 min resting state scans were conducted after the task scans to investigate potential post stimuli-driven effects on intrinsic activity. The results from the post-task resting scans will not be discussed here.

Localizer runs. Each session included 2 localizer runs (4 in total), each lasting 5 min and 40s (340 TRs), and each localizer scan was presented in a blocked fMRI design. Each block of a localizer run contained 20 images of a single category, and those images were different from the images used in the task scans. A fully randomized sequence of eight blocks, consisting of the 7 stimulus categories and a fixation block, was repeated twice within each run. At the beginning and the end of each run, an additional fixation block was presented for 4s and 16s. Within each category block, images were presented for 300ms with an inter-stimulus interval (ISI) of 700ms. A fixation cross was continuously present at the center of the screen during the ISI and during fixation blocks. During category blocks, participants performed a minimally cognitively engaging task by pressing a button if the initially presented image was changed in size or position during the 300ms presentation.

Task runs. Each session included 8 task runs (16 in total), each lasting 5 min and 15s (315 TRs). For each subject and for each run, stimulus presentation order and inter-stimulus intervals were fully randomized using Optseq2 (Dale 1999). Each stimulus presentation lasted

for 300ms and the interval between stimuli was jittered between 3.7s and 8.7s. A fixation cross was continuously present at the center of the screen during the ISI. In each intact-stimulus category, there were 24 separate exemplars (e.g. 24 different faces) and each exemplar was repeated 4 times. In each scrambled category, there were 96 exemplars, each presented once. Participants performed a minimally cognitively engaging task by pressing a button if the presented image changed its size or position during a 300ms presentation, the same task as that performed during the localizer scans.

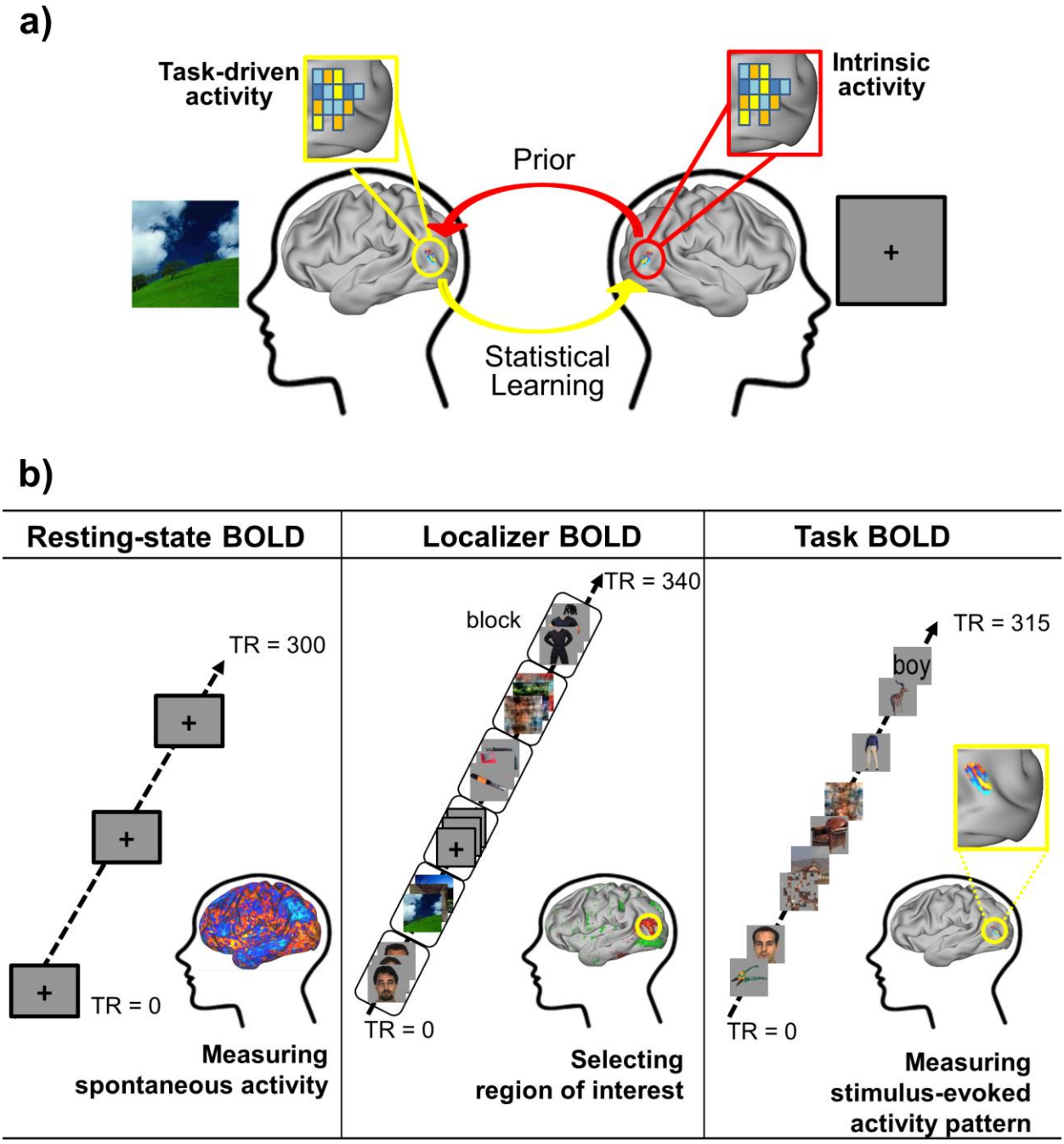

Figure 2.1. (a) The putative cyclic interplay between brain activity evoked by real-world experiences and resting-state activity. **(b)** Experimental design.

2.3.4 Imaging parameters

Data were obtained from a Siemens 3T Prisma MRI scanner. Structural images for atlas transformation and lesion segmentation were acquired using T1-weighted magnetization

prepared-rapid gradient echo (MP-RAGE) (1 x 1 x 1 mm voxels; echo time [TE] = 2.36 ms, repetition time [TR] = 1700 ms, TI=1000 ms, flip angle = 8°) and T2-weighted fast spin echo sequences (1 x 1 x 1 mm voxels; TE = 564 ms, TR = 3200 ms). FMRI scans were collected using a gradient echo-planar sequence sensitive to BOLD contrast (TE = 26.6 ms, flip angle = 58°, 2.4 x 2.4 x 2.4 mm voxels, 48 contiguous slices, TR = 1.0 s, and multiband factor of 4).

2.3.5 fMRI pre-processing

fMRI data underwent pre-processing as previously described (Siegel JS et al. 2016). This included: (1) compensation for asynchronous slice acquisition using sinc interpolation; (2) elimination of odd/even slice intensity differences resulting from interleaved acquisition; (3) whole brain intensity normalization to achieve a mode value of 1000; (4) spatial realignment within and across fMRI runs; and (5) resampling to 2.4 mm cubic voxels in atlas space, including realignment and atlas transformation in one resampling step. Cross-modal (e.g. T2-weighted to T1-weighted) image registration was accomplished by aligning image gradients.

Surface generation and processing of functional data followed procedures similar to Glasser et al (Glasser et al. 2013). First, anatomical surfaces were generated for each subject's T1 MRI using FreeSurfer automated segmentation (Fischl et al. 1999). This step included brain extraction, segmentation, generation of white matter and pial surface, inflation of the surfaces to a sphere, and surface shape-based spherical registration to the subjects' "native" surface to the fs_average surface. The left and right hemispheres were then resampled to 164,000 vertices and registered to each other (Van Essen et al. 2001).

Data were passed through several additional preprocessing steps: (i) removal by regression of the following sources of spurious variance: (a) six parameters obtained by rigid

body correction of head motion, (b) the signal averaged over the whole brain (global signal regression), (c) signal from ventricles and CSF, and (d) signal from white matter; (ii) temporal filtering retaining frequencies in the 0.009−0.08-Hz band; and (iii) frame censoring (framewise displacement (FD) $\geq$ 0.5mm). The first four frames of each BOLD run were excluded.

To account for magnitude variability between different task and resting state runs, the BOLD timeseries for each vertice were Z-normalized across time within the task and the resting state runs. This Z-normalization was not applied to the localizer scans. Also, it was not applied to the Task scans for a separate analysis described below in which task-evoked activation magnitudes were determined (see below, Task scans: **multi-voxel activation patterns**).

2.3.6 Defining ROIs from localizer activation contrasts

ROIs were defined from univariate vertice-wise statistical contrasts on the localizer activation magnitudes for different categories. For example, face-selective areas were defined from the significant vertices for the contrast of faces minus objects, where objects consisted of chairs and tools. First, for each participant a general linear model (GLM) was applied to their functional localizer scans. The GLM consisted of separate regressors for each stimulus category (e.g. faces) using an assumed hemodynamic response function from the Statistical Parametric Mapping (SPM12), a baseline term, and a linear trend term. Condition contrasts were formed to identify vertices showing preferences for each category, using a scheme similar to that of Bracci and Op de Beeck (2016) (Bracci and Op de Beeck 2016): body-preferences (body > objects, i.e. chairs and tools), face-preferences (face > objects), scene-preferences (scene > objects), intact-

stimulus-preferences (face + body + scene + object (chair+tool) > phase-scrambled), and phase-scrambled-preferences (phase-scrambled > face + body + scene + object (chair+tool)).

A group random-effect statistical Z-map for each contrast was then computed from the single-subject GLMs (see Figure 2.2a for the group z-statistic map for each contrast). The Z-values obtained were sorted in magnitude. From the highest Z-values from the map, the group peak with the next highest Z-value was generated until the Z-value was <= 2.0. Group peaks had to be separated by at least 38.4mm (9.6 mm x 4) in the sphere mesh to prevent a vertex being assigned to multiple ROIs in a subject. ROIs were then defined separately for each participant based on the individual's univariate statistical maps (Oosterhof et al. 2012; Wurm et al. 2016). From each group peak defined above, the corresponding peak for an individual subject peak was defined as the vertex with the highest Z-value within a sphere of 9.6 mm radius centered around the group peak in each subject's sphere mesh. The single-subject ROI was formed from the vertices exceeding Z= 2.0 in a sphere of 9.6 mm radius centered around the peak in the subject's mesh. All ROIs used in following analysis contained at least 175 vertices in at least 14 subjects. ROIs in individual subjects with less than 175 vertices were discarded.

To remove differences in BOLD magnitude across MR frames, for each ROI a z-normalization was applied across the vertices of each frame of the resting and task scans. This within-frame Z-normalization was not applied to the localizer scans. Also, it was not applied to the Task scans for a separate analysis described below in which task-evoked activation magnitudes were determined (see below, Task scans: multi-voxel activation patterns)

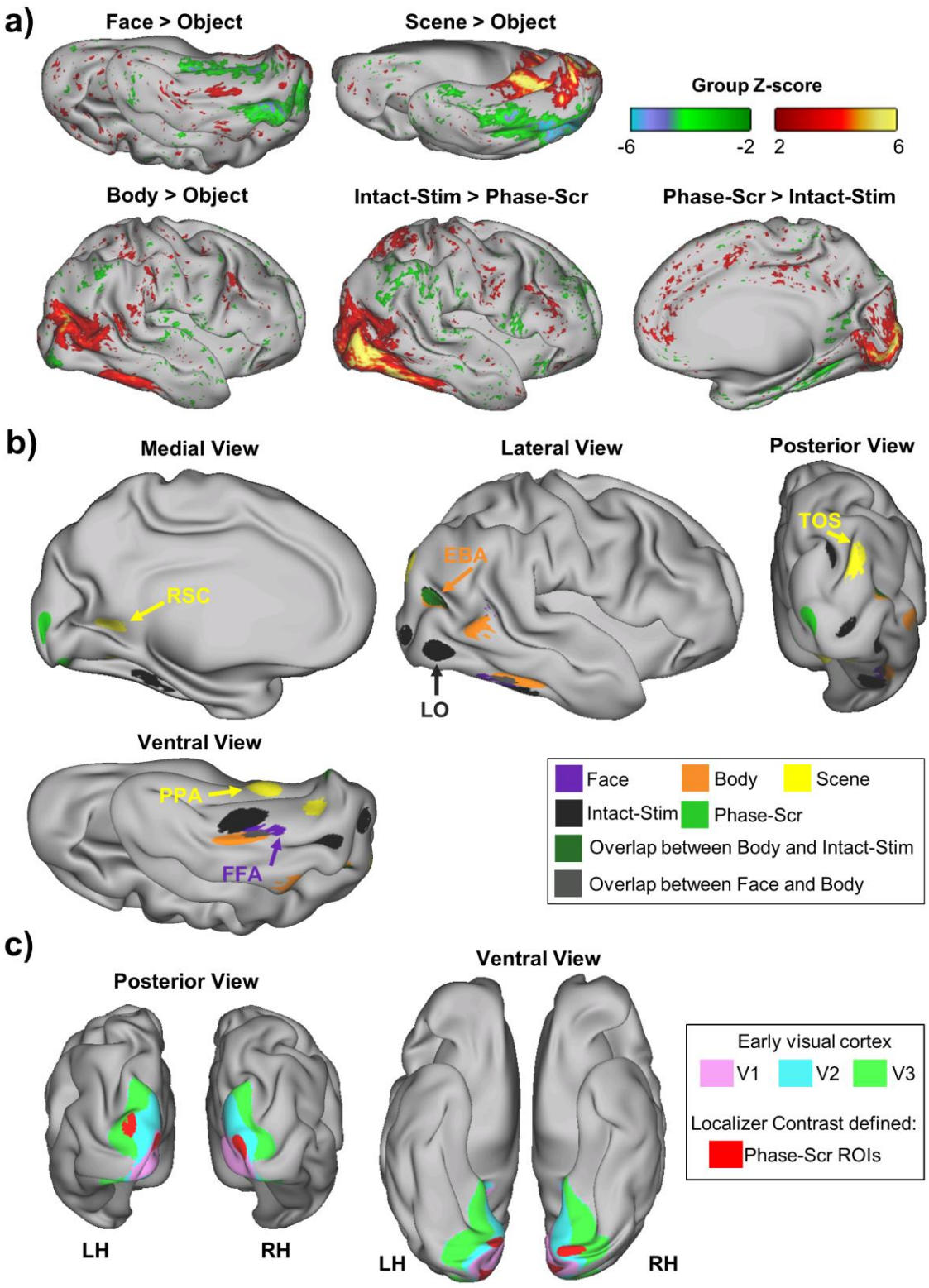

Figure 2.2. (a) Group z-statistic Localizer maps. ROIs were separately defined for individual from their localizer maps using the group foci as a constraint (see Methods, Defining ROIs from localizer activation

contrasts). **(b)** Three sets of category-preferential ROIs were defined for faces, bodies, and scenes using the object category (tools and chairs) as the baseline. The ROIs in each set were combined into a joint-ROI after excluding regions with containing more than 50% of the early visual vertices in the group map. The early visual vertices in V1 to V3 were estimated from the Benson template (Benson et al. 2012). Two additional sets of ROIs were defined by contrasting all intact-stimulus categories (face, body, object, and scene) against the phase-scrambled condition. The positive contrast (i.e. face+body+object+scene > phase-scrambled) and negative contrast (i.e. face+body+object+scene < phase-scrambled) each yielded a set of ROIs that were combined, respectively, into a Intact-Stimulus joint-ROI and a Phase-Scrambled joint-ROI. The locations of the constituent ROIs for each of the five joint-ROIs are schematically shown based on the group locations.

Two sets of ROIs were created for use in different analyses. The first set was created from the localizer-defined ROIs that preferred a particular target category (face, body, or scene) relative to the object category (chairs + tools). We grouped the vertices from the target-preferred ROIs into a single target-preferred joint-ROI. To minimize the effect of retinotopically related low-level feature driven activity from the high-level categorical object gestalts (Strappini et al. 2018), initially generated group ROIs containing more than 50% of its constituent vertices located in early visual areas (V1 to V3) were excluded. The early visual vertices were estimated from surface topology using the template created by Benson et al. (Benson et al. 2012). For each group ROI contains less than 50% of early visual vertices, each subject's individual ROI used its all constituent vertices since the early visual area estimations of V2 and V3 areas in Benson template was not stable. A second set of ROIs consisted of Intact-Stimulus ROIs (face + body + scene + object > phase-scrambled) and Phase-Scrambled ROIs (phase-scrambled > face + body + scene + object). Intact-Stim and Phase-Scrambled ROIs were grouped, respectively, into an Intact-Stim joint-ROI and a Phase-Scrambled joint-ROI. Table 2.1 summarizes the mean MNI coordinate, mean Z-score for the obtained group peak, and mean number of vertices for all constituent ROIs in each joint-ROI. Figure 2.2b schematically indicates the position of all constituent ROIs in a joint-ROI based on their group-peak locations. Figure 2.2c shows the

location of all Phase-Scr ROIs superimposed on a surface map of V1-V3 using the template from Benson et al. (Benson et al. 2012).

Table 2.1. Summary ROI information for all constituent ROIs used for generating a joint-ROI.

		Mean MNI across subjects						# vertices		
Contrast	Hemisphere	x	y	z	Group Peak Z-value	% (Non-EV) in Group Map	# Subject	Mean	STD	ROI Name
Face	RH	41	-50	-16	3.76	100	14	279	54	R-FFA
		54	-49	12	2.71	100	15	246	50	R-STG
Body	LH	-41	-73	12	6.61	100	16	289	45	L-EBA
		-37	-44	-17	4.42	100	14	271	59	
	RH	42	-65	15	6.28	100	15	321	37	R-EBA
		41	-44	-13	4.62	100	14	299	49	
		56	-52	4	3.91	100	14	297	47	
Scene	LH	-21	-47	-4	8.14	67.89	16	327	37	L-PPA
		-14	-51	7	5.88	83.15	16	294	56	L-RSC
		-30	-80	23	3.19	100	14	229	33	L-TOS
	RH	20	-41	-10	8.35	53.15	16	279	45	R-PPA
		27	-68	-10	6.79	56.36	16	254	43	
		35	-77	29	4.55	100	15	281	58	R-TOS
		13	-36	41	4.01	100	14	255	41	
Intact-Stim > Phase-Scr	LH	-41	-73	-1	8.46	100	16	374	31	L-LO
		-35	-66	-12	7.50	100	16	334	36	
		-20	-72	30	5.92	100	15	258	36	
		-30	-83	11	5.71	94.17	16	281	64	
		-26	-39	-14	5.57	100	15	250	40	
		-22	-56	45	4.12	100	14	264	51	
		-51	-59	8	3.10	100	14	243	37	
	RH	44	-72	-7	8.18	100	16	322	38	R-LO
		36	-44	-20	6.47	100	16	295	43	
		28	-82	5	5.34	65.79	14	268	37	
		26	-74	30	5.03	100	15	248	39	
		40	-64	16	4.74	100	14	284	60	
Phase-Scr > Intact-Stim	LH	-5	-89	3	8.25	0	16	276	34	
		-8	-80	-11	5.84	0	16	267	40	
		-19	-89	16	3.71	0	15	282	54	
	RH	10	-93	4	7.41	0	16	354	37	
		9	-77	-4	7.40	0	16	247	35	

2.3.7 Localizer scans: multi-voxel activation patterns

For each joint-ROI from each subject, the multi-vertex activation pattern for each stimulus category from the localizer scans was estimated. To accomplish this, a general linear model (GLM) was constructed using 7 category regressors, and baseline and linear trend regressors for each scan. Each category regressor was convolved with an assumed hemodynamic

response function. The output localizer β weight matrix was a categorical multi-voxel pattern of size Nc x Nv (Nc = Number of the localizer categories & Nv = Number of vertices belong to the ROI). The mean localizer categorical activation magnitude across vertices (a vector of size Nc x 1) was computed from the obtained categorical β weight matrix for each category

2.3.8 Task scans: multi-voxel activation patterns

For each joint-ROI from each subject, the multi-vertex activation pattern for each of the stimulus categories (except the word category) in the task scans was estimated via a GLM that included a category regressor for all stimulus presentations involving a particular category (Fig. 2.3). In addition, the GLM included a target regressor for trials in which a stimulus was perturbed in size or position, and baseline and linear trend regressors for each scan. The category and target regressors were each convolved with an assumed hemodynamic response function, yielding a stimulus-evoked BOLD multi-voxel pattern for each category (e.g. the pattern outlined by the red square in Fig. 2.3) and for the target. In order to determine the task-evoked magnitude for each stimulus category, a β weight matrix was separately computed using spatially non-normalized BOLD timeseries from the task scans.

2.3.9 Determining similarity of resting multi-vertex patterns and stimulus-evoked patterns

For each participant's individual joint-ROI, we determined the degree to which the multi-vertex pattern for a stimulus-evoked template for a category matched the multi-vertex pattern on each resting frame. In this procedure, illustrated in Figures 2.3, framewise intrinsic activity

patterns were obtained from independent resting-state scans. Next, for the averaged stimulus-evoked pattern for a category (e.g. the prototype template for 'scene', Fig. 2.3), the template spatial pattern was spatially correlated with the resting activity pattern on a frame. This procedure was repeated across all resting frames, resulting in a distribution of correlation coefficients (one coefficient per resting frame) for a particular category prototype in a particular joint-ROI. The upper 90% value of each distribution, hereafter termed the U90-value, was then determined. The U90 value computed for a prototype template served as a measure of the relationship between resting activity patterns and the patterns evoked by a category mean. For analyses that involved the Intact-Stimulus and Phase-Scrambled joint-ROI rather than joint-ROIs that preferred a particular category such as faces, U90-values for the six intact-stimulus categories (face, body, mammal, chair, tool, scene) were averaged together to form a intact-stimulus U90 value.

2.3.10 Statistical analysis of U90 values

U90 values were analyzed via repeated measures ANOVAs and paired t-tests. For example, the statistical significance of an overall dependence of U90 values for a joint-ROI on the stimulus category was determined by conducting repeated-measures ANOVAs with Category-Type as factors. Paired t-tests were conducted to test specific contrasts, with a Bonferroni-correction for multiple comparisons. For example, U90 values for intact-stimulus vs. phase-scrambled stimuli were compared in the Intact-Stimulus joint-ROI.

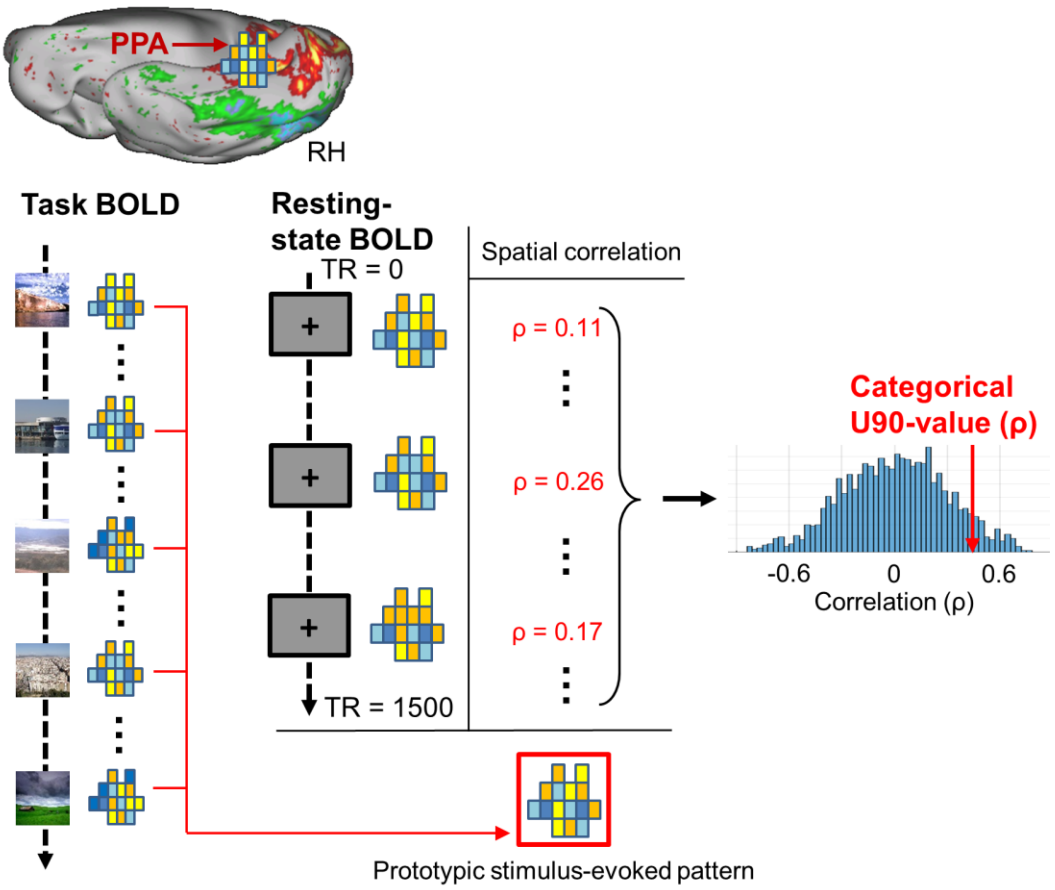

Figure 2.3. (a) Definition of U90-values using a prototype template. At each vertex of each joint-ROI, the categorical β weights for all 96 stimulus presentations from each category were computed, producing a categorical stimulus-evoked pattern or prototype template for each category and joint-ROI (e.g. the scene pattern outlined in red). For each joint-ROI, the spatial correlation between the prototype template and the resting activity pattern on a single resting frame was measured, yielding a spatial correlation coefficient for that frame. This procedure was repeated for all resting-state frames, yielding a distribution of spatial correlation coefficients. The upper 90% value from this distribution, shown by the vertical red arrow, was used as a summary measure of the distribution.

2.4 Results

The primary goal of the experiment was to compare multi-vertex activity patterns in the resting state to stimulus-evoked activity patterns from a variety of stimulus categories, including those that might be considered more or less 'ecological' (e.g. photographs of faces, tools, and

scenes vs. phase-scrambled images of those stimuli). This comparison was conducted 1) in regions of higher-order visual cortex that preferred a particular object category (e.g. faces) relative to other categories (e.g. objects), and 2) in regions of visual cortex that either preferred intact-stimulus categories relative to the phase-scrambled category or showed the reverse preference.

The stimulus-evoked spatial pattern or template for a category in a particular ROI was determined from the β weights estimated for a category regressor in the GLM for the task scans. Therefore, the stimulus-evoked template roughly reflected the average pattern of activation produced by different instances of the category. Instead of analyzing each localizer-defined ROI separately, we grouped each set of category-preferential ROIs for an individual into a single joint-ROI. The corresponding category template for the joint-ROI was the union of the templates for the constituent ROIs. For example, the scene joint-ROI included constituent regions such as PPA and TOS (see Table 2.1 for a complete listing), and the scene template for the joint-ROI consisted of the constituent scene templates for PPA, TOS, and so forth. For each category, the joint-ROI category template was spatially correlated with the activity pattern in the joint-ROI on each resting frame to determine a distribution of correlation coefficients over frames for the category and joint-ROI (Fig. 2.3). For each subject and category, the upper 90% value (U90 value) of the distribution was then used as a summary measure of the relationship between the stimulus-evoked and resting patterns.

U90 values are sensitive to the mean, variance, and skewness of the underlying distribution of correlation coefficients. However, for all categories and ROIs, the distribution of correlation coefficients that defined the U90-value was symmetric and centered very near zero. Figure 2.4b shows the cumulative distribution for all subjects of spatial correlation coefficients

across resting frames in face, body, and scene joint-ROIs for coefficients that were computed using the prototype face, body, and scene templates and the prototype phase-scrambled template. The distributions for intact-stimulus and phase-scrambled stimuli were symmetric and centered on zero, but had different spreads. For the five joint-ROIs (Body, Face, Scene, Intact-Stimulus, Phase-Scrambled) and eight stimulus categories (faces, bodies, mammals, tools, chairs, scenes, phase-scrambled, and grid-scrambled) the largest group averaged value of the distribution mean across the forty distributions of correlation coefficients was 0.011. Consequently, differences in U90 values between categories essentially reflected differences in the variance of the distributions of coefficients. U90-value has an advantage in understanding the relationship between the stimulus-evoked and resting patterns since the value is the actual spatial correlation coefficient value between the stimulus-evoked and resting patterns. In the results below, a larger U90 value indicates the presence of larger positive matches and negative matches of the resting pattern to the category-evoked pattern, rather than the (positive) degree of similarity.

2.4.1 U90 values in joint-ROIs that prefer face, body, and scene categories

We conducted analyses that compared U90 values for a target category vs. other categories in individually-defined ROIs that preferred the target category, as determined by the localizer contrasts used to identify the ROIs. As an example, for the face target category preferred ROIs were defined from the localizer contrast face minus object. Instead of analyzing each ROI separately, we grouped each set of category-preferential ROIs for an individual into a single joint-ROI. We then correlated the category template with the activity pattern on each resting frame across the entire joint-ROI, and derived a single U90 value for the target-preferred joint-ROI. ROIs in early visual cortex, as defined using the Benson template for V1 – V3

(Benson et al. 2012), were not included in category-preferential joint-ROIs, similar to the exclusion in (Strappini et al. 2018).

Figure 2.4a shows the representational similarity matrix of measuring mean pattern similarity values among the all 8 categorical prototype templates across subjects in face, body, and scene joint-ROIs. The animate and inanimate representational hierarchical distinction (Kriegeskorte et al. 2008) was weakly depicted in Face- and Body-preferred joint-ROIs with stronger pattern similarities in animate categories. Table 2.2 shows the actual mean spatial correlation coefficients among face-, body-, and scene- prototype templates in face, body, and scene joint-ROIs.

Figure 2.4c shows U90 values for a joint-ROI's target category (green symbol), non-target intact-stimulus categories (red symbols), grid-scrambled category (blue symbol) and phase-scrambled category (gray symbol). Separate repeated measures analysis of variance (ANOVAs) for each joint-ROI with Category (8 levels) as a factor indicated a significant main effect of Category in all joint-ROIs (Face: $F(7,105)=3.33$, $p=0.003$; Body: $F(7,105)=6.02$, $p=6.56e-6$; Scene: $F(7,105)=6.36$, $p=3.04e-6$). The black symbols indicate significant differences in the U90 value for the joint-ROI's target category vs. each other category (paired t-tests; '+' = Bonferroni-corrected, $p<0.05$, '++' = Bonferroni-corrected, $p<0.005$, '*' = uncorrected, $p<0.05$).

Within the face joint-ROIs, U90 values were larger for the joint-ROI's target category than for inanimate categories (chair, tool, scene) as well as for grid-scrambled objects. Within the body joint-ROIs, U90 values were larger for the joint-ROI's target category than for inanimate categories (chair, tool, scene) as well as for grid- and phase-scrambled objects. Within the scene joint-ROI, U90 values were larger for scenes than for all other intact-stimulus categories as well as for grid- and phase-scrambled objects. These results demonstrate that in

higher-order visual regions that showed stimulus preferences for a particular category, U90 values significantly differed between categories in a manner that partly reflected the higher-order grouping of animate vs. inanimate categories (Kriegeskorte et al. 2008) as well as the distinction between intact and scrambled objects.

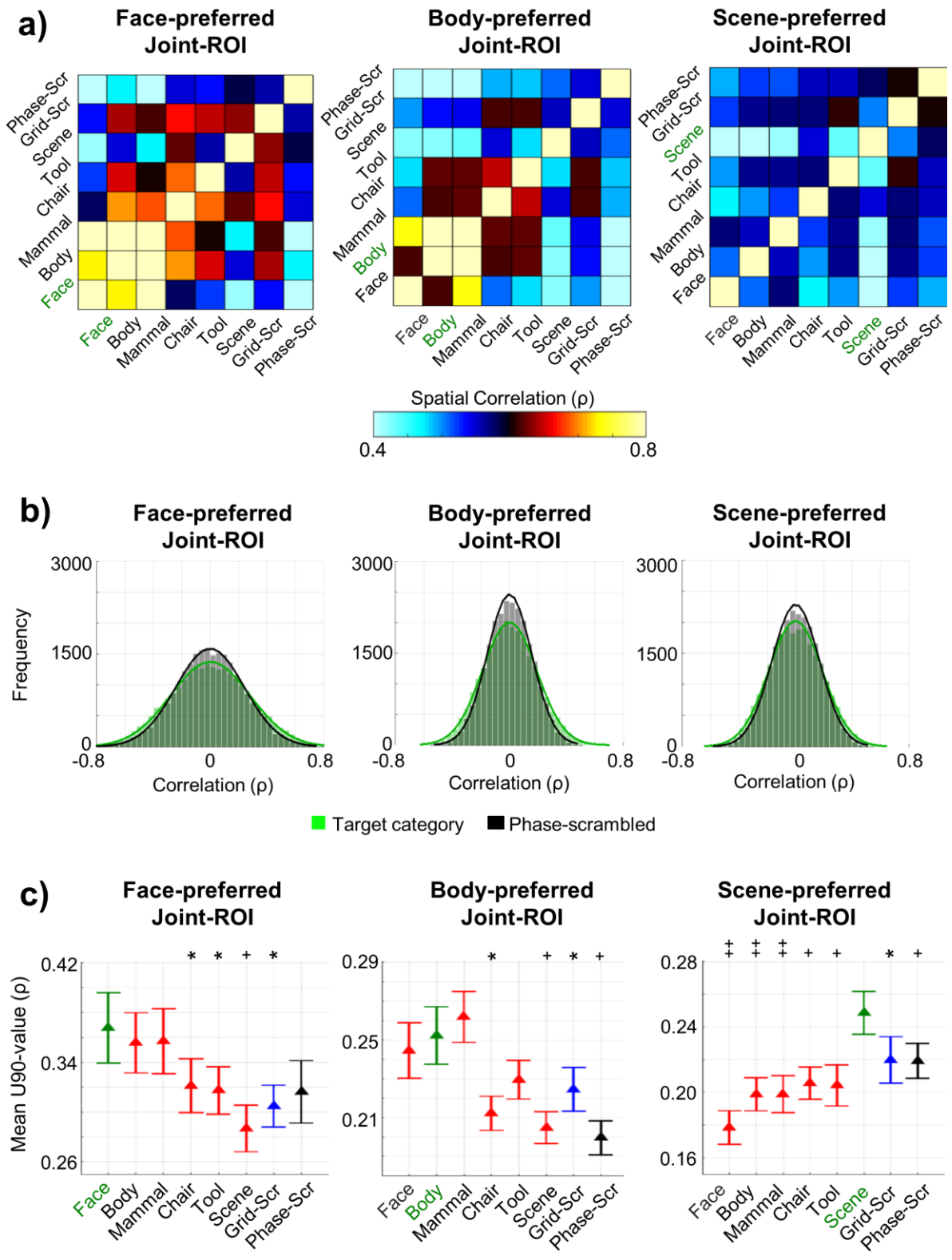

Figure 2.4. (a) Each graph shows representational similarity matrix across all 8 categorical prototype templates for a joint-ROI. **(b)** Each graph shows for a joint-ROI the superimposed distributions of

correlation coefficients between stimulus-evoked and resting activity patterns over frames for the joint-ROI's target category (light green; e.g. Face in the Face-preferred joint-ROI) and for the phase-scrambled category (gray). The stimulus-evoked template for a category corresponded to a 'prototype template' (procedure outlined in Fig. 2.3. Overlapping sections of the two distributions are shown in dark green. The green and black lines have been fit to the distributions for the target and phase-scrambled categories, respectively, using the MATLAB program function 'fitdist.m'. **(c)** Group-averaged U90 values for categories in preferred vs. non-preferred joint-ROIs. For each of three joint-ROIs, the graph plots U90 values for the joint-ROI's target category (green symbol; e.g. U90 values for the face joint-ROI), non-target intact-stimulus categories (red symbols), grid-scrambled category (blue symbol), and phase-scrambled category (gray symbol). Significance of a group paired t-test comparing the U90 values within the preferred joint-ROI for the target category vs each non-target category is indicated by black symbols (+ = Bonferroni-corrected p-val ≤ 0.05; ++ = Bonferroni-corrected p-val ≤ 0.005; * = uncorrected p-val ≤ 0.05).

Table 2.2. Mean spatial correlation coefficients among face-, body-, and scene- prototype templates in face, body, and scene joint-ROIs.

	Similarity (ρ) between Face-Template and Body-Template	Similarity (ρ) between Face-Template and Scene-Template	Similarity (ρ) between Body-Template and Scene-Template
Face Joint-ROI	0.729	0.415	0.550
Body Joint-ROI	0.618	0.421	0.423
Scene Joint-ROI	0.512	0.346	0.372

2.4.2 U90 values in joint-ROIs that prefer phase-scrambled or intact-stimulus images

The above analysis focused on joint-ROIs that showed preferential responses to faces, bodies, or scenes relative to chairs and tools. We also analyzed joint-ROIs in which stimulus-evoked responses were stronger or weaker for the union of the intact-stimulus categories face, body, scene, and object (chair+tools) vs. phase-scrambled stimuli. The resulting 'Intact-stimulus' joint-ROI was located in lateral and ventral visual cortex while the 'Phase-scrambled' joint-ROI was located in medial visual regions (Fig. 2.2).

Figure 2.5b shows that in the Intact-Stimulus joint-ROI, the mean U90 value was larger for intact-stimulus than phase-scrambled objects but not grid-scrambled objects, which contained visual features such as contours, line terminators and junctions. Therefore, when higher-level visual regions were not segregated by category preferences, resting activity did not necessarily differentiate between intact-stimuli objects and scrambled objects that included lower-level visual features. The reverse pattern was observed for the Phase-Scrambled joint-ROI, with higher U90 values for grid- and phase-scrambled objects than intact-stimulus objects.

Confirming the above observations, an ANOVA with ROI-type (Intact-Stimulus, Phase-Scrambled) and category (intact-stimulus, grid-scrambled, phase-scrambled) as factors yielded a significant main effect of Category ($F(2,30)=14.5$, $p=3.99e-5$) and a significant interaction of ROI-type by Category ($F(2,30)=11.5$, $p=0.0002$). A sub-ANOVA with ROI-type (Intact-Stimulus, Phase-Scrambled) and category (intact-stimulus, phase-scrambled) also yielded a significant interaction ($F(1,15)=13.9$, $p=0.002$), indicating that the critical interaction was not driven by the grid-scrambled objects.

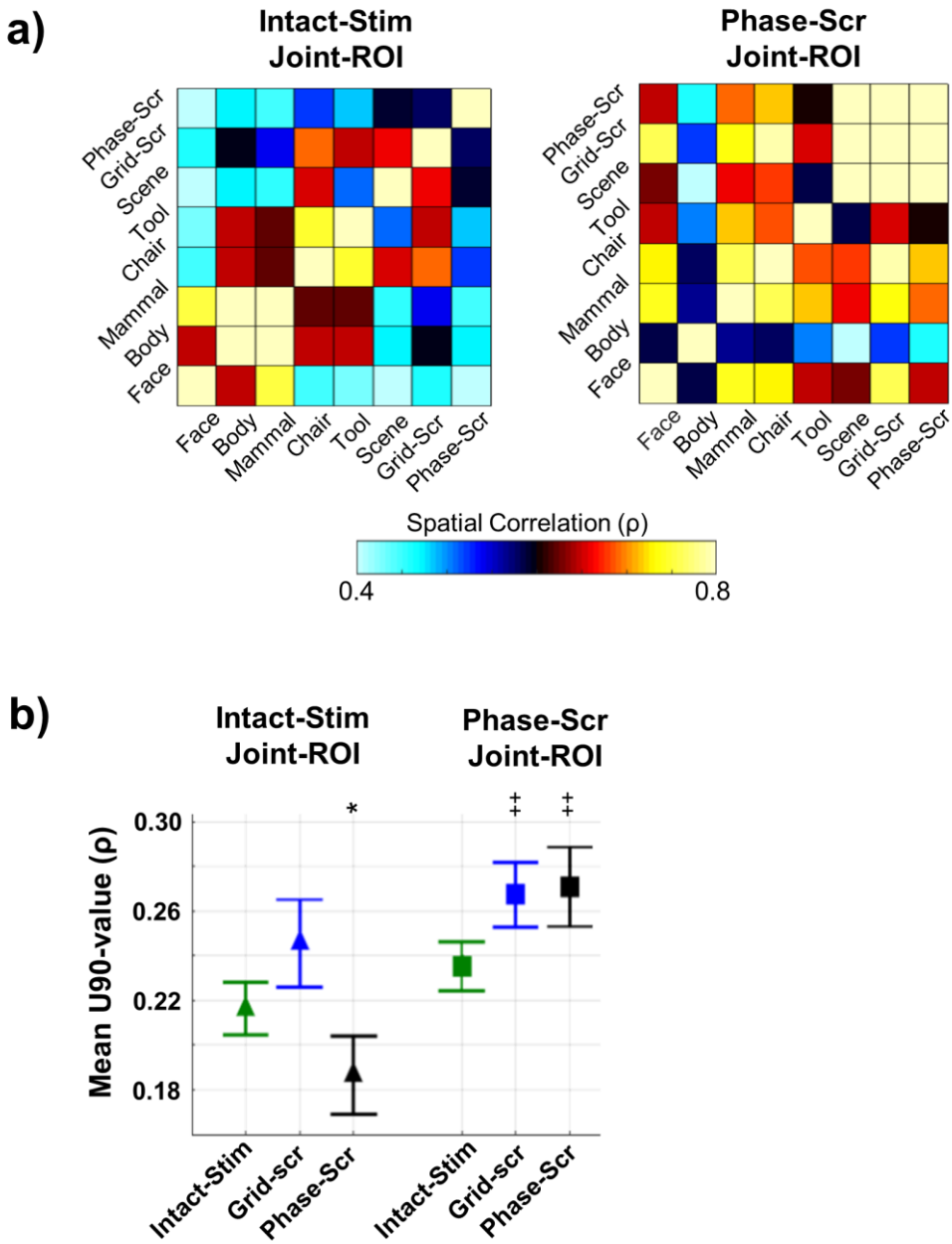

Figure 2.5. (a) Each graph shows representational similarity matrix across all 8 categorical prototype templates for a joint-ROI. **(b)** Group-averaged U90 values in Intact-stimulus and Phase-scrambled joint-ROIs are plotted for intact-stimulus, grid scrambled, and phase-scrambled categories. Black symbols indicate significant differences between the intact-stimulus category and each of the scrambled categories as determined by a group paired t-test (+ = Bonferroni-corrected p-val ≤ 0.05; ++ = Bonferroni-corrected p-val ≤ 0.005; * = uncorrected p-val ≤ 0.05).

2.4.3 U90 values correlate with activation strength

The previous analyses have shown that resting activity patterns showed higher U90 values for the patterns evoked by stimulus categories, whether scrambled or intact-stimulus, which best activated the corresponding joint-ROI. Figure 2.6 shows for Face, Body, Scene, Intact-stimulus, and Phase-scrambled joint-ROIs the mean activation strengths during the Task (first column) and Localizer (second column) scans for each category, as defined from the β weights for the category averaged over subjects and the vertices of each joint-ROI. The task β weights used for the activation strength computation were separately computed from spatially non-normalized task BOLD timeseries (see Methods). The activation strengths in both the Task and Localizer scans followed the general pattern expected from the Localizer contrasts used to define the joint-ROIs. Since the Task scans were independent of the Localizer scans, the presence of the expected pattern in those scans provided an independent confirmation of the suitability of the Localizer-defined regions.

To determine whether the U90 value for a category and joint-ROI was related to the category's activation strength, for each subject and each joint-ROI, we computed the correlation coefficient across categories between the U90-value computed from the resting frames and the activation strength in the task or the localizer conditions. The group average correlation coefficient between U90 values and activation strengths for each Joint-ROI is shown in Figure 2.6 (third column). Group one-sample t-tests indicated that the correlation coefficients were significant for both task and localizer scans in all Joint-ROIs. These results demonstrate that subjects showing a greater similarity between resting state and task patterns for different categories, i.e. larger U90 values for a category, also showed in general stronger task activation in the same ROI for that category. Hence, this result links category selective magnitude of

activation at the regional level, multivoxel category selective patterns of activation, and multivoxel patterns found at rest.

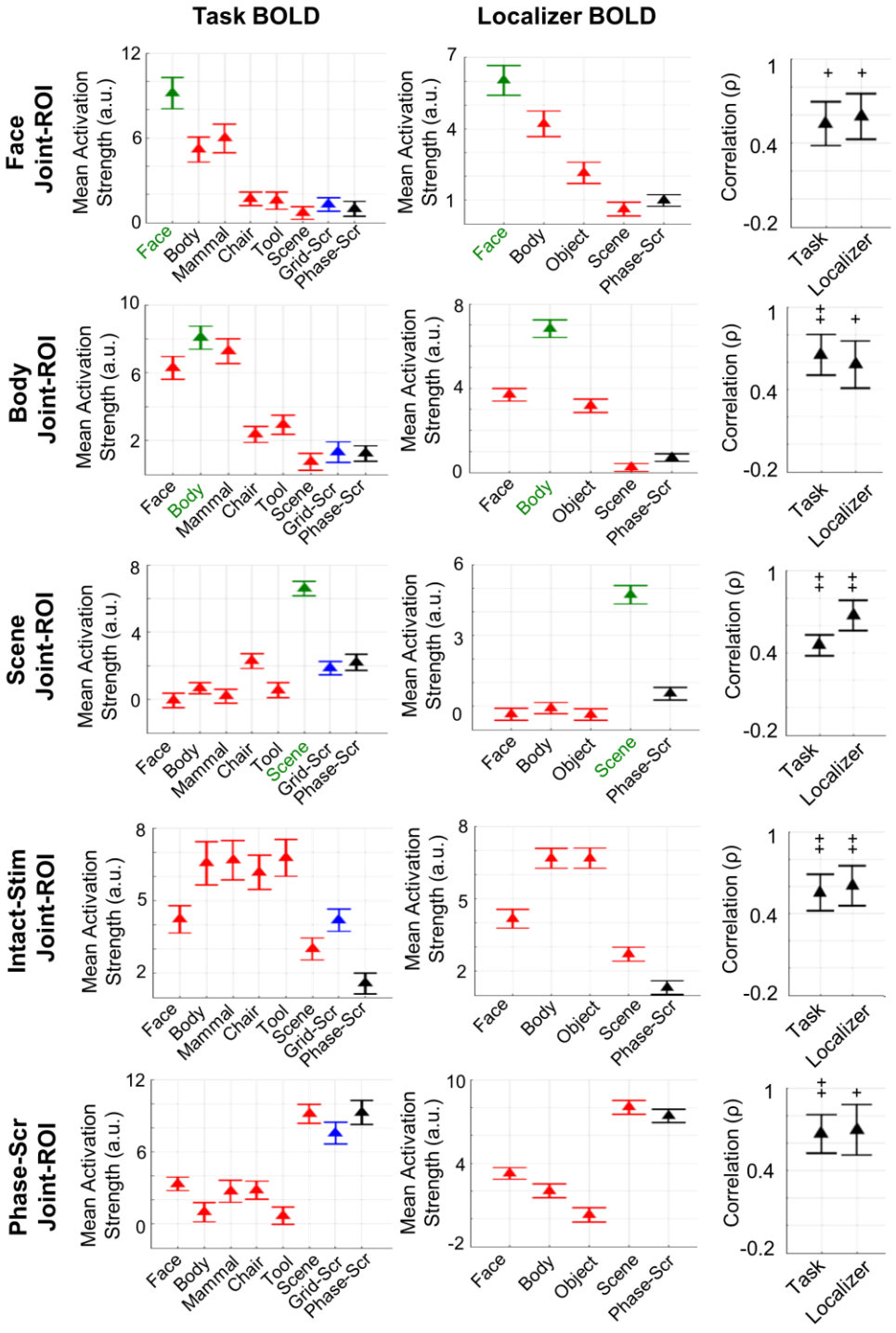

Figure 2.6. The correlation between U90 values and activation strengths. The mean activation strength in Face, Scene, Body, Intact-Stimulus, and Phase-Scrambled joint-ROIs from the task and localizer scans for

all stimulus categories are plotted for in the first and second columns, respectively. The correlation between activation strengths and U90 values across all categories is shown for both task and localizer scans in the third column. Black symbols indicate the significance of each correlation coefficient, as determined by a group 1-sample t-test (+ = Bonferroni-corrected p-val ≤ 0.05; ++ = Bonferroni-corrected p-val ≤ 0.005; * = uncorrected p-val ≤ 0.05)

2.5 Discussion

The goal of the experiment was to determine in regions of visual cortex the relationship between resting multi-vertex activity patterns and the multi-vertex patterns evoked by naturalistic and non-naturalistic visual stimuli. To this end, the multi-vertex patterns of the evoked BOLD activity from common ecological stimulus category objects and from corresponding control stimuli such as phase-scrambled and grid-scrambled objects were correlated with resting multi-vertex patterns in brain regions independently defined using standard localizers.

The overall result, discussed in more detail below, is that on average, resting activity patterns in regions of visual cortex were not more similar to the pattern evoked by one stimulus category as compared to another. However, the variability of resting state patterns in different category specific regions of visual cortex was more similar for preferred stimulus-evoked patterns. For instance, in regions tuned for faces, face specific multivoxel patterns were more likely to have a match in some resting frames than scene specific multivoxel patterns. Interestingly, the higher variance involved not only positive but also negative correlation values, as indexed by the U90 value (Fig. 2.4). Across subjects, the spread of match values was determined by how well a stimulus activated the region.

Therefore, the spatial pattern of resting activity in a distributed set of regions varied in time along an axis that was best aligned with the spatial pattern of the regions' preferred stimulus,

i.e. an axis with two endpoints, preferred- and not-preferred-stimulus values. In high-level visual regions showing categorical object preferences, U90 values were higher for the preferred object category (Fig. 2.4c). In regions of early visual cortex, which were more strongly activated by grid-scrambled or phase-scrambled objects than by real object categories (face, body, mammal, chair, tool, but not scene; Fig. 2.6), U90 values were greater for the scrambled control stimuli (Fig. 2.5). Therefore, also in early visual cortex that contains receptive fields tuned to lower visual properties (e.g. contrast, edges, orientation), the relationship between stimulus evoked patterns and resting state pattern variance was confirmed.

Overall, these results are consistent with a general framework in which resting multivoxel patterns of activity within a brain region are affected by the past history of activity patterns evoked by the external and internal environment (Fiser et al. 2010; Harmelech and Malach 2013). They also show that resting activity patterns can potentially serve a representational function by carrying information about high- and low-level visual features. Interestingly, the variability of resting frames matches stimulus-evoked patterns both in terms of positive and negative correlation, consistently with recent study showing that the variability of response tuning is an important property of control in cortex (Lin et al. 2015). A region's stimulus preference determines an axis along which the resting pattern maximally varies, and links the region's multi-vertex pattern to the multi-vertex patterns of regions that show similar preferences.

2.5.1 Low- and high-level visual correspondences at rest

Resting multivoxel patterns in visual areas were generally related to a region's stimulus preferences, i.e. the stimuli that optimally activated the region. In many higher-level visual ROIs (Fig. 2.4c), these preferences favored particular categories over other categories or corresponding

scrambled control categories. However, in early visual cortex, these preferences favored stimuli that emphasized low-level features (Fig. 2.5). Grid-scrambled stimuli likely included a higher density of contours and line terminators/connectors/junctions than the original naturalistic images, while phase-scrambled images contained dense textures. Both features were also present in scene images (e.g. heterogeneous arrays of multiple small objects, wheat fields, clouds). Correspondingly, in the scene joint-ROI, phase-scrambled and grid-scrambled objects showed relatively high U90 values with respect to most single-object categories (Fig. 2.4c).

The larger U90 values for scrambled control stimuli in early visual cortex do not contradict an overall framework in which resting activity patterns reflect the statistical distribution of features in the environment. Rather, this result suggests that resting activity patterns in regions that primarily extract low-level visual features are relatively independent of the patterns associated with higher-order features/statistics that define categorical objects. Therefore, the link between resting and evoked activity patterns can be driven by a variety of stimulus features that reflect local (e.g. contour-related features) or global (e.g. faces) stimulus characteristics depending on the tested region.

2.5.2 Resting activity as a context-independent prior

An important rationale for postulating a representational function of resting activity is that limits on the information processing capacity of the brain may be mitigated by the incorporation of useful prior information. Appropriate priors will generally depend on context and therefore will change dynamically. The perceptual priors appropriate to walking alone through a forest vs. eating a family meal at the dinner table are quite different. These putative

dynamic changes are thought to reflect generative models of the expected input via top-down pathways (Mumford 1992).

Resting scans are usually conducted under conditions in which subjects lie in a dark tube while fixating a cross in an otherwise blank display, which would not seem a fertile context for a perceptual prior. However, some aspects of an appropriate prior may not heavily depend on context. Under the hypothesis that stimulus tunings reflect the statistical distribution of features in the environment (Fiser et al. 2010), perhaps coupled with additional constraints such as sparsity (Olshausen and Field 1996), the activation pattern corresponding to a region's stimulus preference may serve as an appropriate context-independent prior for a region. In addition, utility might be maximized for a system by including category preferential areas that require less stimulus evidence to generate stimulus-evoked representations of biologically important categories. A category-appropriate resting pattern could provide an appropriate ongoing bias. However, in category-preferential regions we found increases in the variance but not the mean of the spatial match between resting and evoked activity.

An alternative hypothesis is that the increase in variation for a region along the preferred-stimulus/not-preferred-stimulus pattern axis is related to the critical dynamics of the region. Criticality refers to a state whose dynamics enables a transition to a different state(s) in response to a small perturbation, as in a phase transition. Prior studies have suggested that resting activity conforms to critical states that are easily perturbed by stimulus or task inputs (Deco and Jirsa 2012; Tagliazucchi et al. 2012; Chialvo 2010). The alignment of spatial resting patterns along the preferred stimulus/not preferred stimulus axis for a region, coupled with criticality, may better enable departures from the resting state along that axis and lead to better or faster discrimination along that axis. The axis itself may be determined by the joint influences of structural

connectivity and resting functional connectivity (FC). Category specific activations are related to distinct structural connectivity fingerprints (Saygin et al. 2011; Osher et al. 2016), while recent studies have demonstrated mappings between resting FC and voxelwise activation patterns (Cole et al. 2016; Tavor et al. 2016). Resting FC is influenced not only by structural connectivity (Honey et al. 2009) but also by prior experience (Albert et al. 2009; Hasson et al. 2009; Lewis et al. 2009; Tambini et al. 2010), the latter effect thought to be mediated by changes in synaptic weightings.

The description of the poles of the axis of maximal variation in resting activity patterns as preferred-stimulus and not-preferred-stimulus is one of several possible interpretations. For example, van Loon and colleagues (van Loon et al. 2018) studied multivoxel patterns in a region of posterior fusiform cortex that was activated during visual search tasks. Subjects searched through two successive displays, where the target object for the search through each display was different. When subjects searched through the first display, the target objects for both the first and second displays could be decoded. However, the pattern that drove decoding of the second target object was the negative of the pattern that drove decoding of the same object when it served as the first target object. The authors concluded that positive and negative poles of the spatial pattern axis corresponded to current vs prospective working memory representations. Therefore, opposing spatial activity patterns may reflect a variety of functional codes.

2.5.3 Comparison with animal studies

The present work was motivated by the pioneering studies of Grindvald, Arieli, and colleagues (Arieli et al. 1996; Tsodyks et al. 1999; Kenet et al. 2003), who used optical imaging in anaesthetized cats to show that activity patterns in V1 evoked by oriented gratings spatially

matched patterns of spontaneous activity (Kenet et al. 2003). This work was recently extended to monkey by Omer and colleagues (Omer et al. 2018), who correlated spontaneous activity patterns with the differential activity pattern evoked by orthogonally oriented gratings, and compared the resulting distribution of correlation coefficients to a control distribution.

In anaesthetized monkeys, both distributions were centered on zero and the stimulus-evoked distribution had larger positive and negative tails. Presumably, the symmetric distribution reflected the columnar organization of orientation selectivity, since orthogonal gratings would activate disjoint columns. Therefore, the differential spread of the two distributions reflected the similarity of resting and stimulus-evoked patterns. Interestingly, awake monkeys showed evoked and control distributions that completely overlapped, although the authors indicated that FC analyses demonstrated a similar match of resting and evoked pattern but on a smaller spatial scale and faster timescale.

In the present work, the distributions of correlation coefficients used to compute U90 values were symmetric about zero and had larger tails for preferred than non-preferred stimulus categories. However, the results in anaesthetized monkey V1 and awake human visual cortex are not comparable. The underlying columnar architecture in the joint-ROIs is unknown, the evoked template in the current work was not formed from a contrast of orthogonal exemplars, and BOLD activity was not sampled at an analogous spatial or temporal scale.

2.5.4 Limitations

Stimuli were not controlled for low-level variables that might have differentially activated visual regions. As noted, grid-scrambled stimuli may have included contour terminators to a greater extent than single-object stimuli, increasing the activation of early visual

cortex. However, this supposition is only speculative since this factor was not explicitly controlled or manipulated.

Additionally, the naturalistic stimuli of the present study were presented in a decidedly non-naturalistic context. Wilf et al. (Wilf et al. 2017) have shown that in early visual cortex, resting FC patterns are better accounted for by movies than by standard retinotopic stimuli, while Strappini et al. (Strappini et al. 2018) have shown that in higher-level visual cortex, resting FC patterns are better accounted for by movies than by static pictures of objects similar to those used here. Therefore, the present results may underestimate the spatial correspondences between resting and evoked activity patterns.

2.6 References

Albert NB, Robertson EM, Miall RC. 2009. The resting human brain and motor learning. Curr Biol. 19:1023-1027.

Arcaro MJ, Honey CJ, Mruczek RE, Kastner S, Hasson U. 2015. Widespread correlation patterns of fMRI signal across visual cortex reflect eccentricity organization. eLife. 4.

Arieli A, Sterkin A, Grinvald A, Aertsen A. 1996. Dynamics of ongoing activity: explanation of the large variability in evoked cortical responses. Science. 273:1868-1871.

Baldassarre A, Lewis CM, Committeri G, Snyder AZ, Romani GL, Corbetta M. 2012. Individual variability in functional connectivity predicts performance of a perceptual task. Proc Natl Acad Sci U S A. 109:3516-3521.

Benson NC, Butt OH, Datta R, Radoeva PD, Brainard DH, Aguirre GK. 2012. The retinotopic organization of striate cortex is well predicted by surface topology. Curr Biol. 22:2081-2085.

Binder JR, Medler DA, Westbury CF, Liebenthal E, Buchanan L. 2006. Tuning of the human left fusiform gyrus to sublexical orthographic structure. Neuroimage. 33:739-748.

Biswal B, Yetkin FZ, Haughton VM, Hyde JS. 1995. Functional connectivity in the motor cortex of resting human brain using echo-planar MRI. Magnetic resonance in medicine. 34:537-541.

Bracci S, Op de Beeck H. 2016. Dissociations and Associations between Shape and Category Representations in the Two Visual Pathways. J Neurosci. 36:432-444.

Brainard DH. 1997. The Psychophysics Toolbox. Spatial vision. 10(4):433-6.

Chao LL, Haxby JV, Martin A. 1999. Attribute-based neural substrates in temporal cortex for perceiving and knowing about objects. Nat Neurosci. 2:913-919.

Chen RH, Ito T, Kulkarni KR, Cole MW. 2018. The Human Brain Traverses a Common Activation-Pattern State Space Across Task and Rest. Brain Connect.

Chialvo D. 2010. Emergent complex neural dynamics. Nature Physics. 6:744–750.

Cohen L, Dehaene S, Naccache L, Lehericy S, Dehaene-Lambertz G, Henaff MA, Michel F. 2000. The visual word form area: spatial and temporal characterization of an initial stage of reading in normal subjects and posterior split-brain patients. Brain. 123 (Pt 2):291-307.

Cole MW, Bassett DS, Power JD, Braver TS, Petersen SE. 2014. Intrinsic and task-evoked network architectures of the human brain. Neuron. 83:238-251.

Cole MW, Ito T, Bassett DS, Schultz DH. 2016. Activity flow over resting-state networks shapes cognitive task activations. Nat Neurosci. 19:1718-1726.

Dale AM. 1999. Optimal experimental design for event-related fMRI. Hum Brain Mapp. 8:109-114.

de Pasquale F, Della Penna S, Snyder AZ, Lewis C, Mantini D, Marzetti L, Belardinelli P, Ciancetta L, Pizzella V, Romani GL, Corbetta M. 2010. Temporal dynamics of spontaneous MEG activity in brain networks. Proc Natl Acad Sci U S A. 107:6040-6045.

Deco G, Jirsa VK. 2012. Ongoing cortical activity at rest: criticality, multistability, and ghost attractors. J Neurosci. 32:3366-3375.

Dehaene S, Jobert A, Naccache L, Ciuciu P, Poline JB, Le Bihan D, Cohen L. 2004. Letter binding and invariant recognition of masked words: behavioral and neuroimaging evidence. Psychological science. 15:307-313.

Downing PE, Chan AW, Peelen MV, Dodds CM, Kanwisher N. 2006. Domain specificity in visual cortex. Cereb Cortex. 16:1453-1461.

Fischl B, Sereno MI, Tootell RB, Dale AM. 1999. High-resolution intersubject averaging and a coordinate system for the cortical surface. Hum Brain Mapp. 8:272-284.

Fiser J, Berkes P, Orban G, Lengyel M. 2010. Statistically optimal perception and learning: from behavior to neural representations. Trends Cogn Sci. 14:119-130.

Fiser J, Chiu C, Weliky M. 2004. Small modulation of ongoing cortical dynamics by sensory input during natural vision. Nature. 431:573-578.

Fox MD, Corbetta M, Snyder AZ, Vincent JL, Raichle ME. 2006. Spontaneous neuronal activity distinguishes human dorsal and ventral attention systems. Proc Natl Acad Sci U S A. 103:10046-10051.

Fox MD, Snyder AZ, Vincent JL, Corbetta M, Van Essen DC, Raichle ME. 2005. The human brain is intrinsically organized into dynamic, anticorrelated functional networks. Proc Natl Acad Sci U S A. 102:9673-9678.

Fox MD, Snyder AZ, Vincent JL, Raichle ME. 2007. Intrinsic fluctuations within cortical systems account for intertrial variability in human behavior. Neuron. 56:171-184.

Gao LL, Wu T. 2016. The study of brain functional connectivity in Parkinson's disease. Translational neurodegeneration. 5:18.

Glasser MF, Sotiropoulos SN, Wilson JA, Coalson TS, Fischl B, Andersson JL, Xu J, Jbabdi S, Webster M, Polimeni JR, Van Essen DC, Jenkinson M. 2013. The minimal preprocessing pipelines for the Human Connectome Project. Neuroimage. 80:105-124.

Gordon EM, Laumann TO, Gilmore AW, Newbold DJ, Greene DJ, Berg JJ, Ortega M, Hoyt-Drazen C, Gratton C, Sun H, et al. 2017. Precision Functional Mapping of Individual Human Brains. Neuron. 95:791-807.e797.

Gratton C, Laumann TO, Nielsen AN, Greene DJ, Gordon EM, Gilmore AW, Nelson SM, Coalson RS, Snyder AZ, Schlaggar BL, et al. 2018. Functional Brain Networks Are Dominated by Stable Group and Individual Factors, Not Cognitive or Daily Variation. Neuron. 98:439-452.e435.

Greenberg AS, Esterman M, Wilson D, Serences JT, Yantis S. 2010. Control of spatial and feature-based attention in frontoparietal cortex. J Neurosci. 30:14330-14339.

Greicius MD, Krasnow B, Reiss AL, Menon V. 2003. Functional connectivity in the resting brain: a nework analysis of the default mode hypothesis. Proc Natl Acad Sci U S A. 100:253-258.

Harmelech T, Malach R. 2013. Neurocognitive biases and the patterns of spontaneous correlations in the human cortex. Trends Cogn Sci. 17:606-615.

Hasson U, Nusbaum HC, Small SL. 2009. Task-dependent organization of brain regions active during rest. Proc Natl Acad Sci U S A. 106:10841-10846.

Haxby JV, Gobbini MI, Furey ML, Ishai A, Schouten JL, Pietrini P. 2001. Distributed and overlapping representations of faces and objects in ventral temporal cortex. Science. 293:2425-2430.

Haynes JD, Rees G. 2005. Predicting the orientation of invisible stimuli from activity in human primary visual cortex. Nature neuroscience. 8:686-691.

He BJ, Snyder AZ, Vincent JL, Epstein A, Shulman GL, Corbetta M. 2007. Breakdown of functional connectivity in frontoparietal networks underlies behavioral deficits in spatial neglect. Neuron. 53:905-918.

He BJ, Snyder AZ, Zempel JM, Smyth MD, Raichle ME. 2008. Electrophysiological correlates of the brain's intrinsic large-scale functional architecture. Proc Natl Acad Sci U S A. 105:16039-16044.

Heinzle J, Kahnt T, Haynes JD. 2011. Topographically specific functional connectivity between visual field maps in the human brain. Neuroimage. 56:1426-1436.

Honey CJ, Sporns O, Cammoun L, Gigandet X, Thiran JP, Meuli R, Hagmann P. 2009. Predicting human resting-state functional connectivity from structural connectivity. Proc Natl Acad Sci U S A. 106:2035-2040.

Ingram JN, Kording KP, Howard IS, Wolpert DM. 2008. The statistics of natural hand movements. Exp Brain Res. 188:223-236.

Kamitani Y, Tong F. 2005. Decoding the visual and subjective contents of the human brain. Nature neuroscience. 8:679-685.

Kenet T, Bibitchkov D, Tsodyks M, Grinvald A, Arieli A. 2003. Spontaneously emerging cortical representations of visual attributes. Nature. 425(6961):954-956.

Kim D, Kay K, Shulman GL, Corbetta M. 2018. A New Modular Brain Organization of the BOLD Signal during Natural Vision. Cereb Cortex. 28(9):3065-3081.

Kriegeskorte N, Formisano E, Sorger B, Goebel R. 2007. Individual faces elicit distinct response patterns in human anterior temporal cortex. Proc Natl Acad Sci U S A. 104:20600-20605.

Kriegeskorte N, Goebel R, Bandettini P. 2006. Information-based functional brain mapping. Proc Natl Acad Sci U S A. 103:3863-3868.

Kriegeskorte N, Mur M, Ruff DA, Kiani R, Bodurka J, Esteky H, Tanaka K, Bandettini PA. 2008. Matching categorical object representations in inferior temporal cortex of man and monkey. Neuron. 60:1126-1141.

Kuhl BA, Chun MM. 2014. Successful remembering elicits event-specific activity patterns in lateral parietal cortex. J Neurosci. 34:8051-8060.

Laumann TO, Gordon EM, Adeyemo B, Snyder AZ, Joo SJ, Chen MY, Gilmore AW, McDermott KB, Nelson SM, Dosenbach NU, Schlaggar BL, Mumford JA, Poldrack RA, Petersen SE. 2015. Functional System and Areal Organization of a Highly Sampled Individual Human Brain. Neuron. 87:657-670.

Leo A, Handjaras G, Bianchi M, Marino H, Gabiccini M, Guidi A, Scilingo EP, Pietrini P, Bicchi A, Santello M, Ricciardi E. 2016. A synergy-based hand control is encoded in human motor cortical areas. eLife. 5.

Lewis CM, Baldassarre A, Committeri G, Romani GL, Corbetta M. 2009. Learning sculpts the spontaneous activity of the resting human brain. Proc Natl Acad Sci U S A. 106:17558-17563.

Lin IC, Okun M, Carandini M, Harris KD. 2015. The Nature of Shared Cortical Variability. Neuron. 87(3):644-56.

Logan GD. 2002. An instance theory of attention and memory. Psychol Rev. 109:376-400.

Martin A, Wiggs CL, Ungerleider LG, Haxby JV. 1996. Neural correlates of category-specific knowledge. Nature. 379:649-652.

Mumford D. 1992. On the computational architecture of the neocortex. II. The role of cortico-cortical loops. Biological cybernetics. 66:241-251.

Nestor A, Plaut DC, Behrmann M. 2011. Unraveling the distributed neural code of facial identity through spatiotemporal pattern analysis. Proc Natl Acad Sci U S A. 108:9998-10003.

Nir Y, Hasson U, Levy I, Yeshurun Y, Malach R. 2006. Widespread functional connectivity and fMRI fluctuations in human visual cortex in the absence of visual stimulation. Neuroimage. 30:1313-1324.

Nosofsky RM. 1986. Attention, similarity, and the identification-categorization relationship. Journal of experimental psychology General. 115:39-61.

Olshausen BA, Field DJ. 1996. Emergence of simple-cell receptive field properties by learning a sparse code for natural images. Nature. 381:607-609.

Omer DB, Fekete T, Ulchin Y, Hildesheim R, Grinvald A. 2018. Dynamic Patterns of Spontaneous Ongoing Activity in the Visual Cortex of Anesthetized and Awake Monkeys are Different. Cereb Cortex.

Oosterhof NN, Tipper SP, Downing PE. 2012. Viewpoint (in)dependence of action representations: an MVPA study. J Cogn Neurosci. 24:975-989.

Osher DE, Saxe RR, Koldewyn K, Gabrieli JD, Kanwisher N, Saygin ZM. 2016. Structural Connectivity Fingerprints Predict Cortical Selectivity for Multiple Visual Categories across Cortex. Cereb Cortex. 26:1668-1683.

Posner MI, Keele SW. 1968. On the genesis of abstract ideas. Journal of Experimental Psychology. 77:353-363.

Power JD, Cohen AL, Nelson SM, Wig GS, Barnes KA, Church JA, Vogel AC, Laumann TO, Miezin FM, Schlaggar BL, Petersen SE. 2011. Functional network organization of the human brain. Neuron. 72:665-678.

Raemaekers M, Schellekens W, van Wezel RJ, Petridou N, Kristo G, Ramsey NF. 2014. Patterns of resting state connectivity in human primary visual cortical areas: A 7T fMRI study. Neuroimage. 84:911-921.

Santello M, Baud-Bovy G, Jorntell H. 2013. Neural bases of hand synergies. Front Comput Neurosci. 7:23.

Santello M, Flanders M, Soechting JF. 1998. Postural hand synergies for tool use. J Neurosci. 18:10105-10115.

Saygin ZM, Osher DE, Koldewyn K, Reynolds G, Gabrieli JD, Saxe RR. 2011. Anatomical connectivity patterns predict face selectivity in the fusiform gyrus. Nature neuroscience. 15:321-327.

Schieber MH, Santello M. 2004. Hand function: peripheral and central constraints on performance. J Appl Physiol (1985). 96(6):2293-2300.

Serences JT, Boynton GM. 2007. Feature-based attentional modulations in the absence of direct visual stimulation. Neuron. 55:301-312.

Sha L, Haxby JV, Abdi H, Guntupalli JS, Oosterhof NN, Halchenko YO, Connolly AC. 2015. The animacy continuum in the human ventral vision pathway. J Cogn Neurosci. 27:665-678.

Shadlen MN, Newsome WT. 1994. Noise, neural codes and cortical organization. Curr Opin Neurobiol. 4:569-579.

Sharp DJ, Scott G, Leech R. 2014. Network dysfunction after traumatic brain injury. Nature reviews Neurology. 10:156-166.

Sheline YI, Raichle ME. 2013. Resting state functional connectivity in preclinical Alzheimer's disease. Biol Psychiatry. 74:340-347.

Siegel JS, Ramsey LE, Snyder AZ, Metcalf NV, Chacko RV, Weinberger K, Baldassarre A, Hacker CD, Shulman GL, Corbetta M. 2016. Disruptions of network connectivity predict impairment in multiple behavioral domains after stroke. Proc Natl Acad Sci U S A.

Smith SM, Fox PT, Miller KL, Glahn DC, Fox PM, Mackay CE, Filippini N, Watkins KE, Toro R, Laird AR, Beckmann CF. 2009. Correspondence of the brain's functional architecture during activation and rest. Proc Natl Acad Sci U S A. 106:13040-13045.

Strappini F, Wilf M, Karp O, Goldberg H, Harel M, Furman-Haran E, Golan T, Malach R. 2018. Resting-State Activity in High-Order Visual Areas as a Window into Natural Human Brain Activations. Cereb Cortex.

Tagliazucchi E, Balenzuela P, Fraiman D, Chialvo DR. 2012. Criticality in large-scale brain FMRI dynamics unveiled by a novel point process analysis. Frontiers in physiology. 3:15.

Tambini A, Ketz N, Davachi L. 2010. Enhanced brain correlations during rest are related to memory for recent experiences. Neuron. 65:280-290.

Tavor I, Parker Jones O, Mars RB, Smith SM, Behrens TE, Jbabdi S. 2016. Task-free MRI predicts individual differences in brain activity during task performance. Science. 352:216-220.

Tsodyks M, Kenet T, Grinvald A, Arieli A. 1999. Linking spontaneous activity of single cortical neurons and the underlying functional architecture. Science. 286:1943-1946.

Van Essen DC, Drury HA, Dickson J, Harwell J, Hanlon D, Anderson CH. 2001. An integrated software suite for surface-based analyses of cerebral cortex. J Am Med Inform Assoc. 8(5):443-59.

van Loon AM, Olmos-Solis K, Fahrenfort JJ, Olivers CN. 2018. Current and future goals are represented in opposite patterns in object-selective cortex. eLife. 7.

Vinckier F, Dehaene S, Jobert A, Dubus JP, Sigman M, Cohen L. 2007. Hierarchical coding of letter strings in the ventral stream: dissecting the inner organization of the visual word-form system. Neuron. 55:143-156.

Watson DM, Hymers M, Hartley T, Andrews TJ. 2016. Patterns of neural response in scene-selective regions of the human brain are affected by low-level manipulations of spatial frequency. Neuroimage. 124:107-117.

Wilf M, Strappini F, Golan T, Hahamy A, Harel M, Malach R. 2017. Spontaneously Emerging Patterns in Human Visual Cortex Reflect Responses to Naturalistic Sensory Stimuli. Cereb Cortex. 27:750-763.

Wurm MF, Ariani G, Greenlee MW, Lingnau A. 2016. Decoding Concrete and Abstract Action Representations During Explicit and Implicit Conceptual Processing. Cereb Cortex. 26:3390-3401.

Yeo BT, Krienen FM, Sepulcre J, Sabuncu MR, Lashkari D, Hollinshead M, Roffman JL, Smoller JW, Zollei L, Polimeni JR, Fischl B, Liu H, Buckner RL. 2011. The organization of the human cerebral cortex estimated by intrinsic functional connectivity. J Neurophysiol. 106:1125-1165.

Zhang H, Tian J, Liu J, Li J, Lee K. 2009. Intrinsically organized network for face perception during the resting state. Neuroscience letters. 454:1-5.

Zhu Q, Zhang J, Luo YL, Dilks DD, Liu J. 2011. Resting-State Neural Activity across Face-Selective Cortical Regions Is Behaviorally Relevant. J Neurosci. 31:10323-10330.

Chapter 3: Functional connectivity based on temporal task-to-rest activity pattern correspondences

3.1 Abstract

Studies of functional connectivity (FC) of spontaneous activity have yielded important insights into the network organization of the human brain. However, there is no consensus on the mechanisms underlying functional connectivity. Here we used multivoxel pattern analysis to determine if resting FC in high-level visual cortex is modulated by the putative representational content of spontaneous activity. Sixteen participants received resting-state scans, localizer scans to identify cortical regions showing stimulus preferences for bodies and scenes, and task scans to determine the multivoxel patterns or templates in those regions evoked by body and scene images. On each resting state frame, the stimulus-evoked body and scene templates were spatially correlated with the resting multivoxel pattern in each body and scene ROI, frame-by-frame, yielding a time course of the correlation between stimulus template and resting activity. Next, the timeseries associated with a template was then correlated over all scene and body ROIs, yielding a pattern-based resting FC matrix for each stimulus category. Resting spatial activity patterns showed correlated fluctuations across the category specific ROIs that were significantly larger for the ROIs preferred than non-preferred category. For instance, stronger pattern-based resting FC was found in PPA, RSC, and TOS (scene specific regions) for scene template-rest correlation timeseries than body template-rest correlation timeseries.

We conclude that in human visual cortex fluctuations of spontaneous activity, at the level of multi-voxel patterns, are linked to stimulus-evoked patterns.

3.2 Introduction

The task-evoked neural activity that ultimately results in behavior is generated in the context of ongoing, spontaneous activity. Many studies have detailed the spatiotemporal organization of spontaneous activity and considered the possible variables linking spontaneous and task-evoked activity. One explanation for the similarity of task and spontaneous activity is the underlying structural connectivity (Vincent et al. 2007). In whole brain models of spontaneous activity, structural connections and noise account at the group level for about ½ of the spatial correlation (Deco et al. 2011). However, the similarity between task and rest is much stronger during anesthesia, and significantly decreases in the awake state (Barttfeld et al. 2015). Another explanation is that the similarity of spontaneous activity and task-evoked activity comes from the statistical history of co-activation. In the course of development and personal history may affect the organization of spontaneous activity through Hebbian learning (Lewis et al. 2009). Conversely the spatiotemporal organization of spontaneous activity may constrain the activity evoked by a task, predicting whole brain patterns or even topographic individual variations (Cole et al. 2016; Tavor et al. 2016). This reciprocal relationship between spontaneous and task-evoked activity may form a closed loop cycle (Lewis et al. 2009; Kim et al. 2018) through statistical learning and Bayesian prediction.

However, common spatiotemporal patterns may simply reflect common patterns of inter-regional synchronization, as task patterns may be clocked on spontaneous cycles of excitability as in the communication through Coherence hypothesis (Fries P. 2005).

A related, but also different conceptualization is that spontaneous and task-evoked activity share information states (Fiser et al. 2004; Fiser et al. 2010; Harmelech and Malach 2013). An organism's long-term history of task-evoked activity not only shapes the way

networks remain correlated at rest, but also sculpt the distribution of synaptic weights that code for information. Therefore, spontaneous activity may not only represent fluctuations of excitability within/between regions, but also fluctuations of information states that may form the repertoire of available states in cortex at that moment. For distributed coding of semantic information in cortex see Huth et al. (Huth et al. 2012).

This hypothesis about spontaneous activity function may be defined 'representational', insofar patterns of spontaneous activity code for or maintain information about stimuli, responses, etc. There is some support for this hypothesis. Studies in early visual cortex have shown that resting FC is partly organized according to retinotopy (Heinzle et al. 2011; Raemaekers et al. 2014; Arcaro et al. 2015). This has been also shown with local field potentials in monkey visual cortex (Lewis et al. 2016). A retinotopic organization of FC may be consistent with the underlying structural connectivity, as foveal regions in V1 tend to be more strongly connected to foveal regions in V2-V3; the same with more peripheral representation in V1-V3 (Nakamura et al. 1993). There is also evidence that FC variance is better explained by the presentation of real movies than artificial stimuli such as gratings (Wilf et al. 2017). These findings in humans are similar to observations in macaque in which the mean and variance of spontaneous activity was similar to task evoked activity, but more for natural stimuli than synthetic stimuli (Fiser et al. 2004). Similarly, the tuning functions in adult ferret of spontaneous active are much more similar to natural stimuli than artificial ones (Berkes et al. 2011). Also, face-preferential regions show stronger resting FC (Zhu et al. 2011; Nir et al. 2006; Zhang et al. 2009), as compared to regions that do not share the same stimulus selectivity. Finally, the topography of task activation data sets, which mediate behavioral tasks, strongly resemble resting state correlation patterns, or combination thereof (Smith et al. 2009; Power et al. 2011;

Yeo et al. 2011; Laumann et al. 2015; Cole et al. 2016; Gordon et al. 2017; Gratton et al. 2018). However, there are also significant differences as documented in several studies (e.g. Kim et al. 2018).

A more direct testing of the representation hypothesis would be to show that FC patterns code for information states. Information states would be represented, based on multivariate task activation in multi-voxel (multi-vertex in the case of surface analysis) patterns that would occur simultaneously in different functionally related regions. These patterns could be analyzed in a static fashion averaging over time, or dynamically.

Task fMRI has shown that multivoxel patterns within a region or piece of cortex carry important information about stimulus categories, retrieved memories, or cognitive processes such as attention, and can be modulated by learning (Haxby et al. 2001; Haynes and Rees 2005; Kamitani and Tong 2005; Kriegeskorte et al. 2006; Serences and Boynton 2007; Kriegeskorte et al. 2008; Greenberg et al. 2010; Kuhl and Chun 2014). In Chapter 2 we have shown that multi-vertex patterns of spontaneous activity in human visual cortex resemble stimulus-evoked patterns for different categories, and, that these spontaneous patterns are both regional and stimulus specific, as they occur more frequently for a specific stimulus feature in those regions that are specialized (based on localizer or task scans) for that feature.

One important issue is whether across regions in visual cortex, a specific category specific state will occur mainly in functionally specialized regions for that category, or whether it will be distributed across visual cortex. Furthermore, in dynamic terms it is not yet clear whether specific categorical states occur simultaneously in visual cortex, or are somehow temporally segregated.

To test the hypothesis that FC carries information about stimulus category, we adopt recent developments in which the FC organization of regions construed based on the temporal correlation of spatial activity patterns, rather than voxel- or vertice-averaged magnitudes (Coutanche and Thompson-Schill, 2013; Chen et al. 2018).

Furthermore, to test whether categorical states at rest occur locally in functionally specialized regions or more widely in visual cortex, and whether they co-occur or segregate in time, we examined correlations over time in the spatial component of resting activity that corresponds to the representational pattern associated with a stimulus category (pattern-based FC). This analysis determined whether at rest, putative representational multivoxel patterns for a stimulus category (e.g. bodies) fluctuated coherently across regions and whether the representational patterns for different stimulus categories (e.g. bodies and scenes) fluctuated independently in time.

3.3 Methods

The following analysis throughout the Chapter 3 uses exact same dataset analyzed in the previous Chapter 2. The basic experimental setups (e.g. participant information. stimuli, scanning procedure, imaging parameters, fMRI pre-processing, and defining ROIs from localizer activation contrasts) are identical and written in details in Chapter 2 *Method* section.

3.3.1 Regions of Interests

For the following pattern-based FC analysis, we used constituent ROIs from the joint-ROIs analyzed in previous study (Chapter 2). Joint-ROIs of Face-, Body-, and Scene-preferential localizer activation were generated by combining multiple local responsive constituent ROIs (2

ROIs for Face, 5 ROIs for Body, and 7 ROIs for Scene) in visual cortex outside of early visual cortex (V1-V3) estimated by Benson template (Benson et al. 2012). Since only two face constituent ROI exists and one of the ROIs largely overlapped with a Body ROI in ventral temporal cortex, Face ROIs were not included in the current study. We used total of 12 ROIs: 5 from the Body joint-ROI and 7 from the Scene Joint-ROI (see Fig. 3.1b for a schematic view of the ROIs and Table 3.1 for information on each ROI). To remove differences in BOLD magnitude across MR frames, for each ROI a z-normalization was applied across the vertices of each frame of the resting and task scans.

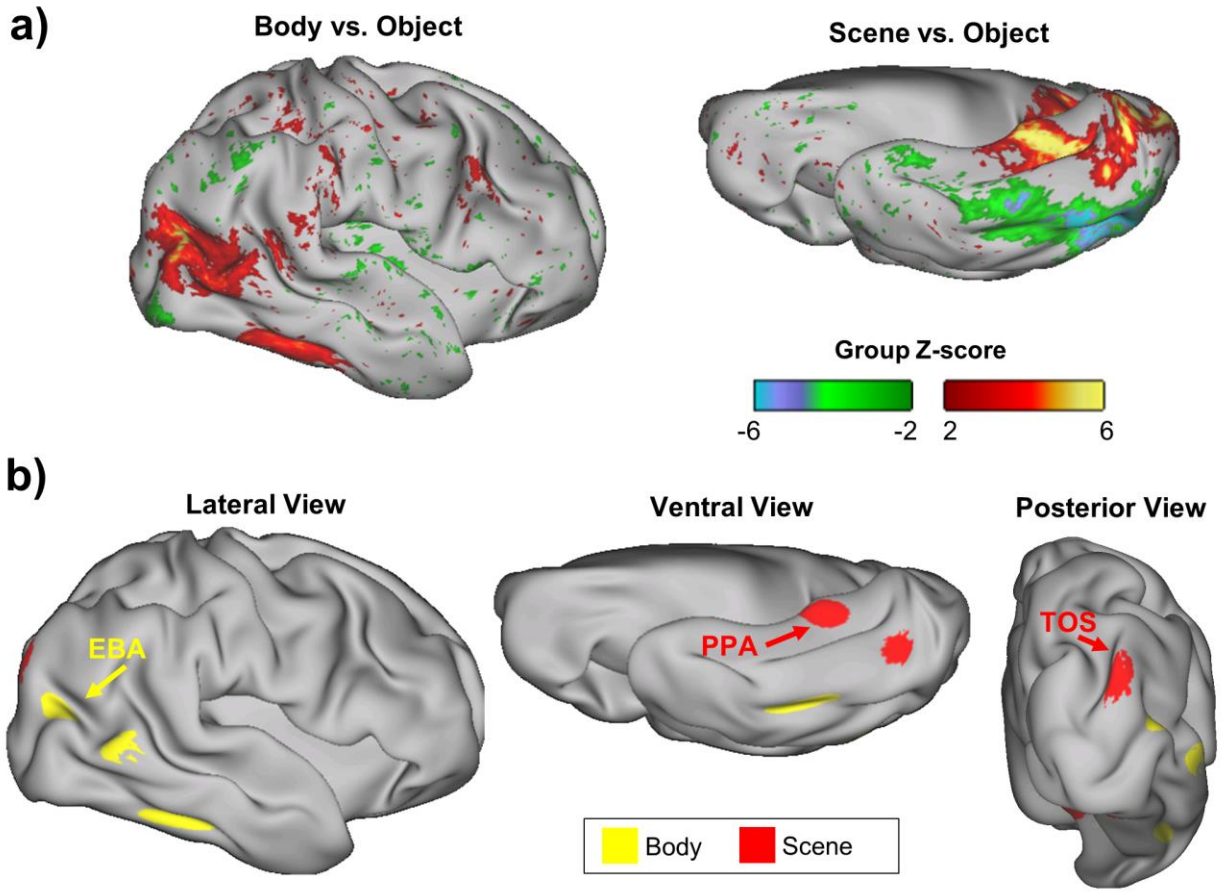

Figure 3.1. (a) Group z-statistic Localizer maps. ROIs were separately defined for individual from their localizer maps using the group foci as a constraint (see Methods, Defining ROIs from

localizer activation contrasts in Chapter 2). **(b)** Category-preferential ROIs of boy and scene categories were defined.

Table 3.1. Summary information for 12 constituent ROIs of Body and Scene joint-ROIs.

		Mean MNI across subjects						# vertices		
Contrast	Hemisphere	x	y	z	Group Peak Z-value	% (Non-EV) in Group Map	# Subject	Mean	STD	ROI Name
Body	LH	-41	-73	12	6.61	100	16	289	45	L-EBA
		-37	-44	-17	4.42	100	14	271	59	
	RH	42	-65	15	6.28	100	15	321	37	R-EBA
		41	-44	-13	4.62	100	14	299	49	
		56	-52	4	3.91	100	14	297	47	
Scene	LH	-21	-47	-4	8.14	67.89	16	327	37	L-PPA
		-14	-51	7	5.88	83.15	16	294	56	L-RSC
		-30	-80	23	3.19	100	14	229	33	L-TOS
	RH	20	-41	-10	8.35	53.15	16	279	45	R-PPA
		27	-68	-10	6.79	56.36	16	254	43	
		35	-77	29	4.55	100	15	281	58	R-TOS
		13	-36	41	4.01	100	14	255	41	

3.3.2 Categorical-pattern-to-rest correlation timeseries

For each participant and ROI, we determined the degree to which the scene and body prototype templates (i.e. the multi-vertex pattern evoked by scenes and bodies; see Fig. 3.2a) matched the multi-vertex pattern measured on each resting frame. In this procedure, framewise intrinsic activity patterns were first obtained for each frame of independent resting-state scans. Then, for each frame the resting multi-vertex pattern was spatially correlated with the scene prototype template, as illustrated in Figure 3.2b, and with the body prototype template. A high positive correlation coefficient indicated that the multi-vertex resting activity pattern on a given frame was very similar to the pattern evoked by the template category. This procedure was repeated across all resting frames, resulting a timeseries of spatial correlation coefficients (categorical-pattern-to-rest correlation timeseries) for a particular template and ROI (e.g. the scene template in PPA).

3.3.3 Pattern-based resting functional connectivity

For each participant, the categorical-pattern-to-rest correlation timeseries for a category and ROI (e.g. the 'scene' timeseries in PPA) was temporally correlated across ROI pairs, resulting in a pattern-based FC matrix for that category (Fig. 3.2c). Separate pattern-based FC matrices were computed for the scene and the body templates. Additionally, a 'preferred template' pattern-based FC matrix was computed. Here, for the 'preferred template' pattern-based FC, the categorical-pattern-to-rest correlation timeseries for body ROIs were computed using the body template and the categorical-pattern-to-rest correlation timeseries for scene ROIs were computed using the scene template. Finally, for a paired body-to-scene ROIs, the categorical-pattern-to-rest correlation timeseries for body ROIs using the body template were temporally correlated to the categorical-pattern-to-rest correlation timeseries for scene ROIs using the body template. This matrix will highlight if there is a stimulus specificity in the pattern-based FC for the category selective ROIs. In fact, we would expect a stronger correlation between body ROIs for body than scene templates, the reverse for scene ROIs. Finally, a vertex-averaged FC matrix was computed by first averaging the resting BOLD timeseries across all vertices of an ROI to generate a vertex-averaged timeseries, and then temporally correlating these averaged timeseries for all pairs of ROIs. Vertex-averaged FC matrices, which correspond to the standard regional FC matrices found in the literature, eliminate any information carried by the spatial pattern of BOLD activity within ROIs.

Pattern-based FC values were analyzed via repeated measures ANOVAs and paired t-tests. For example, we statistically evaluated whether the magnitude of pattern-based FC depended on both the category of the template and the preferred category of the ROIs by conducting a repeated-measures ANOVA with ROI-Type (Body, Scene) and Template-Category

(body, scene) as factors. Paired t-tests were conducted to test differences between specific template/ROI combinations. For example, pattern-based FC values between Body ROIs were compared for correlation timeseries generated using body-templates vs. scene-templates.

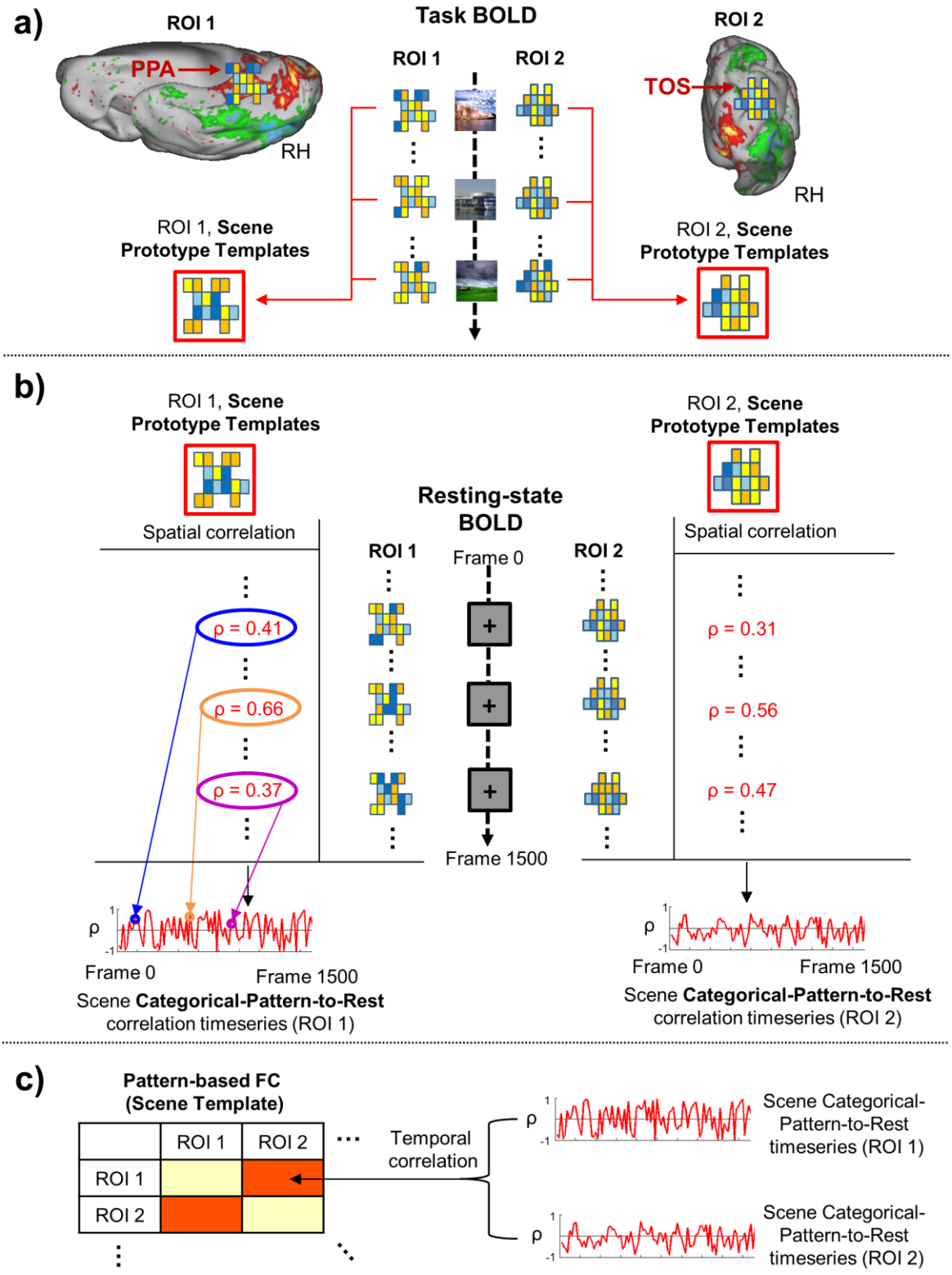

Figure 3.2 (a) At each vertex of each constituent ROI, the β weights for all 96 stimuli from within a category were computed, producing a prototype template. Two scene prototype templates for two scene preferential regions of PPA and TOS were obtained. **(b)** At each

constituent ROI, categorical-pattern-to-rest correlation timeseries was obtained by spatially correlated the scene prototype template with the resting multi-vertex pattern for each resting frame. **(c)** Pattern-based functional correlation was computed by temporally correlating the categorical-pattern-to-rest correlation timeseries for a category across ROIs.

3.4 Result

FC analyses typically evaluate the correlation between the timeseries of activity for single voxels or between voxel-averaged timeseries. However, recent task-based studies have also measured the inter-regional temporal correlation of spatial activity patterns (Coutanche and Thompson-Schill, 2013; Anzellotti et al. 2017 and 2018; Chen et al. 2018). We used a similar approach to determine whether resting fluctuations of the multi-vertex spatial pattern for a category in each constituent ROI of a joint-ROI fluctuated synchronously or independently across the constituent ROIs. Synchronous fluctuations would indicate temporal variations of an inter-regional brain state specific for a particular category.

We first determined whether the similarity of the spatial pattern of activity on a resting state frame to the 'template' spatial pattern evoked by bodies or scenes was temporally correlated over frames between high-level regions of visual cortex preferring bodies or scenes. For each body- and scene-preferring ROI, we computed separate body and scene correlation timeseries based on the spatial correlation of the activity pattern on each resting frame with the scene template and the body template. We then constructed separate body and scene pattern-based resting FC matrices by computing the correlation over all pairs of ROIs, respectively, of the body and scene correlation timeseries (upper left and right panels of Fig. 3.3). The lower left panel shows the 'preferred-template' matrix that was constructed by first computing resting similarity

timeseries in body-preferring regions using the body template and scene preferring regions using the scene template, and then conducting all pairwise regional correlations. Finally, a standard FC matrix (Fig. 3.3, lower right panel) was constructed by computing vertex-averaged resting timeseries for each region, followed by pairwise correlation of the regional timeseries.

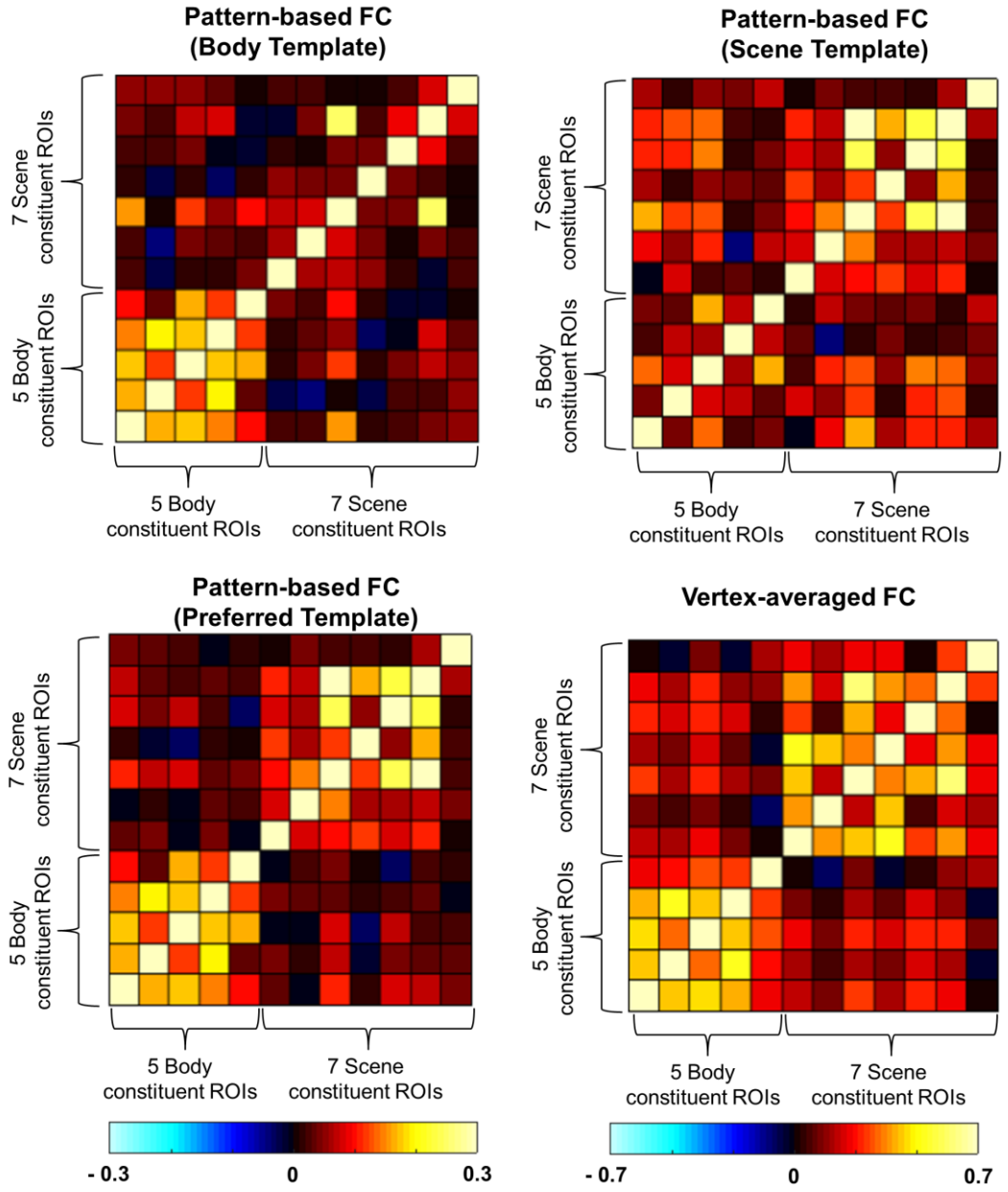

Figure 3.3 Top Left: the pattern-based FC matrix that was constructed by correlating the correlation timeseries associated with the multivoxel body template over all pairs of scene and body regions. **Top Right:** the pattern-based FC matrix that was constructed by correlating the correlation timeseries

associated with the multivoxel scene template over all pairs of scene and body regions. **Bottom Left:** the pattern-based FC matrix constructed using the correlation timeseries in body regions that were generated using a body template and the correlation timeseries in scene regions that were generate using a scene template. Accordingly, the sub-block of 5 body regions is matrix necessarily matched the corresponding blocks from the Top Left Body Template. Similarly, the sub-block of 7 scene regions is matrix necessarily matched the corresponding blocks from the Top Right Scene Template. The blocks of Body-region-to-Scene-region, however, involved the correlation of body region/body template timeseries with scene region/scene template timeseries.
Bottom Right: a standard regional FC matrix generated by first averaging the vertex-wise timeseries of the BOLD signal within each region, and then correlating the resulting timeseries across all pairs of regions.

3.4.1 Pattern-based functional connectivity at rest

Pattern-based resting FC between regions was most evident using stimulus-evoked templates that matched the regions' stimulus preference. Figure 3.4a (leftmost graph) shows that the mean pairwise FC between all body-preferring regions was significantly larger for correlation timeseries computed using a body template than a scene template. Conversely, the mean pairwise FC between all scene-preferring regions was larger for correlation timeseries computed using a scene template than a body template Figure 3.4a (middle graph). A 2-factor ANOVA on the mean pairwise FC values with ROI-type (Body, Scene) and Template-Category (body, scene) as factors yielded a main effect of Template-type ($F(1,15)=5.05$, $p=0.040$), reflecting the larger FC values in body-preferring regions and a significant interaction of ROI-type by Template-Category ($F(1,15)=10.46$, $p=0.0006$), confirming the selectivity of pattern-based FC for matching region preferences and stimulus templates. Paired t-tests indicated that average pairwise FC between body-preferring regions was significantly larger using body than scene templates ($p=8.3e-4$); however, average pairwise FC between scene-preferring regions was not significantly larger using scene than body templates ($p=0.268$).

Interestingly, when pattern-based coherence was computed using the body template, coherence was largely confined to body-preferring regions. Particularly, Body-ROI-to-Scene-ROI correlations were quite low (Fig. 3.4a, rightmost graph), indicating that a general body state that spanned both Body and Scene ROIs was not observed. A similar regionally-selective brain state was observed for the scene category with significant difference ($p=0.025$) indicating that a general scene state that spanned both Body and Scene ROIs was not observed.

We also determined whether body and scene representations fluctuated independently. The lower left panel of Figure 3.3 shows a 'preferred-template' matrix that was constructed using body correlation timeseries in body-preferring regions and scene correlation timeseries in scene preferring regions. The 'Scene-ROIs-to-Body-ROIs' blocks are of primary interest. They indicate that the correlation between scene and body regions was uniformly low under conditions in which the correlation involved timeseries from scene and body regions that respectively indicated the fluctuations of scene and body representations. Therefore, periods in which a body state was maximally present in body-preferring ROIs were largely independent of periods in which a scene state was maximally present in scene-preferring ROIs. Figure 3.4a, rightmost graph, shows the correlation values for scene-body blocks from all three matrices, with the green symbol indicating the scene-body correlations from the preferred-template matrix.

Figure 3.4b shows the average pairwise FC between body ROIs and between scene ROIs using standard vertex-averaged FC. The vertex-averaged FC values were essentially the same for scene-preferring and body-preferring regions and were significantly larger than the values obtained using pattern-based FC. Therefore, pattern-based FC but not vertex-averaged FC isolated a coherent state for a particular representational pattern in a corresponding set of ROIs, resulting in maximal coherence for a single set of constituent ROIs preferring the same category.

Pattern-based FC matrices were moderately-to-strongly correlated with the vertex-averaged FC matrix. As expected, the largest correlation was with the preferred template matrix rather than the matrices generated using a single template (body-template, ρ=0.61; scene-template, ρ=0.54; preferred template, ρ=0.78).

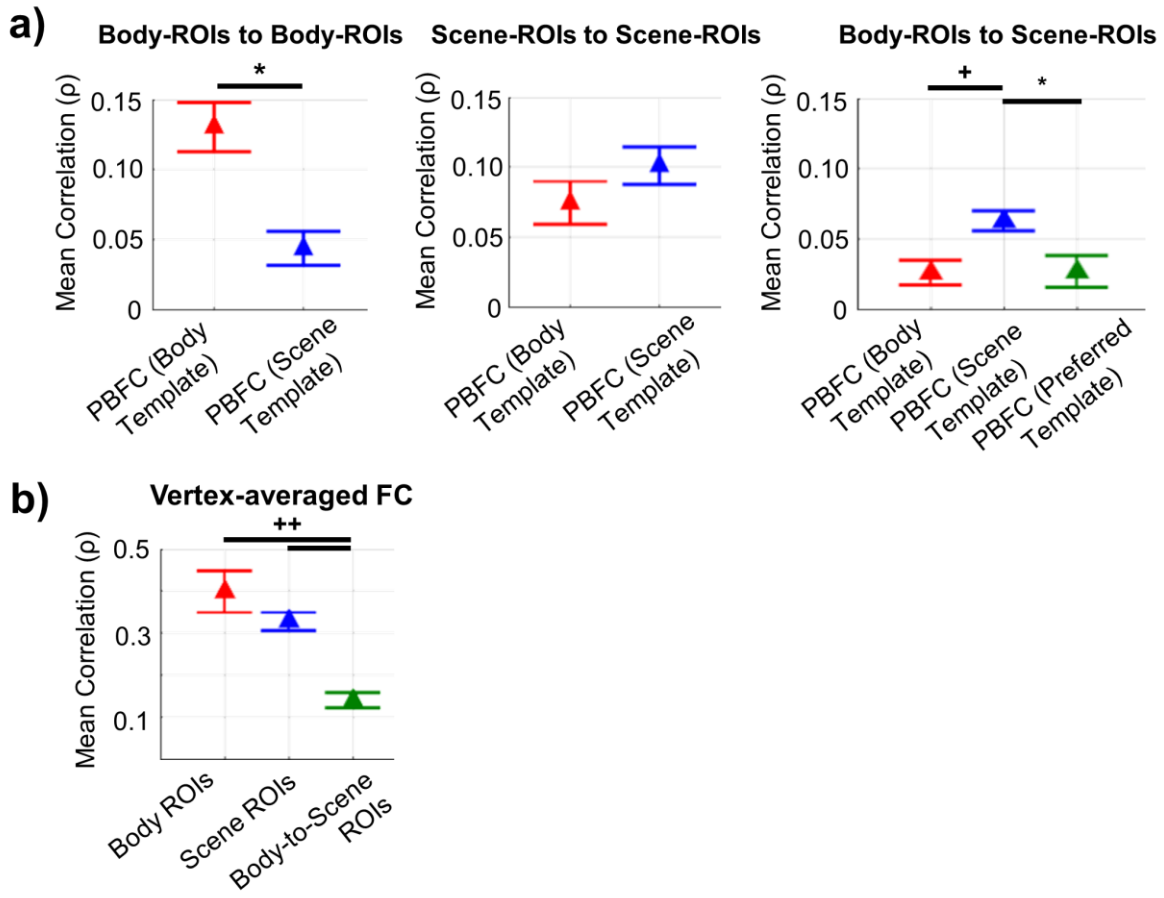

Figure 3.4 (a) Group-averaged pattern-based FC between body regions (left graph) and between scene regions (middle graph) is shown for correlation timeseries generated using body and scene templates. The rightmost graph shows the group-averaged pattern-based FC between body and scene regions for correlation timeseries generated using body templates, scene templates, or the preferred template for the region (i.e. body templates in body regions and scene templates in scene regions). **(b)** The group-averaged vertex-averaged FC between body regions, between scene regions, or between body and scene regions is shown for timeseries generated by averaging the BOLD timeseries for all vertices within a region.

3.4.2 Category selectivity of U90 values in constituent vs. joint-ROIs

The significant different category preferential U90-value profiles shown in the previous Chapter 2 (Fig 2.4) were the measure of U90-value from all combined vertices of a joint-ROI. As each local constituent ROIs might have an overall similar but relevantly different categorical preferences, although the spatial patterns for the constituent ROIs of a joint-ROI fluctuated coherently, we measured the categorical U90 values in each constituent ROIs. The correspondence between the category selectivity of individual constituent ROIs and the joint-ROI varied widely (Fig 3.5). Some constituent regions showed similar categorical U90-value profiles with the profile of the joint-ROI, while other regions showed rather moderately similar or different categorical U90-value profiles (see Fig 2.4 for categorical U90-values of the joint-ROI). Separate repeated measures analysis of variance (ANOVAs) for each constituent ROI with Category (8 levels) as a factor indicated a significant main effect of Category in 5 constituent ROIs (Body ROI#2: $F(7,91)=2.58$, $p=0.018$; Body ROI #4: $F(7,91)=4.09$, $p=6.1e\text{-}4$; Scene ROI #1: $F(7,105)=2.35$, $p=0.028$; Scene ROI #3: $F(7,91)=3.83$, $p=0.001$; Scene ROI #5: $F(7,105)=2.50$, $p=0.020$). Since the ROIs comprising a joint-ROI were determined solely by the activation magnitude for a particular localizer contrast, and there were many fewer vertices in each constituent ROI than in the associated joint-ROI, this variability is perhaps not surprising. In addition, however, the observed differences between the category profiles for a joint-ROI and its constituent ROIs (Fig. 3.5) link the spatial pattern analysis of Figure 2.4 with the spatiotemporal pattern analysis of Figures 3.3 and 3.4, as discussed below.

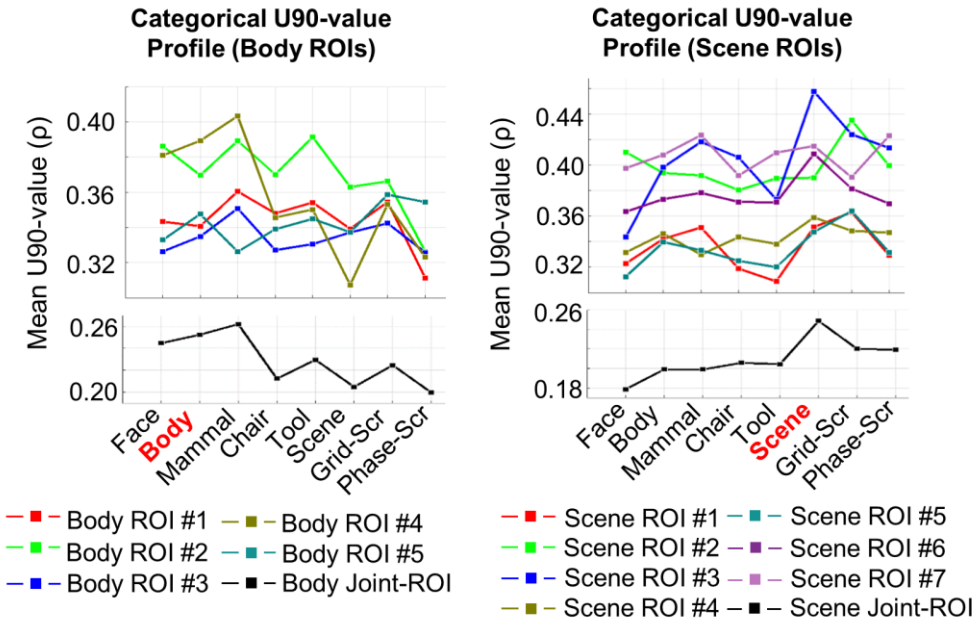

Figure 3.5. A graph of the profile of group-averaged U90 values across stimulus categories for each constituent Body ROIs and Scene ROIs.

3.5 Discussion

The pattern-based FC identified the resting temporal correlations between regions that were related to the multi-vertex pattern evoked by a particular stimulus category. Importantly, the pattern-based FCs were significantly larger for the regions' preferred category. In addition, pattern-based FC computed using a body template was significantly larger in body-preferring regions than in scene-preferring regions, indicating that a 'body' state did not occur throughout category-selective regions. Similar result was observed for scene-templates, resulting in a highly significant interaction of template category by region category that statistically confirmed selectivity. These results distinguished the pattern-based FCs from the vertex-averaged FC since roughly equivalent correlated fluctuations were observed simultaneously within body-preferring and scene-preferring ROIs in the vertex-averaged FC. These results demonstrate that in the

resting-state, the spatial pattern of activity across high-level visual regions preferring a particular category forms a linked brain state that is maximally present for spatial activity patterns evoked by the preferred category.

These results support the notion that the putative representational content of the spontaneous interactions between regions can be measured using pattern-based FC. The current work does not show that the linked spatial activity patterns are behaviorally significant, which is an important correlate of the argument that intrinsic activity serves a representational function. However, the results are consistent with a general framework in which there are joint influences between task-evoked and spontaneous activity (Albert et al. 2009; Hasson et al. 2009; Lewis et al. 2009; Tambini et al. 2010), with the influence here from the spatial pattern of task-evoked activity to the spatial pattern of spontaneous activity.

3.5.1 Selectivity of pattern-based functional connectivity at rest

Selective pattern-based FC did not reflect a greater average similarity of resting patterns to preferred stimulus-evoked patterns, which was not observed (e.g. the distributions of U90 values in Fig. 2.4b). Instead, the correlated fluctuations of the preferred pattern across its associated constituent ROIs were observed in conjunction with an increased variation over resting frames in the magnitude of that pattern over the entire joint-ROI. As shown in Figure 3.5 and Figure 2.4, the variation of U90 values across categories was generally larger within a joint ROI than within many of its constituent ROIs. Large positive or negative similarity values in a joint-ROI occur when the similarity values in the constituent ROIs are simultaneously large and of the same sign. Otherwise, across constituent ROIs the similarity values tend to cancel or average to a lower value. Therefore, a larger spread of similarity values is more likely to be

observed if the similarity values fluctuate in a correlated fashion across the constituent ROIs. If the patterns for a non-preferred category do not fluctuate as coherently across ROIs, the resulting similarity values across frames in the joint-ROI for that category will show less variation from zero. This mechanism, however, likely only partly explains the variance or spread result (Fig. 2.4) since a significant variation of U90 values across categories was also observed within some constituent ROIs (2 out of 5 Body constituent ROIs and 3 out of 7 Scene constituent ROIs showed significant main effect of category in separated ANOVA tests).

3.5.2 Identifying networks from FC

The overall consistency of resting-state FC MRI across subjects has inspired numerous attempts to specify a normative resting-state structure. Papers using different techniques have converged on a structure that is largely consistent with the structure observed in meta-analyses of task activation data, although there is clearly individual variation in this structure (Smith et al. 2009; Power et al. 2011; Yeo et al. 2011; Laumann et al. 2015; Cole et al. 2014; Gordon et al. 2017; Gratton et al. 2018). This normative structure was derived using signals that either corresponded to single voxels or were summed over the voxels in a region and whose putative representational content was not well specified. An interesting possibility is that resting state organization depends on the representational properties of the signals that are correlated across regions, where these representational features are indexed by spatial activity patterns.

Although the putative representational content of resting FC is often unspecified, an important exception comes from studies of early visual cortex, which have shown that resting FC respects the tuning of single voxels for polar angle, eccentricity, and low-level stimulus features (Heinzle et al. 2011; Raemaekers et al. 2014; Arcaro et al. 2015; Ryu and Lee, 2018). Most task-

based studies of representation in higher-order visual and associative regions, however, have not involved measurements of voxelwise tuning functions but instead have identified task-evoked representations through measurements of regional spatial patterns. Therefore, pattern-based FC (Coutanche and Thompson-Schill, 2013; Anzellotti et al. 2017 and 2018; Chen et al. 2018) could provide insights into putative resting representational FC in high-level brain regions that are complementary to those provided by approaches based on the tuning properties of single voxels.

3.5.3 Pattern-based FC application into resting FC

We suggest two ways in which pattern-based FC might inform studies of resting-state organization. First, pattern-based FC may help fractionate existing resting-state networks and identify the functional factors associated with that fractionation. For example, pattern-based resting FC between regions that prefer a particular category might depend on selectivity for features within the category, such as gender for face-preferring regions. Similarly, pattern-based resting FC between regions might depend on the resting selectivity of each region across visual categories.

A second possible contribution of pattern-based FC is to uncover resting FC organizations that differ substantially from the normative structure that has been described over the past decade, although this structure does vary over individuals. In the current work, pattern-based FC was measured within category-preferring regions. Because regions that co-activate (e.g. to bodies) tend to show greater resting FC (Smith et al. 2009), and because previous studies have shown that regions preferring the same category show preferential FC (Nir et al. 2006; Zhang et al. 2009; Zhu et al. 2011; Hutchison et al. 2014; Stevens et al. 2015), novel FC organizations

were not expected. Accordingly, pattern-based FC matrices were moderately-to-strongly correlated with inter-regional vertex-averaged FC matrices.

However, divergent FC organizations may be more likely in studies that use task-evoked templates based on frequently occurring processes that combine different domains: for example, templates based on integration of voice and face information during person-to-person interactions, visuomotor coordination during object manipulation, or biologically significant stimulus-reward or response-reward contingencies. Cross-domain pattern-based connectivity that cuts across standard networks might reflect synergies (Leo et al. 2016) or routines for implementing frequently occurring processes

3.5.3 Limitations

Previous work has shown that naturalistic stimulation from passive viewing of movies better accounts for resting FC throughout occipital cortex than artificial stimuli such as rotating checkerboard wedges or the static pictures of objects used here (Wilf et al. 2017; Strappini et al. 2018). Although the attributes that underlie the greater correspondence between resting FC and movie-evoked FC are unknown, the use of static pictures in the present work may have reduced category-selective, pattern-based FC.

In addition, we measured stimulus-evoked templates using a task that maintained participant alertness but involved discriminations of low-level features unrelated to the category of the stimulus. This procedure was adopted to maximize the influence of automatic encoding processes, but the correspondence of resting FC and the FC evoked by passive viewing of movies suggests that the use of more ecological tasks could result in multivoxel activity patterns that show stronger resting coherence across regions.

3.6 Pattern-based FC using Gordon-Laumann Parcellation

3.6.1 Introduction

The above pattern-based FC computed based on preferential ROIs in terms of stimulus-evoked activations. The task-rest correspondences, therefore, was investigated based on task-based selective region definitions. Another possible ROI definition can be used is RSN-based region definition. The RSN-based region definition would not be optimized in analyzing multi-variate patterns categorizing and discriminating representations of given stimuli since the RSN-based regions are purely organized for the temporal correlations of intrinsic activity. The hypothesis of task-rest correspondences and of a coherent brain resting state representing one stimulus category at a time, however, should be held consistently under the RSN-based region definition with relative categorical preferential responses.

We used multi-vertex activity patterns of task and rest activity registered into the 324 Gordon-Laumann parcels grouped into 13 different resting-state networks (RSN) (Gordon et al. 2016). Out of the 324 GL-Parcels, total 41 parcels with 6 hierarchical clusters showed categorial visual object discriminability (classifications over the chance accuracy) from a trained localizer linear support vector machine (SVM). We computed pattern-based FCs using different categorical templates among the 41 parcels. As expected, similar results to the above were observed.

3.6.2 Method

The data used in the previous sections (Ch.2 and Ch.3) were recruited once again for this analysis; however, there are three important changes need to be clarified.

1) Out of 16 subjects, one subject data was registered relatively poorly in the preprocessing pipeline compared to the data of the subject used in Ch.2 and Ch.3. This is primarily due to the subject's data used in the above sections was re-preprocessed after the analysis conducted in the current section: *3.6. Pattern-based FC using Gordon-Laumann Parcellation.*
2) For the localizer BOLD data, previous analysis in Ch.2 and Ch.3 did not use real-word (RW) and false-font string (FS) categories in the activation-based ROI definitions. In current section (*3.6. Pattern-based FC using Gordon-Laumann Parcellation.*), all localizer contrast categories including RW and FS were used in a region-of-interest definition.
3) The categorical multi-vertex template generated were not prototypic template of a category. In following analysis, 24 heterogeneous templates created by averaging the β weights from four different exemplar instances were used.

Except the above 3 changes, all basic computational methods for the pattern-based FC analysis are same as the previous analyses.

Initially, the preprocessed multi-vertex BOLD timeseries of the resting, the localizer, and the task scans were registered into the 324 Gordon-Laumann parcels (Gordon et al. 2016). While the GL-parcels were purely defined by resting-state temporal correlation structure, we still need to use certain GL-parcels that carries task-relevant information of categorical visual stimuli. A

distinction of task-selective GL-parcels was made by a linear SVM (LIBSVM; Chang and Lin 2011) trained for a category classification.

Since the localizer contains 8 blocks/categories for each of 7 categories, each category was divided into 7 training blocks and 1 testing block. For each GL parcel, a categorical block GLM was computed to obtain localizer block β weights for the parcel (e.g. 8 'face' block weights). A linear SVM was trained from the obtained weights with leave-one-out-cross-validation (LOOCV) with 8 iterations. A chance-level classification accuracy (26.4% for p-val = 0.005) was computed from 50 control simulations of shuffled labels across all GL-parcels. From the obtained classification accuracy for each GL-parcel, total 41 GL-parcels (Fig. 3.6b) were found to be above the chance-level classification accuracy. The categorical classification accuracy profiles of the 41 GL-parcels are illustrated in below Figure 3.6a with 6 clusters from a hierarchical clustering in accuracy profiles. Then, pattern-based FC analysis (see *3.3.2 Pattern-based resting functional connectivity*) of 'face', 'body', 'tool', and 'scene' templates was conducted using the chosen 41 GL-Parcels.

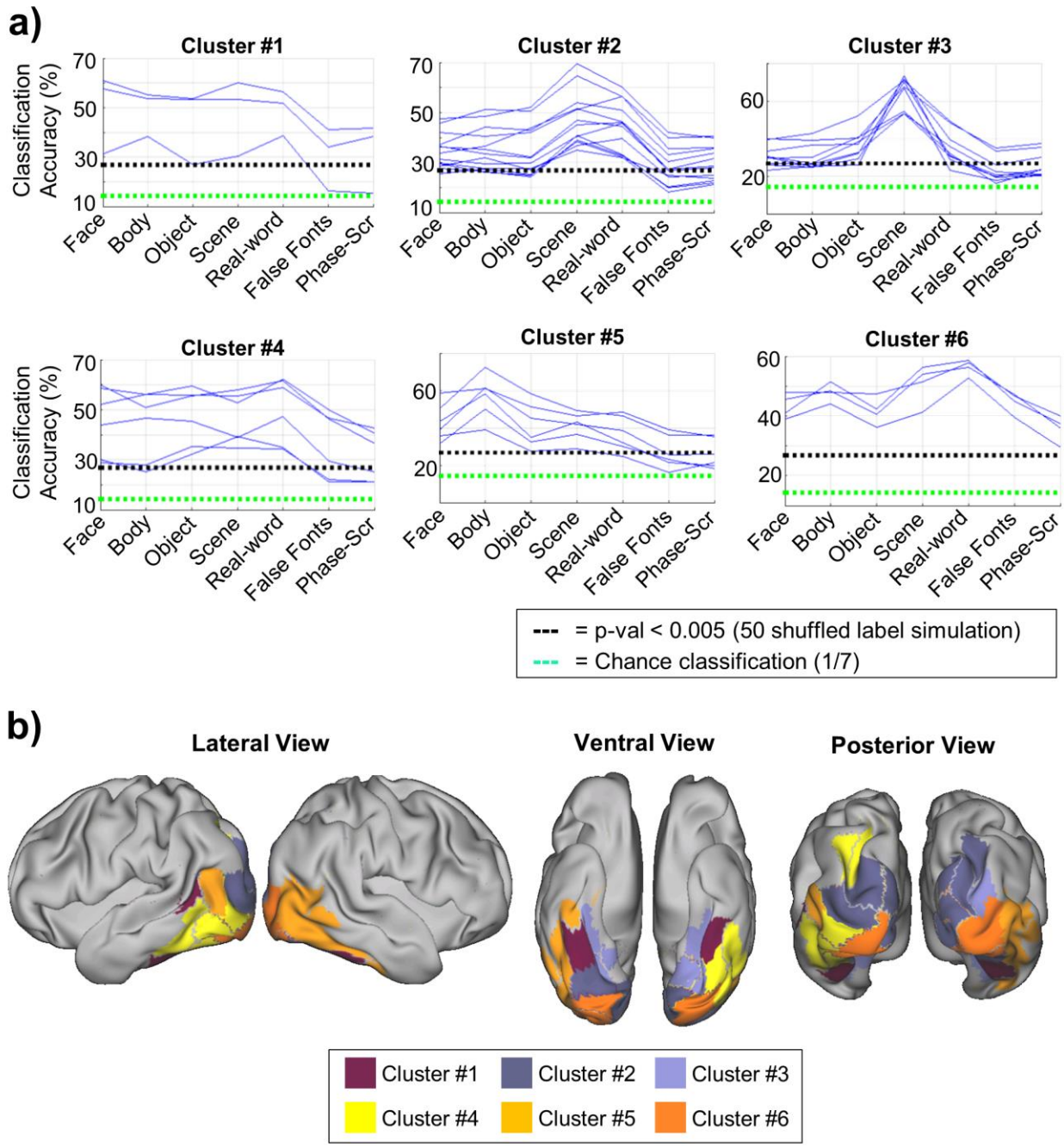

Figure 3.6. 41 Chosen GL-parcels. (a) Each graph plots the categorical classification accuracy predicted from the trained linear SVM for each parcel (thin blue line). Total 6 clusters were obtained from the 41 GL-parcels above the chance-level classification accuracy. **(b)** Locations of the 41 GL-parcels are plotted over a brain surface.

3.6.1 Result

Similar results to the previous results in 3.4 were observed in pattern-based FC across 41 GL-parcels. Figure 3.7 shows the pattern-based FC matrices of 'face', 'body', 'tool', and 'scene' templates and the corresponding vertex-averaged FC. The pattern-based FC's spatial correlation to the vertex-averaged FC were moderate-to-strong: ρ(face) = 0.71; ρ(body) = 0.70; ρ(tool) = 0.66; ρ(scene) = 0.72. Figure 3.7a shows that the overall network structures, but not the sub-network organization, of the pattern-based FCs of 4 templates were similar.

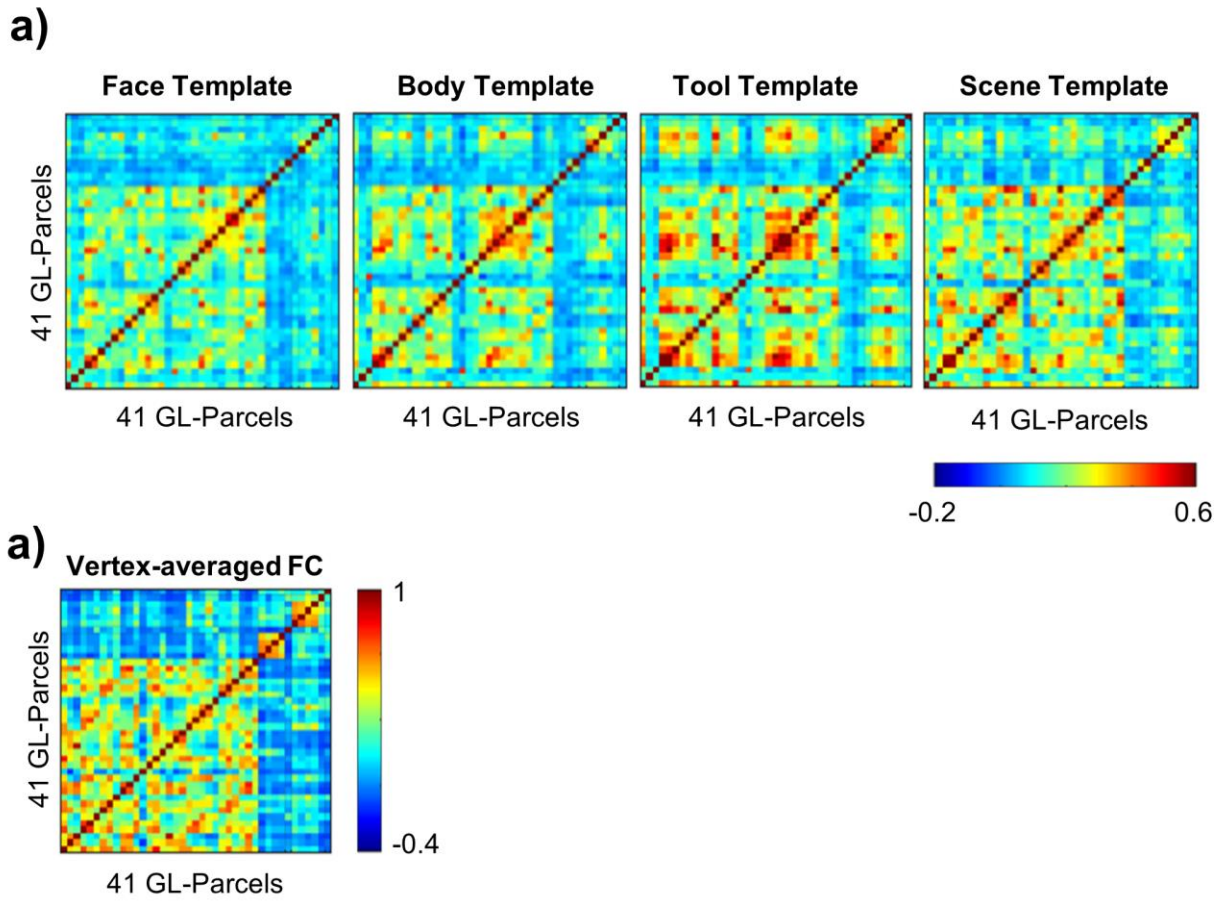

Figure 3.7. Pattern-based FCs across 41 Chosen GL-parcels. (a) Pattern-based FCs of 'face', 'body', 'tool', and 'scene' templates were computed across 41 GL-parcels. **(b)** The corresponding vertex-averaged FC was computed across 41 GL-parcels.

Since the 41-GL parcels were not defined by categorical preferential activation as the previously used Body-ROIs and Scene-ROIs in Fig 3.3, the inter-regional selectivity and coherence analysis could not be performed. An alternative analysis for the coherent categorical pattern representations was performed by making a mixed pattern-based FC with categorical-pattern-to-rest correlation timeseries of different categories for all 41 GL-parcels (e.g. temporal correlation between timeseries using 'body' template and timeseries using 'non-body' templates). This is different to the pattern-based FC of the 'preferred-template' in Fig. 3.3 since the 'non-target category' templates mean using all other category templates (e.g. 'non-body' templates are 'face', 'tool', and 'scene' templates) and since the cross correlation occurred in all pairs of GL-parcels. The paired two-sample t-tests showed significant differences between the pattern-based FC of a single template and the corresponding mixed pattern-based FC. This result indicates existence of a coherent brain resting state representing one stimulus category.

3.7 Reference

Arcaro MJ, Honey CJ, Mruczek RE, Kastner S, Hasson U. 2015. Widespread correlation patterns of fMRI signal across visual cortex reflect eccentricity organization. Elife. 19:4

Albert NB, Robertson EM, Miall RC. 2009. The resting human brain and motor learning. Curr Biol. 19(12):1023–1027

Anzellotti S, Caramazza A, Saxe R. 2017. Multivariate pattern dependence. PLoS Comput Biol. 13(11):e1005799

Anzellotti S, Coutanche MN. 2018. Beyond Functional Connectivity: Investigating Networks of Multivariate Representations. 22(3):258-269 Benson NC, Butt OH, Datta R, Radoeva PD, Brainard DH, Aguirre GK. 2012. The retinotopic organization of striate cortex is well predicted by surface topology. Curr Biol. 22:2081-2085.

Barttfeld P, Uhrig L, Sitt JD, Sigman M, Jarraya B, Dehaene S. 2015. Signature of consciousness in the dynamics of resting-state brain activity. Proc Natl Acad Sci. 2015 Jan 20;112(3):887-92

Benson NC, Butt OH, Datta R, Radoeva PD, Brainard DH, Aguirre GK. 2012. The retinotopic organization of striate cortex is well predicted by surface topology. Curr Biol. 22:2081-2085.

Berkes P, Orban G, Lengyel M, Fiser J. 2011. Spontaneous cortical activity reveals hallmarks of an optimal internal model of the environment. Science. 331(6013):83–87.

Biswal B, Yetkin FZ, Haughton VM, Hyde JS. 1995. Functional connectivity in the motor cortex of resting human brain using echo-planar MRI. Magnetic resonance in medicine. 34:537-541.

Chen RH, Ito T, Kulkarni KR, Cole MW. 2018. The Human Brain Traverses a Common Activation-Pattern State Space Across Task and Rest. Brain Connect.

Cole MW, Ito T, Bassett DS, Schultz DH. 2016. Activity flow over resting-state networks shapes cognitive task activations. Nat Neurosci. 19(12):1718-1726

Coutanche MN, Thompson-Schill SL. 2013. Informational connectivity: identifying synchronized discriminability of multi-voxel patterns across the brain. Front Hum Neurosci. 7:15

Deco G, Jirsa VK, McIntosh AR. 2011. Emerging concepts for the dynamical organization of resting-state activity in the brain. Nat Rev Neurosci. 12(1):43-56.

Fries P. 2005. A mechanism for cognitive dynamics: neuronal communication through neuronal coherence. Trends Cogn Sci. 9(10):474-80.

Gordon EM, Laumann TO, Adeyemo B, Huckins JF, Kelley WM, Petersen SE. 2016. Generation and Evaluation of a Cortical Area Parcellation from Resting-State Correlations. Cereb Cortex. 26 (1):288-303

Gordon EM, Laumann TO, Gilmore AW, Newbold DJ, Greene DJ, Berg JJ, Ortega M, Hoyt-Drazen C, Gratton C, Sun H, et al. 2017. Precision Functional Mapping of Individual Human Brains. Neuron. 95:791-807.e797.

Gratton C, Laumann TO, Nielsen AN, Greene DJ, Gordon EM, Gilmore AW, Nelson SM, Coalson RS, Snyder AZ, Schlaggar BL, et al. 2018. Functional Brain Networks Are Dominated by Stable Group and Individual Factors, Not Cognitive or Daily Variation. Neuron. 98:439-452.e435.

Greenberg AS, Esterman M, Wilson D, Serences JT, Yantis S. 2010. Control of spatial and feature-based attention in frontoparietal cortex. J Neurosci. 30:14330-14339.

Greicius MD, Krasnow B, Reiss AL, Menon V. 2003. Functional connectivity in the resting brain: a network analysis of the default mode hypothesis. Proc Natl Acad Sci USA. 100:253-258.

Harmelech T, Malach R. 2013. Neurocognitive biases and the patterns of spontaneous correlations in the human cortex. Trends Cogn Sci. 17(12):606–615.

Hasson U, Nusbaum HC, Small SL. 2009. Task-dependent organization of brain regions active during rest. Proc Natl Acad Sci. 106(26):10841–10846.

Haxby JV, Gobbini MI, Furey ML, Ishai A, Schouten JL, Pietrini P. 2001. Distributed and overlapping representations of faces and objects in ventral temporal cortex. Science. 293:2425-2430.

Haynes JD, Rees G. 2006. Decoding mental states from brain activity in humans. Nat Rev Neurosci. 7(7):523–534.

Heinzle J, Kahnt T, Haynes JD. 2011. Topographically specific functional connectivity between visual field maps in the human brain. Neuroimage. 56:1426-1436.

Hutchison RM, Culham JC, Everling S, Flanagan JR, Gallivan JP. 2014. Distinct and distributed functional connectivity patterns across cortex reflect the domain-specific constraints of object, face, scene, body, and tool category-selective modules in the ventral visual pathway. Neuroimage. 96:216-36.

Huth AG, Nishimoto S, Vu AT, Gallant JL. 2012. A continuous semantic space describes the representation of thousands of object and action categories across the human brain. Neuron. 76(6): 1210–1224.

Fiser J, Chiu C, Weliky M. 2004. Small modulation of ongoing cortical dynamics by sensory input during natural vision. Nature. 431(7009):573–578.

Fox MD, Corbetta M, Snyder AZ, Vincent JL, Raichle ME. 2006. Spontaneous neuronal activity distinguishes human dorsal and ventral attention systems. Proc Natl Acad Sci USA. 103:10046-10051.

Kamitani Y, Tong F. 2005. Decoding the visual and subjective contents of the human brain. Nature neuroscience. 8:679-685.

Kriegeskorte N, Goebel R, Bandettini P. 2006. Information-based functional brain mapping. Proc Natl Acad Sci U S A. 103:3863-3868.

Kriegeskorte N, Mur M, Ruff DA, Kiani R, Bodurka J, Esteky H, Tanaka K, Bandettini PA. 2008. Matching categorical object representations in inferior temporal cortex of man and monkey. Neuron. 60:1126-1141.

Kuhl BA, Chun MM. 2014. Successful remembering elicits event-specific activity patterns in lateral parietal cortex. J Neurosci. 34:8051-8060.

Laumann TO, Gordon EM, Adeyemo B, Snyder AZ, Joo SJ, Chen MY, Gilmore AW, McDermott KB, Nelson SM, Dosenbach NU, Schlaggar BL, Mumford JA, Poldrack RA, Petersen SE. 2015. Functional System and Areal Organization of a Highly Sampled Individual Human Brain. Neuron. 87:657-670.

Lewis CM, Baldassarre A, Committeri G, Romani GL, Corbetta M. 2009. Learning sculpts the spontaneous activity of the resting human brain. Proc Natl Acad Sci U S A. 106:17558-17563.

Lewis CM, Bosman CA, Womelsdorf T, Fries P. 2016. Stimulus-induced visual cortical networks are recapitulated by spontaneous local and interareal synchronization. Proc Natl Acad Sci U S A. 113(5):E606-15.

Leo A, Handjaras G, Bianchi M, Marino H, Gabiccini M, Guidi A, Scilingo EP, Pietrini P, Bicchi A, Santello M, Ricciardi E. 2016. A synergy-based hand control is encoded in human motor cortical areas. eLife. 5.

Nakamura H, Gattass R, Desimone R, Ungerleider LG. 1993. The modular organization of projections from areas V1 and V2 to areas V4 and TEO in macaques. J Neurosci. 13(9):3681-91.

Nir Y, Hasson U, Levy I, Yeshurun Y, Malach R. 2006. Widespread functional connectivity and fMRI fluctuations in human visual cortex in the absence of visual stimulation. Neuroimage. 30:1313-1324.

Power JD, Cohen AL, Nelson SM, Wig GS, Barnes KA, Church JA, Vogel AC, Laumann TO, Miezin FM, Schlaggar BL, Petersen SE. 2011. Functional network organization of the human brain. Neuron. 72:665-678.

Raemaekers M, Schellekens W, van Wezel RJ, Petridou N, Kristo G, Ramsey NF. 2014. Patterns of resting state connectivity in human primary visual cortical areas: A 7T fMRI study. Neuroimage. 84:911-921

Ryu J, Lee SH. 2018. Stimulus-Tuned Structure of Correlated fMRI Activity in Human Visual Cortex. Cereb Cortex. 28(2):693-712

Serences JT, Boynton GM. 2007. Feature-based attentional modulations in the absence of direct visual stimulation. Neuron. 55:301-312.

Smith SM, Fox PT, Miller KL, Glahn DC, Fox PM, Mackay CE, Filippini N, Watkins KE, Toro R, Laird AR, Beckmann CF. 2009. Correspondence of the brain's functional architecture during activation and rest. Proc Natl Acad Sci U S A. 106:13040-13045.

Strappini F, Wilf M, Karp O, Goldberg H, Harel M, Furman-Haran E, Golan T, Malach R. 2018. Resting-State Activity in High-Order Visual Areas as a Window into Natural Human Brain Activations. Cereb Cortex

Stevens WD, Tessler MH, Peng CS, Martin A. 2015. Functional connectivity constrains the category-related organization of human ventral occipitotemporal cortex. Hum Brain Mapp. 36(6):2187-206.

Tambini A, Ketz N, Davachi L. 2010. Enhanced Brain Correlations during Rest Are Related to Memory for Recent Experiences. Neuron. 65(2):280–290.

Tavor I, Parker Jones O, Mars RB, Smith SM, Behrens TE, Jbabdi S. 2016. Task-free MRI predicts individual differences in brain activity during task performance. Science. 352:216-220.

Vincent JL, Patel GH, Fox MD, Snyder AZ, Baker JT, Van Essen DC, Zempel JM, Snyder LH, Corbetta M, Raichle ME. 2007. Intrinsic functional architecture in the anaesthetized monkey brain.

Wilf M, Strappini F, Golan T, Hahamy A, Harel M, Malach R. 2017. Spontaneously Emerging Patterns in Human Visual Cortex Reflect Responses to Naturalistic Sensory Stimuli. Cereb Cortex. 27:750-763.

Yeo BT, Krienen FM, Sepulcre J, Sabuncu MR, Lashkari D, Hollinshead M, Roffman JL, Smoller JW, Zollei L, Polimeni JR, Fischl B, Liu H, Buckner RL. 2011. The organization of the human cerebral cortex estimated by intrinsic functional connectivity. J Neurophysiol. 106:1125-1165.

Zhang H, Tian J, Liu J, Li J, Lee K. 2009. Intrinsically organized network for face perception during the resting state. Neuroscience letters. 454:1-5.

Zhu Q, Zhang J, Luo YL, Dilks DD, Liu J. 2011. Resting-State Neural Activity across Face-Selective Cortical Regions Is Behaviorally Relevant. J Neurosci. 31:10323-10330.

Chapter 4: Word recognition activity and intrinsic activity in language system

4.1 Abstract

In the previous chapters, the relationship between spontaneous and task-evoked brain activity was investigated along human ventral occipito-temporal cortex using real world visual object categories. It was shown that spontaneous multi-voxel activity patterns are linked to stimulus-evoked patterns. The task-rest correspondence is assumed to originate from task-evoked activity patterns being sculpted into spontaneous activity by experience through a Hebbian learning process.

Here, we examined if similar rules apply to visual words. The visual word form is a representation of letter strings that can be only acquired through reading for many years. Visual words (letter strings, etc.), therefore, represent an excellent test of the hypothesis that patterns of spontaneous activity are entrained in the brain by experience. Here, we ask if spontaneous multivoxel activity patterns are linked to patterns evoked by linguistic (e.g. real word, consonant strings, letters), pseudo-linguistic (e.g. false font letters or strings), and non-linguistic (e.g. phase-scrambled real word) visual stimuli.

The similarity of task evoked patterns with resting state patterns was higher for word-like stimuli (real words, consonant strings, false fonts) than phase scrambled words. There was no preferential representation for linguistic stimuli. In addition, while task response patterns were consistent in showing higher responses for real words, in contrast to the first experiment, there was no correlation between pattern similarity in task vs. rest, and magnitude of response across subjects. Control analyses show a weak correlation with word features like familiarity and

imaginability. Finally, we show that across categories most of the effects are driven by the difference between real word stimuli and artificial (phase scrambled) stimuli.

4.2 Introduction

In previous chapter, we established an approach to compare the multi-vertex resting-state activity pattern and multi-vertex stimuli-evoked activity pattern in laboratory conditions by using categorical visual object stimuli that are prevalent in everyday life. The regions of interest are found in ventral occipito-temporal cortex where strong activations were evoked to specific object categories such as faces (Allison et al. 1994; Kanwisher et al. 1997; Ishai et al. 2000;), body parts (Downing et al. 2001; Grossman and Blake 2002), and places (Aguirre et al. 1998a and 1998b; Epstein and Kanwisher 1998; Ishai et al. 2000). One known categorical-preferential responsive regions not tested in previous chapters is the visual word form area (VWFA), which is consistently activated for word reading (Cohen et al. 2002; Dehaene et al. 2002; Jobard et al. 2003; Cohen and Dehaene 2004). VWFA in human VOTC is located next to the left fusiform face area, and is tuned for visual words across different languages such as Japanese, Chinese, and Roman (Bolger et al. 2005). It was reported that resting state BOLD signals in VWFA correlate with the other core regions of language systems including Wernicke's area, and that the correlation of the BOLD signals between VWFA and Wernicke's area predicts accuracy on a semantic classification task (Stevens et al. 2017). Additionally, Stevens and colleagues reported success in learning a second-language was positively correlated with the connectivity strength between the VWFA and the left middle superior temporal gyrus.

The visual word form is an abstract size-, font-, case-, and position-invariant representation of letter strings that can be only acquired by expert readers through long-term

reading training over years of education (Warrington and Shallice, 1980; Aghababian and Nazir, 2000). It should be emphasized that training alone is not what makes visual words special. Most ecological object categories tested in previous chapters (e.g. face) are also highly trained as their analysis is critical for survival. There is evidence that some face specific mechanisms are genetically determined, as in developmental prosopagnosia (Behrmann and Avidan. 2005), and that they are active early on in life, since babies can smile to faces immediately after birth (Modloch et al. 1999). In contrast, the VWFA is a brain mechanism that is exclusively related to training during development, since the oldest known record of writing system dates to the Babylonians about 5000 years ago; and, that literacy was low until the development of a public education system.

The VWFA region shows increasing responsivity as a function of expertise for reading (Shaywitz et al. 2002; Maurer et al. 2006). VWFA activation is also positively correlated with reading speed accounting for about half of the variability in reading fluency (Dehaene et al. 2010). A recent study by Dehane-Labertz and colleagues showed the activation-based emergence of the VWFA area from longitudinal fMRI scans of 6 years old children during reading acquisition (Dehane-Labertz et al. 2018). They found that children's VWFA, positioned next to the face-selective region, was not specialized early on in recognizing written words, but rather was slightly responsive to tools. As reading training progressed, children's VWFA became selective to written word, while stronger face-selective responses were observed in the right hemisphere homologous region. The authors claimed that an induced reorientation of cortical maps for letter-selectivity during reading acquisition partly replaced selectivity for other categories within the region. VWFA may obtain its functionality through a putative mechanism called "neuronal recycling" (Dehaene 2005). According to the neuronal recycling hypothesis,

human brain organization in its early state is constrained by anatomical neuronal connections shaped through evolutions. This constraint biases subsequent functional development within a region. The circuit, however, is plastic enough to recycle the given biased function onto a novel process such as responsiveness to written words. It has been reported that the location of the developing VWFA in a child at age 8 can be predicted by the connectivity structure of the child at age 5, supporting the idea of neuronal recycling within the initial framework given by anatomical connections (Saygin et al. 2016).

While the above studies support a specific role of the VWFA in the analysis of written word, other studies suggest the VWFA is a more general visual processor (Price and Devlin 2003). Stronger responses for words than consonant strings and false fonts were observed in some studies (Cohen et al. 2002; Baker et al. 2007; Vinckier et al. 2007), however, weaker responses were observed in other studies (Tagamets et al. 2000; Cohen et al. 2003; Xue et al. 2006, Vogel et al. 2012b). For instance, Vogel and colleagues showed that VWFA responds to other high-spatial frequency high contrast stimuli, including line drawings, comparably to words or letter strings (Vogel et al. 2012).

The aim of this study is to reveal correspondences between intrinsic activity and task-evoked activity to highly trained linguistic (e.g. alphabetic letter, consonant string, real word), pseudo-linguistic (false font and false font string), and non-linguistic (phase-scrambled alphabetic letter and phase-scrambled real word) visual stimuli. These visual stimuli are ideal for testing the hypothesis that intrinsic activity is shaped by repeated exposures to specific task patterns. The hypothesis that the VWFA is specifically dedicated to words/letters would predict that these stimuli would be more frequently coded in intrinsic activity than pseudo-words or -letters. On the other hand, if VWFA is a more general processor dedicated to high frequency line

stimuli then we would not expect a difference. However, both linguistic and non-linguistic pseudo-words and -letters should be more frequently coded in this region than phase scrambled stimuli.

In addition to studying regions in visual cortex, we also examined these questions in classical language processing regions, such as Broca's area and superior temporal cortex.

Subjects received resting scans, localizer scans, and task scans. Localizer scans determined the tested ROIs and task scans identified the multi-voxel 'representational' patterns evoked by the different stimulus categories. These representational patterns were then correlated with the multi-voxel patterns measured on each frame of resting-scans. The resulting distribution of correlation coefficients indicated the extent to which resting activity patterns matched stimulus-evoked patterns.

We specifically examined whether resting state multivoxel patterns: 1) corresponded better to multivoxel patterns evoked by linguistic categories (e.g. real word or letters) as compared to consonant strings or false fonts, consistent with a predominant role in processing linguistic material ; 2) corresponded better to line patterns (words, letters, pseudo-words or letters) than non-line patterns (e.g. phase-scrambled real word), consistent with a role in processing high frequency high contrast line stimuli. In addition, we determined whether resting activity patterns correlated with stimulus-evoked patterns coding for individual exemplars, either alphabetic letters or real words, and whether there was a correlation with linguistic properties such as word or letter frequency.

4.3 Methods

The general experimental design structure and analysis methods are analogous to those of the categorical object experiment described in Chapter 2.

4.3.1 Participants

The study included 16 healthy young adult volunteers (11 female; age 19 – 35 years-old) with no prior history of neurological or psychiatric disorders. All participants were right-handed native English speakers with normal or corrected-to-normal vision. All participants gave informed consent to take part in the experiment, and the study was approved by the Institutional Review Board (IRB) of Washington University in St. Louis School of Medicine.

4.3.2 Stimuli

Seven linguistic categories of grey-color images subtending 4^o x 4^o of visual angle were included in event-related 'task' fMRI scans (Fig 4.0). Three categories consisted of the linguistic stimuli that are composed with English characters: single letter, real word, and consonant strings.

24 exemplars of the single letter category consisted of 24 lower case English alphabets in Arial font style. The letter "q" and "z" were not used based on their low lexical frequencies. 24 exemplars of the real word category consisted of six ecological and frequently encountered natural object categories of human-types (e.g. boy and girl), body-parts (e.g. hand), mammals (e.g. dog), tools (e.g. hammer), non-tool objects (e.g. window), and scene-types (e.g. sea). Human-types, body-parts and mammals served as animate categories, and non-tool objects, tools and scene-types served as inanimate categories – matching hierarchical categorical object

representations in human VOTC (Kriegeskorte et al. 2008). The six ecological natural object categories were chosen for the possible investigation of a relationship between previously explored object visual recognition responses (Kim et al. 2019) and categorical semantic responses. Exemplars of the real word category are frequently used visually concrete words. From a large pool of norms of 2,311 nouns (Clark & Paivio, 2004), an initial word selection was made based on three linguistic criteria: imaginability, familiarity, frequency of use by log Kucera–Francis frequency. Imaginability of the word is reported with a 7-point scale, with 1 indicating low scores, and 7, high scores. The initially chosen words have an imaginability score over 5 (some words don't have an imaginability score, reported as 0). Familiarity of the word is reported with a 7-point scale, with 1 indicating low scores, and 7, high scores. The initially chosen words have imaginability score over 5 (some words don't have imaginability score, reported as 0). Among words reached criteria (137 words), 41 categorical words were extracted. These chosen categorical words have mean imaginability of 6.41 ± 0.38, mean familiarity of 6.06 ± 0.61, and mean frequency of use (log Kucera–Francis frequency) of 1.77 ± 0.57. Similar to the categorical representation structure in visual pathways, semantic relationships show a representation structure among words reflecting higher level linguistic cognitive processes. Three parameters (free association strength, latent semantic analysis, and Word2Vec) were applied to analyze semantic structures among the extracted categorical words (Maki et al. 2004; Mikolov et al. 2013; Nelson et al. 2004). Free association strength is an index of relative accessibility of related words in memory scored between 0 and 1, with 0 indicating no free association, and 1, perfect free association (Nelson et al. 2004). Free association strength for all the pairs of the extracted categorical words was determined. Latent semantic analysis (LSA) is a measure of semantic organization based on lexical co-occurrence (Landauer and Dumais, 1997).

The semantic distances (cosine similarity values) based on LSA were determined from WordNet (Maki et al. 2004; Buchanan et al. 2013) For a pair of words, the LSA scored between 0 and 1, with 0 indicating no lexical co-occurrence, and 1, perfect lexical co-occurrence. For example, "Husband" and "Wife" has high lexical co-occurrence and scored 0.87 in LSA. LSA scores for all the pairs of the extracted categorical words were recruited. Word2Vec is an embedding of 300 corpus data as vectors (Mikolov et al. 2013). Each word has a vector of 300 parameters which comes from 300 different corpus, then trained with 2-layer neural networks. By correlating the word vectors, Word2Vec shows the semantic relationship between paired words. Correlation values for all pairs of the extracted categorical words were computed. Four words within a category were chosen based on the averaged value of 3 parameters of word x word associative matrix. Each chosen word is written in Arial font placed on the center of gray background. Because each character (e.g. 'a') had the same size irrespective of the string (e.g. 'cat') in which it appeared, the shortest word width was the 3-character word "cat" while the longest word was the 8-character word "mountain".

24 unpronounceable consonant string exemplars were generated that had the same numbers of characters as the 24 real word exemplars (3 to 8 characters). The consonant string exemplars were generated from the English Lexicon Project by minimizing the number of orthographic neighbors and bigram frequency (http://elexicon.wustl.edu/).

Two control, non-trained linguistic stimulus categories were constructed from the linguistic stimuli used in the experiment. A low-level control consisted of phase-scrambled stimuli that preserved the spatial frequency amplitude spectrum of the linguistic stimulus images. 2D phase scrambled images were generated by applying the same set of random phases to each 2-dimensional frequency component of the original image while keeping the magnitude constant

(Watson et al. 2016). Exemplars from single letter category were 2D phase scrambled, yielding a total of 24 2D phase scrambled single letter stimuli. Similarly, exemplars from the real word category were 2D phase scrambled, yielding a total of 24 2D phase scrambled real word stimuli.

Intermediate-level control images were constructed from false fonts which preserve local visual properties of the linguistic stimulus images such as line segments and connectors. Each 24-alphabet used in the single letter category was transformed into 24 false fonts with the method described in (Grotheer et al. 2016). Simply, local components (up to 4) of a particular character were moved randomly to a different position. Therefore, the local statistics of the original alphabet characters were preserved while the false fonts would not be recognized and processed as the original characters. Additionally, using the above generated false-fonts, 24 false font string images were generated as an intermediate-level control of the real word category. 24 false font string exemplars were generated while having the same numbers of characters as the 24 real word exemplars (3 to 8 characters) and preserving the alphabetical frequencies.

Grey-colored images of exemplars from five categories were included in localizer scans: real words, false font strings, human faces, scenes, and phase scrambled real word images. The categories for the localizer scans differed from the categories for the task scans since the former was only used to define the regions of interest (ROIs).

Stimuli were presented using the Psychophysics Toolbox package (Brainard 1997) in MATLAB (The MathWorks). Stimulus images were projected onto a screen and were viewed through a mirror mounted on the head coil. All stimuli were presented centrally on a gray background. For the linguistic stimuli of Alphabetic single letter (SL), real word (RW), consonant string (CS), false-font (FF), false-font string (FS), phase-scrambled alphabetic single letter (Scr-SL), and phase-scrambled real (Scr-RW), the size of each alphabetical character and

its corresponding control stimuli presented was kept constant across scans. The maximum pixel width of the linguistic stimuli found from the 8-letter real word “mountain”, subtended horizontally 4^{o} of visual angle, and determined the horizontal visual angle of the other stimuli.

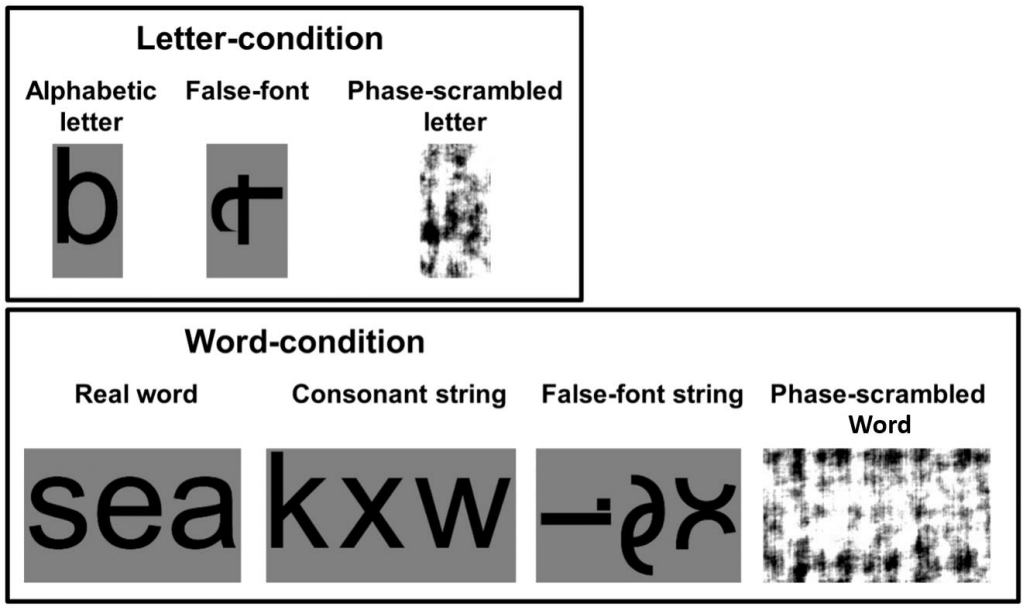

Figure 4.0. Experimental Stimuli.

4.3.3 Scanning Procedure

The study consisted of two separate sessions, each conducted on a separate day. In session one, subjects received 3 resting state runs, 3 localizer runs, and 8 task runs. In session 2, subjects received 2 resting state runs, 3 localizer runs, 8 task runs, and 2 post-task resting state runs.

Resting state runs. Participants received a total of 7 resting state scans, each lasting 5 min (300 TRs). During a scan the participant was asked to maintain fixation on a cross that was displayed at the center of the screen during the entire run. Five resting scans (3 for first session

and 2 for second session) were conducted before any localizer or task scans to collect stimulus-free intrinsic activities. For the second session only, two additional 5 min resting state scans were conducted after the task scans to investigate potential post stimuli-driven effects on intrinsic activity. The results from the post-task resting scans will not be discussed here.

Localizer runs. Each session included 3 localizer runs (6 in total), each lasting 4 min and 20s (260 TRs), and each localizer scan was presented in a blocked fMRI design. Each block of a localizer run contained 20 images of a single category, and those images were different from the images used in the task scans. A fully randomized sequence of eight blocks, consisting of the 5 stimulus categories and a fixation block, was repeated twice within each run. At the beginning and the end of each run, an additional fixation block was presented for 4s and 16s. Within each category block, images were presented for 300ms with an inter-stimulus interval (ISI) of 700ms. A fixation cross was continuously present at the center of the screen during the ISI and during fixation blocks. During category blocks, participants performed a minimally cognitively engaging task by pressing a button if the initially presented image was changed in size or position during the 300ms presentation.

Task runs. Each session included 8 task runs (16 in total), each lasting 4 min and 45s (285 TRs). For each subject and for each run, stimulus presentation order and inter-stimulus intervals were fully randomized using Optseq2 (Dale 1999). Each stimulus presentation lasted for 300ms and the interval between stimuli was jittered between 3.7s and 8.7s. A fixation cross was continuously present at the center of the screen during the ISI. In each category, there were 24 separate exemplars (e.g. 24 different words) and each exemplar was repeated 4 times.

Participants performed a minimally cognitively engaging task by pressing a button if the presented image changed its size or position during a 300ms presentation, the same task as that performed during the localizer scans.

4.3.4 Imaging Parameter

Data were obtained from a Siemens 3T Prisma MRI scanner. Structural images for atlas transformation and lesion segmentation were acquired using T1-weighted magnetization prepared-rapid gradient echo (MP-RAGE) (1 x 1 x 1 mm voxels; echo time [TE] = 2.36 ms, repetition time [TR] = 1700 ms, TI=1000 ms, flip angle = 8°) and T2-weighted fast spin echo sequences (1 x 1 x 1 mm voxels; TE = 564 ms, TR = 3200 ms). FMRI scans were collected using a gradient echo-planar sequence sensitive to BOLD contrast (TE = 26.6 ms, flip angle = 58°, 2.4 x 2.4 x 2.4 mm voxels, 48 contiguous slices, TR = 1.0 s, and multiband factor of 4).

4.3.5 fMRI pre-processing

FMRI data underwent pre-processing as previously described (Siegel et al. 2016). This included: (1) compensation for asynchronous slice acquisition using sinc interpolation; (2) elimination of odd/even slice intensity differences resulting from interleaved acquisition; (3) whole brain intensity normalization to achieve a mode value of 1000; (4) spatial realignment within and across fMRI runs; and (5) resampling to 2.4 mm cubic voxels in atlas space, including realignment and atlas transformation in one resampling step. Cross-modal (e.g. T2-weighted to T1-weighted) image registration was accomplished by aligning image gradients.

Surface generation and processing of functional data followed procedures similar to Glasser et al (Glasser et al. 2013). First, anatomical surfaces were generated for each subject's

T1 MRI using FreeSurfer automated segmentation (Fischl et al. 1999). This step included brain extraction, segmentation, generation of white matter and pial surface, inflation of the surfaces to a sphere, and surface shape-based spherical registration to the subjects' "native" surface to the fs_average surface. The left and right hemispheres were then resampled to 164,000 vertices and registered to each other (Van Essen et al. 2001).

Data were passed through several additional preprocessing steps: (i) removal by regression of the following sources of spurious variance: (a) six parameters obtained by rigid body correction of head motion, (b) the signal averaged over the whole brain (global signal regression), (c) signal from ventricles and CSF, and (d) signal from white matter; (ii) temporal filtering retaining frequencies in the 0.009–0.08-Hz band; and (iii) frame censoring (framewise displacement (FD) $\geq$ 0.5mm). The first four frames of each BOLD run were excluded.

To account for magnitude variability between different task and resting state runs, the BOLD timeseries for each vertex were Z-normalized across time within the task and the resting state runs. This Z-normalization was not applied to the localizer scans. Also, it was not applied to the Task scans for a separate analysis described below in which task-evoked activation magnitudes were determined.

4.3.6 Defining ROIs from localizer activation contrasts

ROIs were defined from univariate vertice-wise statistical contrasts on the localizer activation magnitudes for different categories. For example, word-selective areas were defined from the significant vertices for the contrast of real words minus false font string or scrambled real words. First, spatial smoothing with a Gaussian kernel of 6 mm FWHM was first applied to the minimally pre-processed data to improve signal-to-noise ratio as well as anatomy

correspondence between individuals. Second, for each participant a general linear model (GLM) was applied to their functional localizer scans. The GLM consisted of separate regressors for each stimulus category (e.g. real words) using an assumed hemodynamic response function from the Statistical Parametric Mapping (SPM12), a baseline term, and a linear trend term. Condition contrasts were formed to identify vertices showing preferences for each category: words-preferred (a: real word > false font string, or b: real word > phase scrambled real word), face-preferred (face > scene), scene-preferred (scene > face), and phase-scrambled-preferred (phase-scrambled real word > real word).

A group random-effect statistical Z-map for each contrast was then computed from the single-subject GLMs (see Figure 4.1a for the group z-statistic map for each contrast). The Z-values obtained were sorted in magnitude. From the highest Z-values from the map, the group peak with the next highest Z-value was generated until the Z-value was <= 2.0. Group peaks had to be separated by at least 38.4mm (9.6 mm x 4) in the sphere mesh to prevent a vertex being assigned to multiple ROIs in a subject. ROIs were then defined separately for each participant based on the individual's univariate statistical maps (Oosterhof et al. 2012; Wurm et al. 2016). From each group peak defined above, the corresponding peak for an individual subject peak was defined as the vertex with the highest Z-value within a sphere of 9.6 mm radius centered around the group peak in each subject's sphere mesh. The single-subject ROI was formed from the vertices exceeding Z= 2.0 in a sphere of 9.6 mm radius centered around the peak in the subject's mesh. All ROIs used in following analysis contained at least 150 vertices in at least 14 subjects. ROIs in individual subjects with less than 150 vertices were discarded.

To remove differences in BOLD magnitude across MR frames, for each ROI a z-normalization was applied across the vertices of each frame of the resting and task scans. This

within-frame Z-normalization was not applied to the localizer scans. Also, it was not applied to the Task scans for a separate analysis described below in which task-evoked activation magnitudes were determined (see below, Task scans: multi-voxel activation patterns). We grouped the vertices from the target-preferred ROIs into a single target-preferred joint-ROI. For each joint-ROI, all vertices located in early visual areas (V1 to V3) were excluded (Strappini et al. 2018), as estimated from surface topology using the template created by Benson et al. (Benson et al. 2012). Table 4.1 and Table 4.2 summarize the mean MNI coordinate, mean Z-score for the obtained group peak, and mean number of vertices for all constituent ROIs in each joint-ROI. Figure 4.1b schematically indicates the position of all constituent ROIs in a joint-ROI based on their group-peak locations.

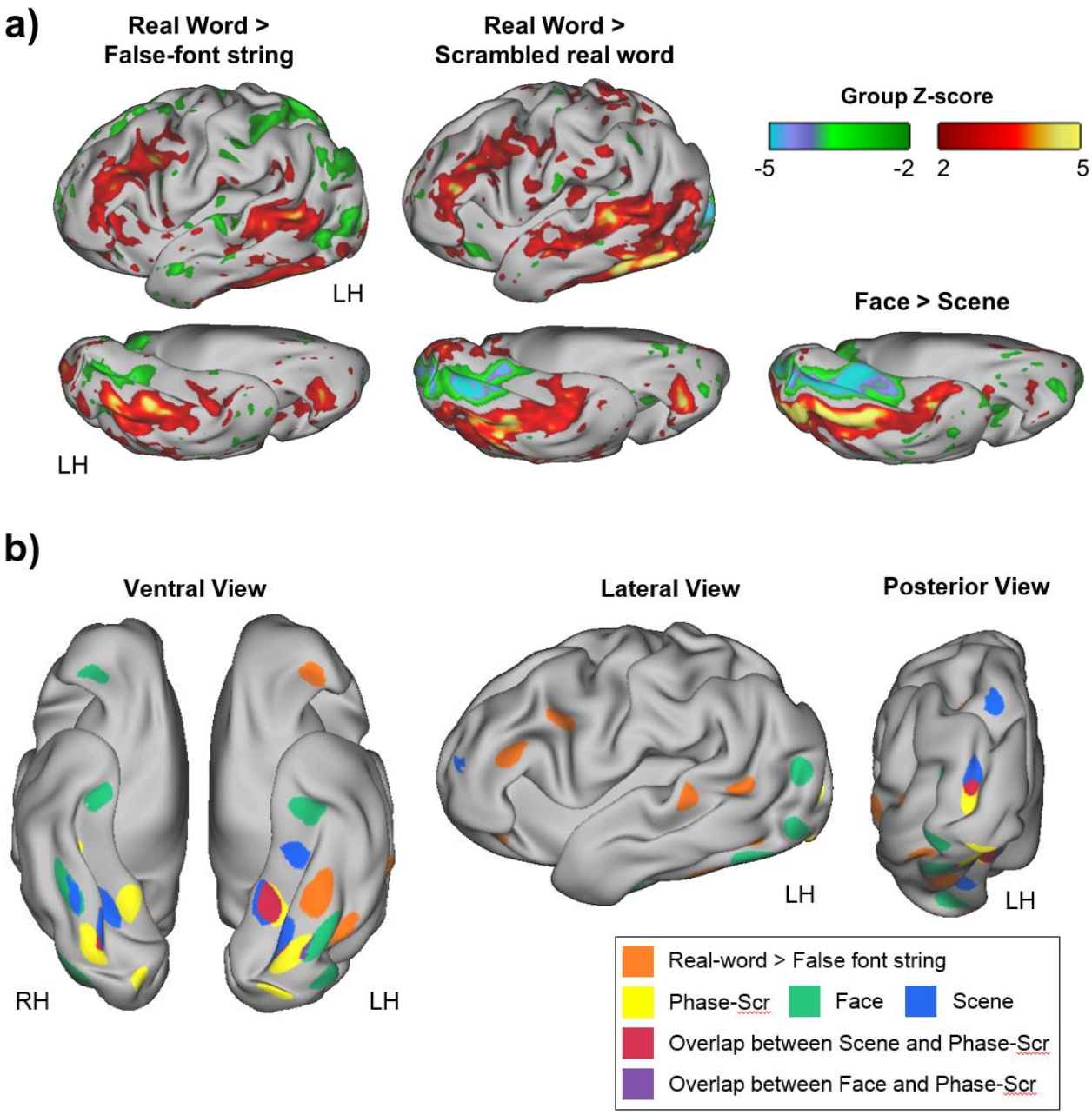

Figure 4.1. (a) Group z-statistic Localizer maps. ROIs were separately defined for individual from their localizer maps using the group foci as a constraint (see Methods, Defining ROIs from localizer activation contrasts). **(b)** Sets of category-preferential ROIs were defined for faces, scenes, real-word, and phase-scrambled real-word. The ROIs in each set were combined into a joint-ROI after excluding regions in V1-V3 as determined from the Benson template (Benson et al. 2012) except for the phase-scrambled ROIs.

Table 4.1 Summary ROI Information for real-word ROIs and phase-scrambled ROIs.

		Mean MNI across subjects				# vertices			
Contrast	Hemisphere	x	y	z	Group Peak Z-value	# Subject	Mean	STD	ROI Name
RW > FS	LH	-31	-46	-17	4.85	14	312	58	
		-36	1	31	4.65	15	271	54	Broca's
		-41	-47	12	4.25	14	240	43	
		-43	24	18	3.96	15	243	51	
		-42	-54	-7	3.76	14	254	44	L-VWFA
		-33	27	-8	3.75	15	228	60	
		-56	-34	6	3.68	14	272	53	
		-26	-49	35	2.87	14	247	71	
		-5	5	50	2.80	14	308	69	
	RH	5	14	51	2.87	14	250	36	
		57	-42	1	2.86	14	284	97	
		36	-48	-16	2.65	14	244	49	
RW > Scr-RW	LH	-39	-60	-12	6.76	16	310	39	
		-47	-37	7	5.12	14	305	41	
		-33	28	-7	4.76	14	255	55	
		-36	17	24	4.73	14	294	49	
		-24	-51	39	4.13	14	283	44	
		-31	-20	-24	4.03	14	313	97	
		-18	-69	36	3.94	15	252	54	
		-36	0	35	3.73	14	241	53	
		-39	-78	2	3.66	16	284	80	
		-44	30	9	3.45	14	213	56	
		-5	15	50	3.07	14	247	70	
		-50	-18	-4	3.07	14	276	71	
		-54	-54	8	2.96	14	243	55	
	RH	40	-62	-2	3.97	14	223	52	
		19	-13	60	3.88	14	266	69	
		41	-51	-14	3.16	14	246	73	
		31	-39	56	2.93	14	240	75	
Scr-RW > RW	LH	-26	-69	-12	7.08	16	322	37	
		-24	-79	8	5.86	16	324	56	
		-21	-45	-4	4.36	14	278	72	
	RH	30	-66	-11	8.36	16	336	39	
		28	-86	4	7.64	16	324	32	
		20	-46	-8	6.43	16	276	37	
		24	-72	18	3.31	14	263	67	
		33	-31	-17	3.12	14	240	61	
		57	-31	14	2.94	14	202	44	
		49	-48	39	2.91	14	262	77	
		8	-65	39	2.77	14	258	77	
		41	-71	22	2.20	14	256	76	

Table 4.2 Summary ROI Information for face and scene ROIs.

Contrast	Hemisphere	Mean MNI across subjects x	y	z	Group Peak Z-value	# Subject	# vertices Mean	STD	ROI Name
Face > Scene	LH	-39	-62	-16	7.84	16	347	34	L-FFA
		-36	-78	-7	7.29	15	341	30	
		-37	-65	14	5.78	16	287	54	
		-32	-16	-25	4.77	15	367	86	
		-36	-4	-12	3.33	14	233	69	
	RH	39	-46	-17	7.57	16	339	36	R-FFA
		40	-81	-8	7.57	16	351	40	
		44	-60	6	5.41	16	339	80	
		29	-12	-29	5.28	14	273	47	
		43	-43	18	4.14	14	337	85	
		9	-51	40	3.47	15	252	66	
		47	-14	-10	3.28	14	236	45	
		29	4	-24	3.15	14	226	57	
		32	27	-9	2.60	14	237	63	
		35	-59	43	2.46	14	266	73	
		5	13	45	2.31	14	226	59	
		39	31	13	2.27	14	226	52	
Scene > Face	LH	-19	-45	-6	8.54	14	250	65	L-PPA
		-21	-60	-10	8.31	14	268	61	
		-27	-82	12	7.79	16	300	49	L-TOS
		-17	-59	41	3.94	14	273	68	
		-28	-28	-17	3.29	14	333	75	
		-35	43	17	2.20	14	214	52	
	RH	28	-47	-4	8.99	14	305	74	R-PPA
		33	-80	18	8.33	16	303	50	R-TOS
		23	-57	44	2.35	14	261	54	
		29	-58	-13	2.21	15	266	55	

4.3.7 Task scans: multi-voxel activation patterns

For each Joint-ROI from each subject, the multi-vertex activation pattern for each of the 96 stimulus presentations for a category in the task scans was estimated via a GLM that included a separate regressor for each stimulus presentation (Fig. 4.2). In addition, the GLM included a target regressor for the trials in which a stimulus was perturbed in size or position, and baseline and linear trend regressors for each scan. Each stimulus regressor was convolved with an assumed hemodynamic response function. The output task β weight matrix was a presentation-

specific stimulus-evoked BOLD multi-voxel pattern of size Np x Nv (Np = 96 presentations by category x 7 stimuli categories & Nv = Number of vertices belong to the joint-ROI).

Two kinds of stimulus-evoked spatial patterns or templates were computed for each category and joint-ROI from the β weight matrix. First, an averaged stimulus-evoked pattern or prototype template was computed by averaging the β weights from all 96 presentations of a category at each vertex of the joint-ROI (red pattern in Fig. 4.2a). Second, as each of the 24 exemplars from each category was repeated four times, a 'homogenous' template was created for each of the 24 exemplars by averaging the β weights from the four presentations of each exemplar (4 instances of single letter 'a' as magenta pattern in Fig. 4.2b). As a control condition, a 'heterogeneous' template was created by averaging the β weights from four different exemplar instances (e.g. single letter 'a', 'c', 'f', and 'g').

In order to determine the mean task-evoked categorical magnitudes, a β weight matrix was separately computed using spatially non-normalized BOLD timeseries from the task scans. The mean task categorical activation magnitude for each category (a vector of size Nc x 1) was computed by averaging the β weight matrix across vertices and presentations within a category.

4.3.8 Determining similarity of resting multi-vertex patterns and stimulus-evoked patterns

For each participant's individual joint-ROI, we determined the degree to which the multi-vertex pattern for a stimulus-evoked template for a category matched the multi-vertex pattern on each resting frame based on derived parameter used in the previous study called the U90-value (Kim et al. 2019). In this procedure, illustrated in Figures 4.2a and 4.2b, framewise intrinsic activity patterns were obtained from independent resting-state scans. Next, for the averaged

stimulus-evoked pattern for a category (e.g. the prototype template for ‘alphabetic single letter’, Fig. 4.2a), the template spatial pattern was spatially correlated with the resting activity pattern on a frame. This procedure was repeated across all resting frames, resulting in a distribution of correlation coefficients (one coefficient per resting frame) for a particular category prototype in a particular joint-ROI. The upper 90% value of each distribution, hereafter termed the U90-value, was then determined.

U90 values were analyzed via repeated measures ANOVAs and paired t-tests. For example, the statistical significance of an overall dependence of U90 values for a joint-ROI on the stimulus category was determined by conducting repeated-measures ANOVAs with Category-Type as factors. Paired t-tests were conducted to test specific contrasts, with a Bonferroni-correction for multiple comparisons. To analyze the local linguistic effect, the above U90 value analysis was additionally repeated for each constituent ROIs of the RW > FS joint ROI.

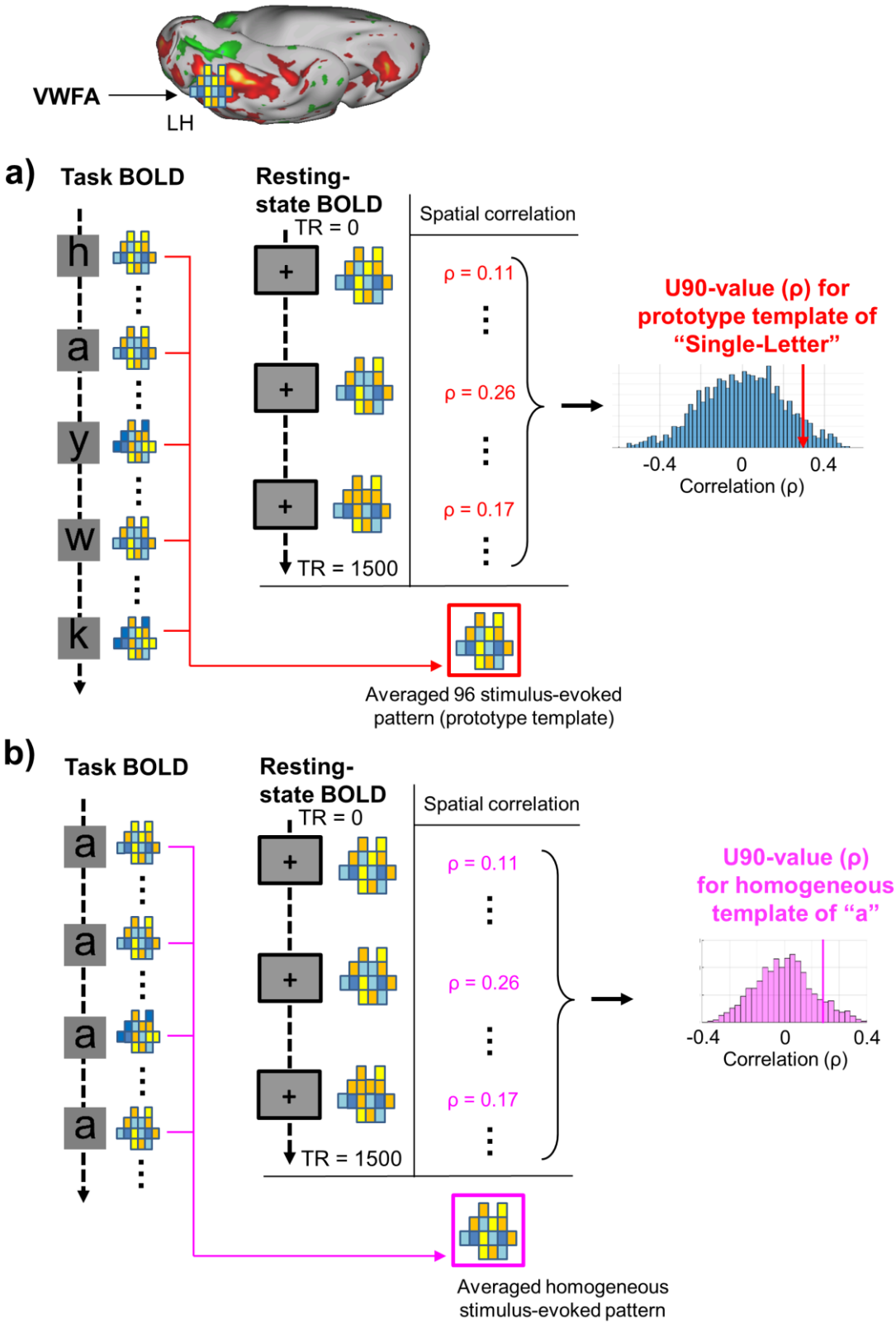

Figure 4.2. (a) Definition of U90-values using a prototype template. At each vertex of each joint-ROI, the β weights for the 96 stimuli from each category were averaged, producing an averaged stimulus-evoked

pattern or prototype template for each category and joint-ROI (e.g. the Alphabetic single letter pattern outlined in red). For each joint-ROI, the spatial correlation between the prototype template and the resting activity pattern on a single resting frame was measured, yielding a spatial correlation coefficient for that frame. This procedure was repeated for all resting-state frames, yielding a distribution of spatial correlation coefficients. The upper 90% value from this distribution, shown by the vertical red arrow, was used as a summary measure of the distribution. **(b)** Definition of U90-values using homogeneous exemplar templates. At each vertex of each joint-ROI, the β weights for 4 stimulus presentation of a single exemplar from a category comprised a homogeneous template for the exemplar (e.g. the magenta pattern represents a homogeneous template for the Alphabetic single letter "a"). For each joint-ROI, the spatial correlation between a homogeneous template and the resting activity pattern on a single resting frame was measured, yielding a spatial correlation coefficient for that frame. This procedure was repeated for all resting-state frames, yielding a distribution of spatial correlation coefficients for the homogeneous template. The upper 90% value from this distribution, shown by the colored vertical line, was used as a summary measure of the distribution for that exemplar.

4.4 Results

The primary goal of the experiment was to compare multi-vertex activity patterns in the resting state to stimulus-evoked activity patterns from linguistic and non-linguistic stimuli. In the main analyses discussed below, 3 types of templates were used: prototype, homogeneous and heterogeneous. Prototype templates were obtained by averaging the β weights for the ninety-six stimulus presentations within a category. Homogeneous and heterogeneous templates were obtained by averaging 4 instances of same and different exemplars within a category. Prototype templates were used to analyze whether a region of interest shows linguistic effects in the multi-vertex activity patterns in the resting state. Additionally, homogeneous and heterogeneous templates were used to analyze whether a region of interest has character-specific or word-specific effects in the resting state.

The stimulus-evoked template for a category, whether a prototype, homogeneous or heterogeneous, was spatially correlated with the activity pattern in an ROI on each resting frame to determine a distribution of correlation coefficients over frames for the category and ROI (Fig.

4.2**)**. The upper 90% value (U90 value) of the distribution was then used as a summary measure of the relationship between the stimulus-evoked and resting patterns like the previous categorical visual objects study (Kim et al. 2019).

4.4.1 U90-values in the real-word preferred (RW > FS) joint-ROI represent line stimuli more than linguistic stimuli.

First, we conducted an analysis that compared U90 values for letter conditions (including 3 stimulus categories of SL: single alphabet letter; FF: false font; and Scr-SL: phase-scrambled single alphabet letter) and word conditions (including 4 stimulus categories of RW: real word; SC: consonant string; FS: false-font string; and Scr-RW: phase-scrambled real word) in the real-word preferred (RW > FS) joint-ROI defined in the localizer scans. The RW > FS joint-ROI contains the regions with the strongest selectivity for visual words, with (ROI #5, Fig.4.4) corresponds to the VWFA. Figure 4.3a left panel shows U90 values for a joint-ROI's linguistic-stimuli (red symbol: SL, RW, and CS), pseudo-linguistic categories (blue symbols: FF and FS), and phase-scrambled category (black symbols: Scr-SL and Scr-RW).

Separate repeated measures analysis of variance (ANOVAs) with all Category (7 levels) as a factor indicated a significant main effect of Category in the RW > FS joint-ROI ($F(6,90) = 2.258$, $p = 0.045$). The ANOVA was re-run separately using only the letter-conditions (3 levels) or the word-conditions (4 levels). There was no significant main effects of Category in the letter-conditions ($F(2,30) = 0.761$, $p = 0.476$). In contrast, there was a significant main effects of Category using the word-conditions ($F(3,45) = 4.048$, $p = 0.013$). Paired two-sample t-tests with Bonferroni corrections showed no difference between Real Words, Consonant strings, or False Font Strings. However, a significant difference was found with Phase scrambled words

(Bonferroni-corrected significance for Consonant Strings and uncorrected significance for Real Words). Therefore, this analysis does not support the idea that intrinsic activity in regions responding preferentially to visual words code preferentially for linguistic stimuli, as compared to non-linguistic (consonant) or line strings (false fonts). However, the higher frequency of resting states coding 'realistic' line stimuli as compared to scrambled line stimuli is consistent with the first experiment on faces, bodies, and scenes.

The previous study of categorical objects demonstrated that the U90 value for a category and joint-ROI was related to the category's activation strength (Kim et al. 2019). Figure 4.3a middle panel shows the mean response for each category in the RW > FS joint-ROI. The β weights for the task response were separately computed from spatially non-normalized task BOLD timeseries. Separate repeated measures analysis of variance (ANOVAs) for the mean categorical activation strength with all category (7 levels) as a factor indicated a significant main effect of Category in the RW > FS joint-ROI ($F(6,90) = 24.785$, $p < 0.0001$). The ANOVA analysis was re-run separately in the letter-conditions (3 levels) and word-conditions (4 levels) as factors. There was significant main effects of Category in both the letter-conditions ($F(2,30) = 10.684$, $p = 3.14e\text{-}4$) and word-conditions ($F(2,30) = 37.212$, $p < 0.0001$). For the letter conditions, there was no difference between real letter and false fonts ($p = 0.2462$ after Bonferroni-correction), while both of them differed from scrambled letters ($p = 0.003$ and $p = 0.012$ after Bonferroni-correction). For the word conditions, the linguistic stimuli (real words and consonant strings) significantly differed from false fonts and scrambled words. These patterns are consistent with the patterns of task activation reported in the literature, and show a difference in linguistic materials for words, and a difference between line like stimuli and phase scrambled stimuli.

However, in contrast to the previous experiment, we did not find a significant correlation across stimulus categories between U90 values and the strength of the activation response. Figure 4.3a right panel shows the correlation coefficient between the U90-value computed from the resting frames and the activation strength for the different letter conditions (SL, FF, and Scr-SL), and word conditions (RW, CS, FS, and Scr-RW). Group one-sample t-tests indicated that the correlation coefficients were not significant for all 3 cases after Bonferroni-correction. This interesting difference suggests that the coding of words in intrinsic activity follows different rules than other stimuli (face, bodies, scenes).

We also ran a series of control analyses to examine other properties of intrinsic activity patterns coding for word like stimuli.

First, we looked at whether task patterns in intrinsic activity for letter or word like stimuli were character-specific or word-specific, or whether more robust patterns of intrinsic activity were obtained for average templates. Accordingly, U90-values for every SL and RW exemplar homogeneous templates were obtained (Fig 4.3b), and were separately tested in ANOVAs with character or word exemplars as a factor (24 levels). The ANOVA showed no significant main effects of Alphabetic characters ($F(23,345)=1.394$, $p<0.1093$), and no significant main effects of word exemplars ($F(23,345)=0.813$, $p<0.7156$). Overall, it appears that the average (prototype) template yields higher U90 values.

Secondly, we were interested in examining if there was a relationship between U90 values in intrinsic activity for individual stimuli and letter/word parameters in the real world. We found a correlation of $r=-0.258$ between U90 values and alphabetic frequencies of SL exemplars in the (RW > FS) joint-ROI. Similarly, we found weak/moderate correlations between U90

values and word-linguist parameters of character-length (r=-0.175), familiarity (r=-0.399), imaginability (r=0.124), and LKFR-frequency (r=-0.214).

Thirdly, we examined if the frequency of task patterns in resting activity varied according to whether the template was homogeneous (averaging same stimulus n=4 across trials) or heterogeneous (averaging n=4 different stimuli). Figure 4.3c shows the within-category averaged U90 values for homogeneous and heterogeneous templates. For the letter conditions, separate repeated measures analysis of variance (ANOVAs) with template-type (homogeneous and heterogeneous) and category (SL, FF, and Scr-SL) as factors yielded a significant main effect of template ($F(1,15)=4.832$, $p=0.044$), no significant main effect of category ($F(2,30)=0.685$, $p=0.512$), and no significant interaction of template-type by category ($F(2,30)=0.9$, $p=0.412$). Similarly for the word conditions, separate repeated measures analysis of variance (ANOVAs) with template-type (homogeneous and heterogeneous) and category (RW, CS, FS, and Scr-RW) as factors yielded a significant main effect of template ($F(1,15)=9.248$, $p=0.008$), a significant main effect of category ($F(3,45)=5.262$, $p=0.003$), and no significant interaction of template-type by category ($F(3,45)=0.049$, $p=0.691$).

The absence of statistically significant effect in the above analyses is consistent with the absence of language specific effects in the real-word preferred (RW > FS) joint-ROI. Because each exemplar was only presented four times, however, the statistical power of homogenous and heterogeneous templates was restricted.

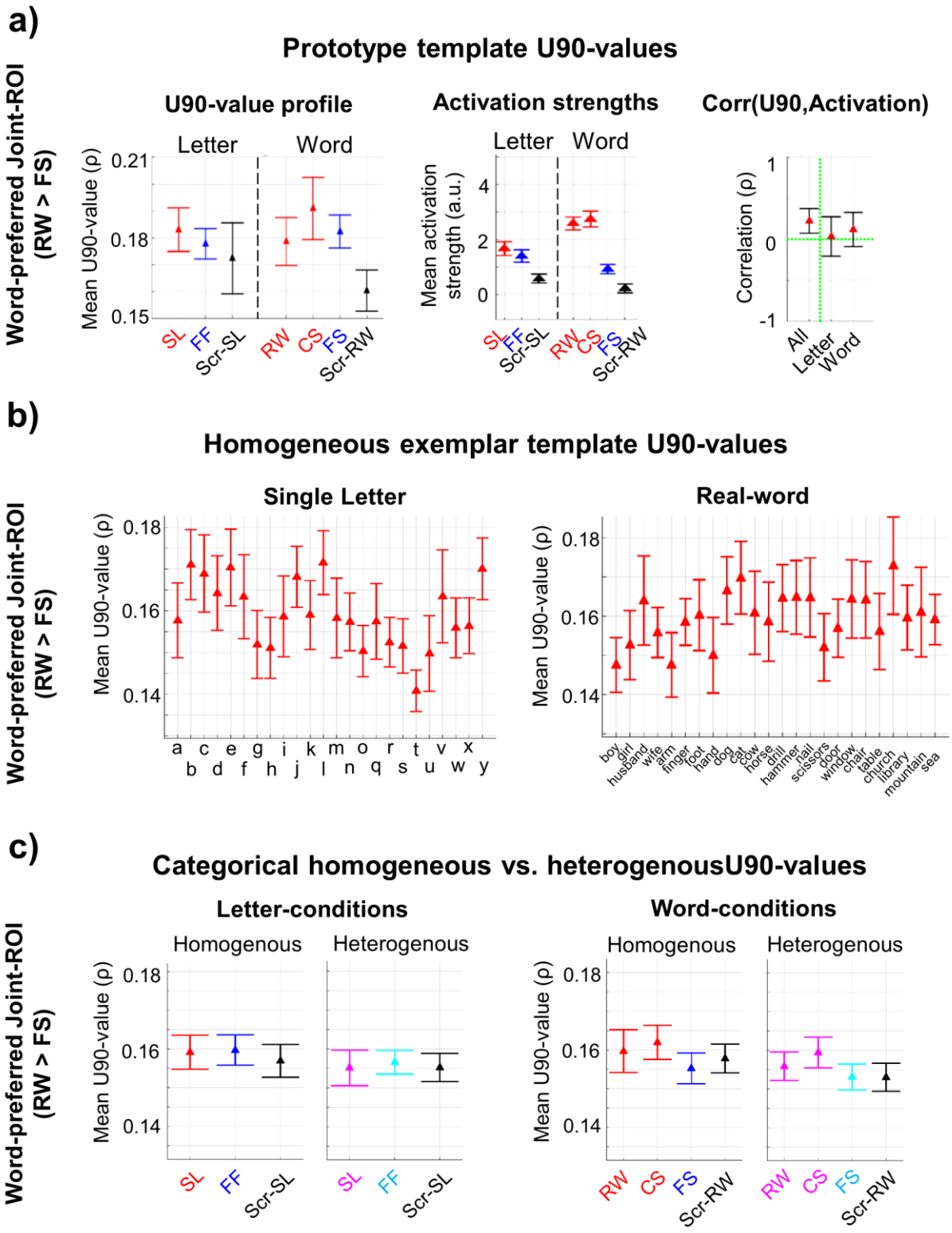

Figure 4.3 (a) The graph plots categorical U90 values (Left Panel) and mean activation strength (Middle Panel) for the joint-ROI's linguistic category (Red symbol), pseudo-linguistic categories (blue symbols), and phase-scrambled category (black symbol). The group-averaged correlation between activation

strengths and U90 values across all categories, letter-condition, and word-condition are plotted (Right Panel). **(b)** The graph plots homogeneous U90 values for the joint-ROI's each Alphabetic single letter (Left Panel) and real-word (Right Panel) exemplar. **(c)** Within-category averaged homogeneous and heterogeneous U90-value across categories are plotted by letter-conditions (Left Panel) and by word-conditions (Right Panel).

4.4.2 No linguistic effects from U90-values in constituent linguistic (RW > FS) ROIs.

The real-word (RW >FS) joint-ROI contains vertices not only from ventral occipito-temporal area, but also from higher-level language processing areas such as Broca's area. To examine the coding of letter and word like stimuli in intrinsic activity, we computed U90 values separately for each ROIs that preferentially responded more strongly to real words than false font strings.

Figure 4.4a shows the six ROIs used to generate the real-word preferred (RW > FS) joint-ROI including the visual word form area (VWFA, ROI #5), Broca's (ROI #2), and Wernicke's area (ROI #3). Figure 4.4b shows categorical U90 values across the different ROIs. ANOVAs using the letter-conditions (3 levels) as levels on the Category factor were significant in ROI #2 (Broca's) and #7 (middle temporal gyrus) (p-value = 0.014 and 0.017). For these two ROIs, two-sample t-tests of SL vs. FF and SL vs. Scr-SL were performed, and significant difference between SL and Scr-SL was found only in ROI #2 only (corrected p-val = 0.033). Similarly, ANOVAs using the word-conditions (4 levels) as levels on a Category factor were significant in ROI #3 (Wernicke's) and #5 (VWFA) (p-value = 0.008 and 0.004). For these two ROIs, two-sample t-tests of RW vs. CS, RW vs. FS, RW vs. Scr-RW, CS vs. FS, and CS vs. Scr-RW were performed. A significant difference between CS and Scr-RW was found in ROI #5 (corrected p-val = 0.034). Figure 4.4c shows the mean correlation coefficient between the ROI's categorical

U90-value and the categorical activation strength in the task across the six local linguistic constituent ROIs by using all 7 categories, letter conditions only, and word conditions only. Group one-sample t-tests were performed across ROIs and conditions yielding no significant correlations after Bonferroni multiple correction.

This analysis shows that a linguistic explanation does not apply to the patterns observed in the resting state. However, several regions of the language network beyond VWFA showed greater U90 values for word like or line segment stimuli than phase scrambled stimuli. The lack of correlation between U90 patterns and task response is confirmed in other individual ROIs, consistent with the joint-ROI analysis.

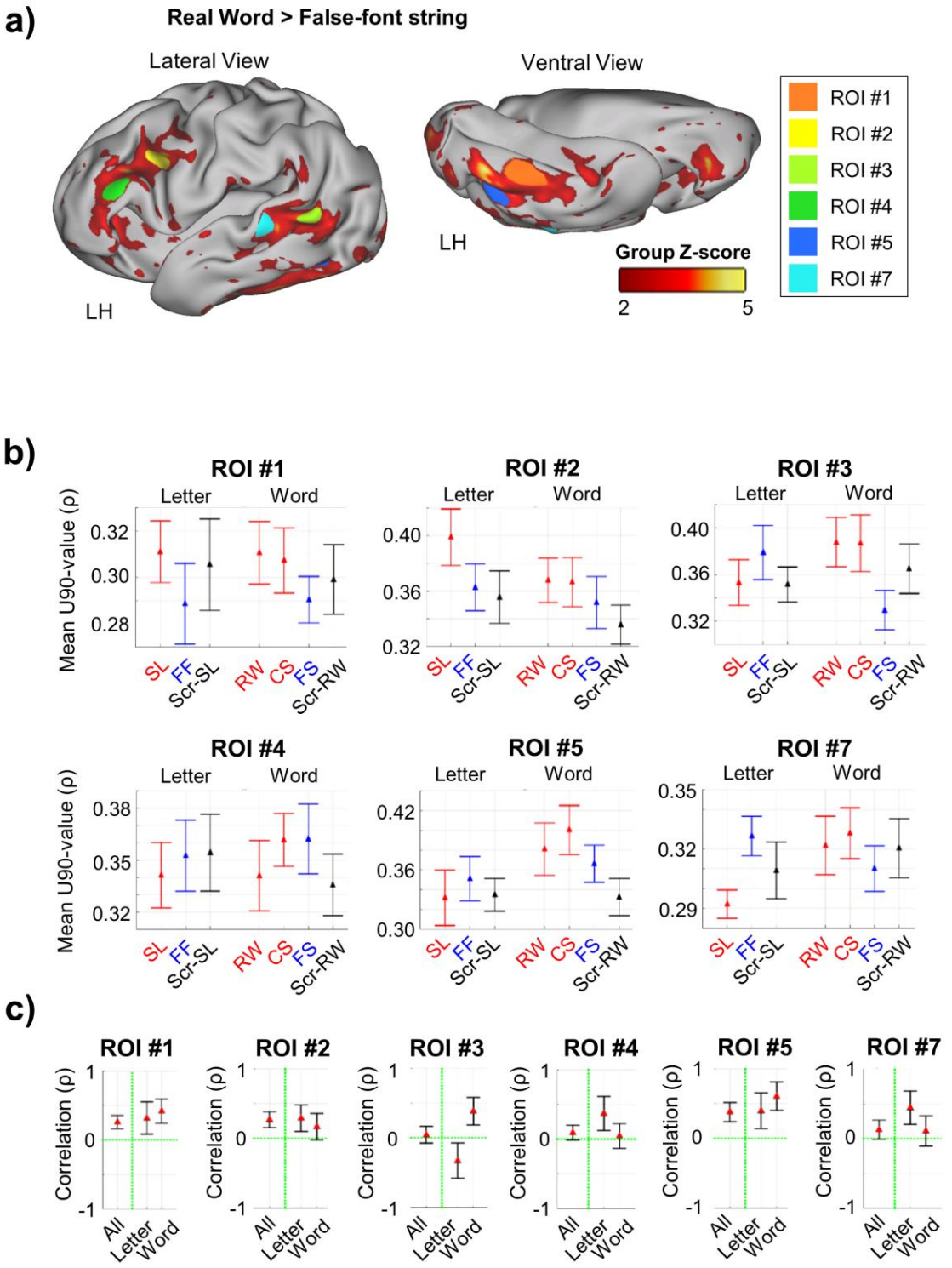

Figure 4.4. (a) Six constituent RW > FS ROIs were schematically shown based on the group locations and group contrast map of RW > FS. **(b)** The graph plots categorical U90 values of linguistic category (Red symbol), pseudo-linguistic categories (blue symbols), and phase-scrambled category (black symbol) for each constituent ROI. **(c)** The group-averaged correlation between activation strengths and U90 values across all categories, letter-condition, and word-condition are plotted for each constituent ROI.

4.4.3 U90-value profiles across different category preferential joint-ROIs shows that differences are driven by phase-scrambled images.

To test for the category selectivity of word like stimuli in resting state activity, we measured the U90 values on letter and word (like) stimuli in 4 sets of joint-ROIs: (1) word category (RW > Phase-scrambled RW); (2) face category (Face > Scene), scene category (Scene > Face), and phase-scrambled (Phase-scrambled RW > RW) based on localizer scan responses. As the linguistic stimuli used in this study were presented with a small visual aperture of about 4o at the center, we expected stronger foveal than peripheral responses. As face specific ROIs also emphasize foveal regions of the visual field, while scene specific ROIs prefer the periphery, (Hasson et al. 2002; Malach et al. 2002) we expected visual stimuli in this experiment to be preferentially represented in more foveal (e.g. face) than peripheral (e.g. scene) ROIs. The face joint-ROI and scene joint-ROI are a set of contrasting ROIs for the foveal vs. peripheral extended-eccentricity organization of the human visual system.

Figure 4.5 shows all 4 joint-ROIs' U90-values profile across stimulus categories (Left Panel), mean activation strength profiles (Middle Panel), and correlation coefficient across categories between the U90-value computed from the resting frames and the activation strength in the task (Right Panel). ANOVAs with all conditions (7 levels) as levels on a Category factor yielded significant effects in the word, face, and phase-scrambled joint-ROIs (p-value = 0.001, 0.001, and 0.014). ANOVAs using only the letter-conditions (3 levels) yielded significant effects in the generic word, face, and phase-scrambled joint-ROIs (p-value = 0.001, 0.001, and 0.048). Finally, ANOVAs using only the word-conditions (4 levels) yielded significant effects in the word and face joint-ROIs only (p-value = 0.001 and 0.001). For the above three joint-ROIs, two-

sample t-tests of SL vs. FF, SL vs. Scr-SL, RW vs. CS, RW vs. FS, RW vs. Scr-RW, CS vs. FS, and CS vs. Scr-RW were performed. Significant differences in letter-conditions were found only for the SL vs. Scr-SL in the generic word and face preferred joint-ROIs (p-value = 0.001 and 0.016 after Bonferroni-correction). Significant differences in word-conditions were found for the RW vs. Scr-RW in the generic word and face preferred joint-ROIs (p-value = 0.005 and 0.048 after Bonferroni-correction) and for the CS vs. Scr-RW in the generic word preferred joint-ROI (p-value = 0.001 after Bonferroni-correction) only. Therefore, no significance differences among linguistic stimuli were found, and all significance differences were driven by the phase-scrambled stimuli set. In other words, the higher frequency of positive and negative matches between resting frame patterns and task-evoked patterns was mainly driven by the difference between real world vs. artificial stimuli. Note also that letter/word like stimuli drive the face and word joint-ROIs, which favor the fovea, but not the periphery-preferring scene joint ROI. In contrast scrambled word/letter stimuli were more represented in early visual regions, as in experiment 1.

The correlation coefficient across categories between the U90-value computed from the resting frames and the activation strength in the task was computed by using all categories, letter conditions only (SL, FF, and Scr-SL), and word conditions only (RW, CS, FS, and Scr-RW). Group one-sample t-tests indicated that the correlation coefficients were significant for all categories in the generic word, face, and phase-scrambled preferred joint-ROIs (p-value = 0.001, 0.001 and 0.029 after Bonferroni-correction), significant for letter-conditions in the generic word and face preferred joint-ROIs (p-value = 0.011 and 0.001 after Bonferroni-correction), and significant for word-conditions in the generic word and face preferred joint-ROIs (p-value = 0.007 and 0.011 after Bonferroni-correction). The significant correlations between categorical

U90 values and mean activation strengths, however, were no longer significant if phase-scrambled control stimuli (Scr-SL and Scr-RW) were excluded. The relationship between categorical U90-values and mean activation strengths from the object study in Chapter 2, therefore, is maintained in this experiment – but the main effect is driven by the phase-scrambled stimuli.

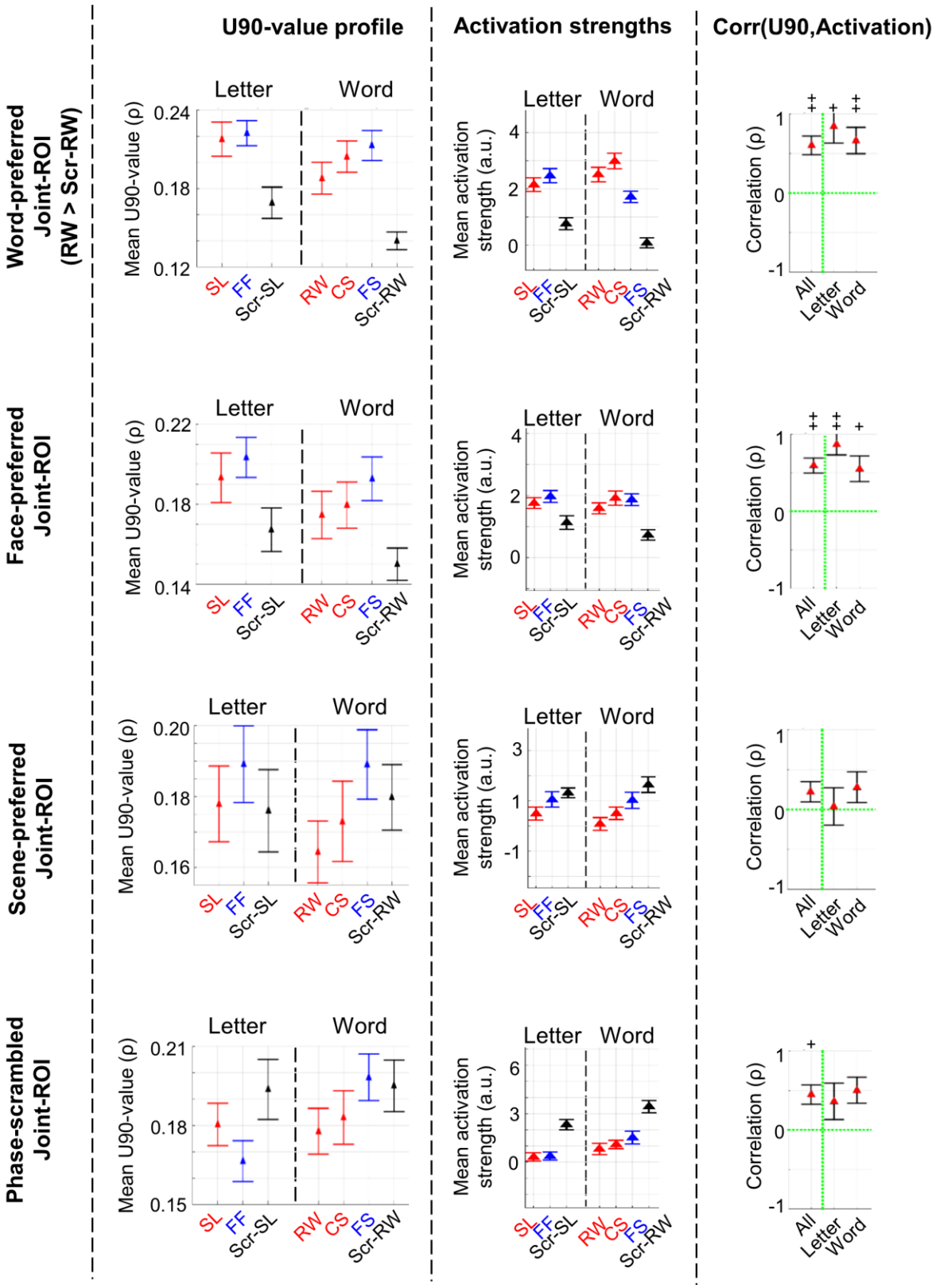

Figure 4.5. The graph plots categorical U90 values (Left Panel) and mean activation strength (Middle Panel) of linguistic category (Red symbol), pseudo-linguistic categories (blue symbols), and phase-

scrambled category (black symbol) for each joint-ROI. The group-averaged correlation between activation strengths and U90 values across all categories, letter-condition, and word-condition are plotted for each joint-ROI (Right Panel). Black symbols indicate the significance of each correlation coefficient, as determined by a group 1-sample t-test (+ = Bonferroni-corrected p-val $\leq$ 0.05; ++ = Bonferroni-corrected p-val $\leq$ 0.005; * = uncorrected p-val $\leq$ 0.05).

4.5 Discussion

The goal of the experiment was to determine the relationship between resting multi-vertex activity patterns and multi-vertex patterns evoked by linguistic and non-linguistic visual stimuli in regions of the language network, particularly the visual-word area in left ventral occipital temporal cortex. To this end, the multi-vertex patterns of the evoked BOLD activity from linguistic stimuli with varying levels of visual word form and corresponding non-linguistic stimuli were correlated with resting multi-vertex patterns in brain regions independently defined using standard localizers. The task-rest correspondence was measured in the U90 parameter that reflects the spread of positive and negative matches with resting activity patterns (Kim et al. 2019).

Linguistic stimuli used in this experiment are 24 alphabetic single letters, 24 real words with 3-8 letters for categorical objects matching to previous object experiment (Chapter 2), and 24 consonant strings. Pseudo-linguistic stimuli used are 24 false-fonts and false-font strings with 3-8 letters corresponding to real-word stimuli. Finally, non-linguistic stimuli used are 24 phase-scrambled Alphabetic single letters and phase-scrambled real words.

Under the hypothesis that task states driven by visual words are sculpted in resting state activity through extensive writing and reading and Hebbian learning, the U90-values across categories are expected to rank in the following orders: Linguistic stimuli > Pseudo-linguistic

stimuli > non-linguistic stimuli. However, an alternative hypothesis posits that the VWFA is a general processor for high frequency high contrast line stimuli. Under this hypothesis, we would predict a strong difference of all line stimuli (word, letters, consonant strings, false fonts) vs. scrambled letters and words. The results are more consistent with the latter hypothesis.

4.5.1 No linguistic-specific visual correspondences at rest

Resting multivoxel patterns in the real-word preferential (RW >FS) joint-ROI containing vertices from language regions were not necessarily related to the patterns evoked by linguistic stimuli since no statistically significant differences in two-sample paired t-tests were found between SL and other letter-type control stimuli and between RW and other word-type control stimuli. Since the previous study of categorical objects demonstrated that the U90 value for a category and joint-ROI was related to the category's activation strength (Kim et al., 2019), the correlation between the categorical U90-value and activation strengths were measured for all letter conditions only (SL, FF, and Scr-SL), and word conditions only (RW, CS, FS, and Scr-RW) in Fig 3a right panel. Group one-sample t-tests, however, indicated that the correlation coefficients were not significant for all 3 cases after Bonferroni-correction.

To rule out the possible contaminations of higher-level linguistic processes, the above analyses were repeated in the constituent linguistic (RW > FS) ROIs. Among the constituent ROIs, the VWFA area was of particular interest since this region, based on the neuronal recycling hypothesis, has reoriented its function for visual word perception from general categorical object perception. Figure 4 shows the categorical U90 values and correlation between the categorical U90 values and the categorical mean activations across different constituent ROIs. Although the VWFA (ROI #5) and Broca's area (ROI #2) appear to show higher U90-

values for linguistic stimuli, statistically significant differences were only found in SL vs. Scr-SL (ROI #2) and in CS vs. Scr-RW (ROI #5). The significant differences between linguistic stimuli and phase-scrambled non-linguistic stimuli agree with the previous demonstrations in object study (Chapter 2) for high-level vs. low-level visual features. The initial assumption of written-word preferred (RW > FS) regions having ranked categorical U90-value based on neuronal recycling hypothesis, however, was not met indicating no linguistic-specific effects were found at rest.

The selectivity of the VWFA for written words has been strongly debated in the literature. Some studies reported stronger responses for words than consonant strings and false font strings in the VWFA (Cohen et al. 2002; Baker et al. 2007; Vinckier et al. 2007) while other studies reported opposite findings (Tagamets et al. 2000; Cohen et al. 2003; Xue et al. 2006, Vogel et al. 2012). Vogel and colleagues showed that VWFA responded to other high-spatial frequency high contrast stimuli including line drawings in similar degree to words or letter strings responses, and claimed that the VWFA is not a specialized region for visual-word form but is rather a general visual processing region (Vogel et al. 2012). Other studies showed that the VWFA is activated by non-word visual stimuli (e.g. pictures) supporting the idea of VWFA region as a general visual processing region (Price and Devlin 2003; Ben-Shachar et al. 2007; Starrfelt and Gerlach 2007; Van Doren et al. 2010; Kherif et al. 2011; Song et al. 2012). The current results, which found no linguistic specific task-rest correspondence, support the hypothesis that the VWFA does not respond selectively to visual word form but responds generally for line drawings.

4.5.2 No character-specific or word-specific effect were found at rest.

Figure 3b describes U90-values for 24 alphabetic single letter exemplars and 24 real-word exemplars to analyze possible character-specific or word-specific effects in the resting state. The one-way ANOVA with all character or word exemplar (24 levels) as a factor did not show any statistical significance.

It has previously been shown greater word frequency is associated with decreasing activations (Kuo et al. 2003; Kronbichler et al. 2004; Schuster et al. 2016). The frequency effect was explained by a "predictive coding" framework: the reciprocal sensorimotor activation that conveys experience-dependent predictions of a stimulus. The higher activation from infrequent words was explained as a larger error signal. Additionally, Schuster et al. (2016) reported that increasing word length is associated with increasing activations due to linked eye movements during reading.

To test for effects associated with various linguistic properties, U90 values were correlated with character-length, familiarity, imaginability, and LKFR-frequency of the RW exemplars and to alphabet frequency. The interpretation of the results is different than in Schuster et al. since the U90-value is a measure of spatial pattern similarity between resting activity patterns and specific word exemplar evoked activity patterns. Under the initial hypothesis of task-rest correspondence, a more frequently experienced stimulus with a higher LKFR-frequency or a higher alphabetic frequency would be shaped more into resting activity patterns, and therefore would be expected to yield a higher U90-value. Against this initial prediction, negative correlations were found between the homogeneous RW exemplar U90-value and the LKFR-frequency and between the homogeneous SL exemplar U90-value and alphabetic

letter frequency. Additionally, negative correlations for character length and for familiarity scores were found.

4.5.3 Phase-scrambled stimuli drive task-rest correspondences mostly.

In Chapter 2, we discovered that resting multivoxel patterns in visual areas were not necessarily related to the patterns evoked by ecological objects but were more related to a region's stimulus preferences for high- or low-level visual features (e.g. Intact-stimuli in high level visual region and phase-scrambled in low-level visual region).

In the current study, figure 4.5 shows all 4 joint-ROIs' U90-values profile across stimulus categories (Left Panel), mean activation strength profiles (Middle Panel), and correlation coefficient across categories between the U90-value computed from the resting frames and the activation strength in the task (Right Panel). From the one-way ANOVA across ROIs and the two-sample paired t-tests across categories and 4 different joint-ROIs, it was shown that significant differences in U90-values are mainly driven by differences between the other stimulus categories and the phase-scrambled control stimuli. Additionally, the complementary foveal-bias vs. peripheral-bias of the extended organization of the human visual system was consistent with the results across different joint-ROIs (Hasson et al. 2002; Malach et al. 2002). Intact-stimuli (both linguistic stimuli and pseudo-linguistic stimuli) were mostly processed in foveal-biased regions, consistent with the acuity demands of readings. The foveal bias for intact-stimuli resulted in higher U90-values for intact-stimuli than phase-scrambled stimuli in the foveal-biased face (Face > Scene) joint-ROI and the generic word preferred (RW > Scr-RW) joint-ROI. In contrast, the phase-scrambled control images (Scr-SL and Scr-RW) showed higher U90-values in the periphery-biased scene (Scene > Face) joint-ROI and phase-scrambled

preferred (Scr-RW > RW) joint-ROI. Therefore, the task-rest correspondences for intact-stimuli vs. phase-scrambled stimuli across joint-ROIs were consistent with the conclusions of the previous study (Chapter 2).

4.5.4 Limitations of the study

First, the linguistic stimuli of the present study were presented in a decidedly non-naturalistic context since only single stimuli were presented in the context of a minimally cognitive engaging detection task. It is possible that the current procedure was not sufficient to evoke the linguistic activation patterns evoked by naturalistic reading; therefore, the finding of no linguistic-specific effects may be misleading.

Second, compared to the previous study of visual categorical object recognition bounded in VOTC (Chapter 2), the current study used word-preferred joint ROIs (RW > FS or RW > Scr-RW) containing different language areas across the entire brain. Since the recruited regions outside of VOTC play a role in higher-level cognitive processing such as semantic processing and integration of different modalities (e.g., sound and visual stimuli), the task-evoked activity patterns measured would be contaminated by those higher-level cognitive processes. However, the main conclusions of the paper were clearly not due to this factor. We separately repeated analyses in the constituent ROIs of the real-word preferential (RW >FS) joint-ROI, and still linguistic-specific effects were not found.

The temporal resolution of the fMRI BOLD signal might limit the power of the spatial similarity measures of task-evoked activity patterns. The activation time-courses for real-words, consonants, and false fonts were identified with fMRI and Magnetoencephalography (MEG) (Thesen et al., 2012). Different activation peaks and profiles were found across categories with

several hundred milliseconds differences across language network regions. Since the time resolution of the current study is TR = 1 second, the activity patterns we obtained might not represent the optimal activity patterns. Additionally, the U90 value measurement came from direct spatial correlations between resting-state activity patterns and task-evoked activity patterns. This simple comparison might not be proper if the task-evoked activity patterns are convolved with hidden layers specific to visual word form due to the induced reorientation of cortical maps. While categorical object recognition is a built-in function (e.g. a baby responds and distinguishes faces), linguistic recognition only happens after long-term training; therefore, the differences between the results for objects in Chapter 2 and linguistic stimuli in the current study may reflect developmental factors.

Finally, because each exemplar was only presented four times, the comparison of homogenous vs. heterogeneous templates was restricted in power. The correlations between U90-values and linguistic parameters (e.g letter type) could be affected by the small sample size for each homogeneous template.

4.6 Reference

Aghababian V, and Nazir TA. 2000. Developing normal reading skills: aspects of the visual processes underlying word recognition. J. Exp. Child Psychol. 76, 123–150

Aguirre GK, Zarahn E, D'Esposito M. 1998. An area within human ventral cortex sensitive to "building" stimuli: evidence and implications. Neuron 21, 373–383

Aguirre GK, Zarahn E, D'Esposito M. 1998. Neural components of topographical representation. Proc Natl Acad Sci USA. 95(3):839-46.

Allison T, McCarthy G, Nobre A, Puce A, Belger A. 1994. Human Extrastriate Visual Cortex and the Perception of Faces, Words, Numbers, and Colors. Cereb Cortex. 4(5):544-54.

Baker CI, Liu J, Wald LL, Kwong KK, Benner T, Kanwisher N. 2007. Visual word processing and experiential origins of functional selectivity in human extrastriate cortex. Proc. Natl. Acad. Sci. USA. 104, 9087–9092.

Benson NC, Butt OH, Datta R, Radoeva PD, Brainard DH, Aguirre GK. 2012. The retinotopic organization of striate cortex is well predicted by surface topology. Curr Biol. 22:2081-2085.

Behrmann M, Avidan G. 2005. Congenital prosopagnosia: face-blind from birth. Trends Cogn Sci. 9(4):180-7.

Bolger DJ, Perfetti CA, Schneider W. 2005. Cross-cultural effect on the brain revisited: universal structures plus writing system variation. Hum Brain Mapp. 25(1):92-104.

Brainard DH. 1997. The Psychophysics Toolbox. Spatial vision. 10(4):433-6.

Buchanan EM, Holmes JL, Teasley ML, Hutchison KA. 2013. English semantic word-pair norms and a searchable Web portal for experimental stimulus creation. Behav Res Methods. 45(3):746-57.

Clark JM, Paivio A. 2004. Extensions of the Paivio, Yuille, and Madigan (1968) norms. Behav Res Methods Instrum Comput. 36(3):371-83.

Cohen L, Lehéricy S, Chochon F, Lemer C, Rivaud S, Dehaene S. 2002. Language-specific tuning of visual cortex? Functional properties of the Visual Word Form Area. Brain. 125(Pt 5):1054-69

Cohen L, Martinaud O, Lemer C, Lehericy S, Samson Y, Obadia M, Slachevsky A, Dehaene S. 2003. Visual word recognition in the left and right hemispheres: anatomical and functional correlates of peripheral alexias. Cereb Cortex. 13:1313-1333

Cohen L, Dehaene S. 2004. Specialization within the ventral stream: the case for the visual word form area. Neuroimage. 22(1):466-76.

Dehaene S, Le Clec'H G, Poline JB, Le Bihan D, Cohen L. 2002. The visual word form area: a prelexical representation of visual words in the fusiform gyrus. Neuroreport. 13(3):321-5.

Dehaene S, Cohen L, Sigman M, Vinckier F. 2005. The neural code for written words: A proposal. Trends Cogn Sci. 9(7):335-41.

Dehaene S, Pegado F, Braga LW, Ventura P, Nunes Filho G, Jobert A, Dehaene-Lambertz G, Kolinsky R, Morais J, Cohen L. 2010. How learning to read changes the cortical networks for vision and language. Science. 330(6009):1359-64.

Dehaene-Lambertz G, Monzalvo K, Dehaene S. 2018. The emergence of the visual word form: Longitudinal evolution of category-specific ventral visual areas during reading acquisition. PLoS Biol. 16(3):e2004103.

Downing PE, Jiang Y, Shuman M, Kanwisher N. 2001. A cortical area selective for visual processing of the human body. Science. 293(5539):2470-3.

Epstein R, Kanwisher N. 1998. A cortical representation of the local visual environment. Nature. 392(6676):598-601.

Fischl B, Sereno MI, Tootell RB, Dale AM. 1999. High-resolution intersubject averaging and a coordinate system for the cortical surface. Hum Brain Mapp. 8:272-284.

Glasser MF, Sotiropoulos SN, Wilson JA, Coalson TS, Fischl B, Andersson JL, Xu J, Jbabdi S, Webster M, Polimeni JR, Van Essen DC, Jenkinson M. 2013. The minimal preprocessing pipelines for the Human Connectome Project. Neuroimage. 80:105-124.

Grotheer M, Herrmann KH, Kovács G. 2016. Neuroimaging Evidence of a Bilateral Representation for Visually Presented Numbers. J Neurosci. 36(1):88-97.

Grossman ED, Blake R. 2002. Brain areas active during visual perception of biological motion. Neuron. 35(6):1167-75.

Hasson U, Levy I, Behrmann M, Hendler T, Malach R. 2002. Eccentricity Bias as an Organizing Principle for Human High-Order Object Areas. Neuron. 34(3):479-90.

Ishai A, Ungerleider LG, Martin A, Haxby JV. 2000. Distributed representation of objects in the human ventral visual pathway. J Cogn Neurosci. 12 Suppl 2:35-51.

Jobard G, Crivello F, Tzourio-Mazoyer N. 2003. Evaluation of the dual route theory of reading: A metanalysis of 35 neuroimaging studies. Neuroimage. 20(2):693-712.

Kanwisher N, McDermott J, Chun MM. 1997. The fusiform face area: a module in human extrastriate cortex specialized for face perception. J Neurosci. 17(11):4302-11.

Kim D, Livne T, Metcalf NV, Corbetta M, Shulamn GL. 2019. Resting multivoxel activity patterns in human visual cortex are linked to patterns evoked by preferred visual stimuli. BioRxiv. doi: https://doi.org/10.1101/518712

Kherif F, Josse G, Price CJ. 2011. Automatic top-down processing explains common left occipito-temporal responses to visual words and objects. Cereb Cortex. 21(1):103-14

Kriegeskorte N, Mur M, Ruff DA, Kiani R, Bodurka J, Esteky H, Tanaka K, Bandettini PA. 2008. Matching categorical object representations in inferior temporal cortex of man and monkey. Neuron. 60:1126-1141.

Kronbichler M, Hutzler F, Wimmer H, Mair A, Staffen W, Ladurner G. 2004. The visual word form area and the fre- quency with which words are encountered: evidence from a parametric fMRI study. Neuroimage. 21:946–953.

Kuo WJ, Yeh TC, Lee CY, Yu Wu, Chou CC, Ho LT, Hung DL, Tzeng OJ, Hsieh JC. 2003. Frequency effects of Chinese character processing in the brain: an event-related fMRI study. Neuroimage. 18:720–730.

Landauer TK, Dumais ST. 1997. A solution to Plato's problem: The latent semantic analysis theory of acquisition, induction, and representation of knowledge. Psychological Review, 104(2), 211-240.

Maki WS, McKinley LN, Thompson AG. 2004. Semantic distance norms computed from an electronic dictionary (WordNet). Behav Res Methods Instrum Comput. 36(3):421-31.

Malach R, Levy I, Hasson U. 2002. The topography of high-order human object areas. Trends Cogn Sci. 6(4):176-184.

Mikolov T, Chen K, Corrado G, Dean J. 2013. Efficient Estimation of Word Representations in Vector Space. Proceedings of the International Conference on Learning Representations (ICLR 2013). arXiv:1301.3781

Modloch CJ, Lewis TL, Budreau D, Mauere D, Dannemiller J, Stephens BR, Kleiner-Gathercoal KA. 1999. Face Perception During Early Infancy. Psychological Science. 10 (5): 419-422

Nelson DL, McEvoy CL, Schreiber TA. 2004. The University of South Florida free association, rhyme, and word fragment norms. Behav Res Methods Instrum Comput. 36(3):402-7.

Oosterhof NN, Tipper SP, Downing PE. 2012. Viewpoint (in)dependence of action representations: an MVPA study. J Cogn Neurosci. 24:975-989.

Price CJ, Devlin JT. 2003. The myth of the visual word form area. Neuroimage. 19(3):473-81.

Saygin ZM, Osher DE, Norton ES, Youssoufian DA, Beach SD, Feather J, Gaab N, Gabrieli JD, Kanwisher N. 2016. Connectivity precedes function in the development of the visual word form area. Nat Neurosci. 19(9):1250-5

Schuster S, Hawelka S, Hutzler F, Kronbichler M, Richlan F. 2016. Words in Context: The Effects of Length, Frequency, and Predictability on Brain Responses during Natural Reading. Cereb Cortex. 26(10):3889-3904.

Shaywitz BA, Shaywitz SE, Pugh KR, Mencl WE, Fulbright RK, Skudlarski P, Constable RT, Marchione KE, Fletcher JM, Lyon GR, Gore JC. 2002. Disruption of posterior brain

systems for reading in children with developmental dyslexia. Biol Psychiatry. 52(2):101-10.

Siegel JS, Ramsey LE, Snyder AZ, Metcalf NV, Chacko RV, Weinberger K, Baldassarre A, Hacker CD, Shulman GL, Corbetta M. 2016. Disruptions of network connectivity predict impairment in multiple behavioral domains after stroke. Proc Natl Acad Sci. 113(30):E4367-76

Song Y, Tian M, Liu J. 2012. Top-Down Processing of Symbolic Meanings Modulates the Visual Word Form Area. J Neurosci. 32(35):12277-83

Starrfelt R, Gerlach C. 2007. The visual what for area: words and pictures in the left fusiform gyrus. Neuroimage. 35(1):334-42.

Strappini F, Wilf M, Karp O, Goldberg H, Harel M, Furman-Haran E, Golan T, Malach R. 2018. Resting-State Activity in High-Order Visual Areas as a Window into Natural Human Brain Activations. Cereb Cortex

Stevens WD, Kravitz DJ, Peng CS, Tessler MH, Martin A. 2017. Privileged Functional Connectivity Between the Visual Word Form Area and the Language System. J Neurosci. 37(21):5288-5297

Tagamets MA, Novick JM, Chalmers ML, Friedman RB. 2000. A parametric approach to orthographic processing in the brain: an fMRI study. J Cogn Neurosci. 12(2):281-97.

Thesen T, McDonald CR, Carlson C, Doyle W, Cash S, Sherfey J, Felsovalyi O, Girard H, Barr W, Devinsky O, Kuzniecky R, Halgren E. 2012. Sequential then interactive processing of letters and words in the left fusiform gyrus. Nat Commun. 3:1284.

Van Doren L, Dupont P, De Grauwe S, Peeters R, Vandenberghe R. 2010. The amodal system for conscious word and picture identification in the absence of a semantic task. Neuroimage. 49(4):3295-307

Van Essen DC, Drury HA, Dickson J, Harwell J, Hanlon D, Anderson CH. 2001. An integrated software suite for surface-based analyses of cerebral cortex. J Am Med Inform Assoc. 8(5):443-59.

Vinckier F, Dehaene S, Jobert A, Dubus JP, Sigman M, Cohen L. 2007. Hierarchical coding of letter strings in the ventral stream: dissecting the inner organization of the visual word-form system. Neuron. 55:143-156.

Vogel AC, Miezin FM, Petersen SE, Schlaggar BL. 2012. The putative visual word form area is functionally connected to the dorsal attention network. Cereb Cortex. 22(3):537-49.

Vogel AC, Petersen SE, Schlaggar BL. 2012. The left occipitotemporal cortex does not show preferential activity for words. Cereb Cortex. 22(12):2715-32

Warrington ET, Shallice T. 1980. Word form dyslexia. Brain. 103:99-112.

Watson DM, Hymers M, Hartley T, Andrews TJ. 2016. Patterns of neural response in scene-selective regions of the human brain are affected by low-level manipulations of spatial-frequency. Neuroimage. 124:107-117.

Wilf M, Strappini F, Golan T, Hahamy A, Harel M, Malach R. 2017. Spontaneously Emerging Patterns in Human Visual Cortex Reflect Responses to Naturalistic Sensory Stimuli. Cereb Cortex. 27:750-763.

Wurm MF, Ariani G, Greenlee MW, Lingnau A. 2016. Decoding Concrete and Abstract Action Representations During Explicit and Implicit Conceptual Processing. Cereb Cortex. 26:3390-3401.

Xue G, Chen C, Jin Z, Dong Q. 2006. Language experience shapes fusiform activation when processing a logographic artificial language: An fMRI training study. Neuroimage. 31(3):1315-26

Chapter 5: Functional connectivity structure in resting-state and during natural vision.

The main results discussed in this chapter has been published as a journal article. The citation is:

Kim D, Kay K, Shulman GL, Corbetta M. (2018). A New Modular Brain Organization of the BOLD Signal during Natural Vision. *Cereb Cortex*, 28(9):3065-3081.

The visual stimuli used in Chapter 2 to 4 are designed specifically for a laboratory environment that does not correspond to realistic ecological environments. In Chapter 5, to overcome this limitation, we use the more naturalistic visual experience of movie-watching and compare the whole-brain FC network structure of movie-watching and of resting-state.

5.1 Abstract

The resting blood-oxygenation-level-dependent (BOLD) signal is synchronized in large-scale brain networks (resting-state networks, RSNs) defined by inter-regional temporal correlations (functional connectivity, FC). RSNs are thought to place strong constraints on task-evoked processing since they largely match the networks observed during task performance. However, this result may simply reflect the presence of spontaneous activity during both rest and task. Here we examined the BOLD network structure of natural vision, as simulated by viewing of movies, using procedures that minimized the contribution of spontaneous activity. We found that the correlation between resting and movie-evoked FC ($\rho = 0.60$) was lower than previously reported. Hierarchical clustering and graph-theory analyses indicated a well-defined network structure during natural vision that differed from the resting structure, and emphasized functional

groupings adaptive for natural vision. The visual network merged with a network for navigation, scene analysis, and scene memory. Conversely, the dorsal attention network was split and re-integrated into two groupings likely related to vision/scene and sound/action processing. Finally, higher-order groupings from the clustering analysis combined internally-directed and externally-directed RSNs violating the large-scale distinction that governs resting-state organization. We conclude that the BOLD FC evoked by natural vision is only partly constrained by the resting network structure.

5.2 Introduction

Recent evidence indicates that spontaneous activity in the brain is not random, as traditionally modeled based on the variability of sensory response to identical stimuli, but is systematically organized as spatial patterns of temporally correlated activity (from neurons to whole brain networks) (Tsodyks et al. 1999; Varela et al. 2001; Fiser et al. 2004; Fox et al. 2005; He et al. 2008; Nir et al. 2008; de Pasquale et al. 2010; Berkes et al. 2011; Brookes et al. 2011; Florin and Baillet 2015). In fMRI studies, for example, the spatial topography of inter-regional temporal correlations (functional connectivity, FC) of the blood-oxygenation-level-dependent (BOLD) signal at rest, i.e. in the absence of any stimulation or task, is well described by a relatively small number of spatio-temporal clusters or networks (so called resting state networks, RSNs). Interestingly, the topography of BOLD RSNs is very similar to the topographies of BOLD task activity evoked by different sensory, motor, and cognitive tasks and the FC measured during those tasks (Biswal et al. 1995; Smith et al. 2009; Mennes et al. 2013; Cole et al. 2014).

One explanation for this task-rest correspondence is that task states have been sculpted into the brain by evolution, development, and experience (Fiser et al. 2004; Albert et al.

2009; Hasson et al. 2009; Lewis et al. 2009; Tambini et al. 2010; Raichle 2011; Petersen and Sporns 2015). On this view, specific tasks represent different subsets of the repertoire of states that the brain explores at rest (Kenet et al. 2003). As a result, the neural activity that enables adaptive behavior during tasks is strongly constrained by the activity observed at rest. However, if similar sources of intrinsic activity are present at rest and during tasks, similar FC matrices will be observed for both states even if task-evoked FC is very different than resting FC. In line with this view, several authors have proposed that rest states represent a default or idling state from which many different task states can be generated through unknown mechanisms (Betti et al. 2013; Spadone et al. 2015). Therefore, the FC from adaptive neural activity, i.e. activity evoked by a task, may be largely unrelated to resting FC. The first but not second view predicts that task and resting BOLD FC will be similar even if the influence of intrinsic activity during a task is removed.

In this study we compared the topography of resting state patterns of functional connectivity to the topography induced by natural vision, as simulated by viewing a series of short movies. Importantly, this comparison occurred after isolating the movie-evoked component free of any ongoing spontaneous or intrinsic activity, insuring that task-rest correspondences did not simply reflect the presence of intrinsic activity during both. One approach to removing intrinsic activity is to average BOLD timeseries across subjects, on the assumption that ongoing spontaneous activity in different subjects is not temporally synchronized. However, Henrikkson et al. reported that the effects of intrinsic activity on representational dissimilarity matrices were only partly removed by averaging BOLD timeseries across subjects (Henriksson et al. 2015). A different approach, called inter-subject functional correlation (ISFC), was recently reported (Simony et al. 2016) (see also Mantini et al. 2012). To compute the functional connectivity

between regions A and B, the BOLD timeseries from region A was averaged over one group of subjects, the BOLD timeseries from region B was averaged over a separate group of subjects, and then the timeseries for regions A and B were correlated.

In the first part of this paper, we show that the ISFC procedure eliminates intrinsic signals more effectively than simple averaging of timeseries across subjects within a group, but that at large sample sizes the two methods yield very similar results. We then use the ISFC procedure to show that the correlation between FC matrices for natural vision and rest is lower than previously reported. This result indicates that BOLD task-rest correspondences have been overestimated due to the common presence of intrinsic activity. Finally, by applying hierarchical clustering and graph-based analyses to the resting and movie-evoked FC matrices, we show that natural vision induces a modular network organization of the BOLD signal that differs from the organization at rest.

5.3 Method

5.3.1 Human Connectome Project (HCP) Data

Seventy participants (28 Male, age 22~35, including pairs of identical twins) were obtained from the Washington University-Minnesota Consortium Human Connectome Project (WU-Minn HCP Data – 900 Subjects + 7T; June 2016) (Van Essen et al. 2012). Blood oxygenation level dependent (BOLD) signals were acquired in two consecutive days of experiments on a 7T scanner (SC72 gradient coil 70 ~ 100 mT/m, Multi-Band factor of 5, TE = 22ms, TR = 1sec, 1.6 mm voxel size) installed at the University of Minnesota (Uğurbil et al. 2013). On the first day, participants were scanned while maintaining fixation on a black screen for 2 scans, each 15 minutes in duration (Resting state). Next, participants were scanned while

watching movie clips for 2 scans, each 15 minutes in duration (Movie task). Each movie watching scan contained 3 to 4 short movie clips with a repeated short clip for validation of possible regression models inserted at the end of each movie session. A twenty second period of fixation on a black screen was inserted prior to the first movie clip, in between movie clips, and following the last movie clip. The same procedure was repeated for the second day. Two of the movie sessions were composed of short clip compilations of 3 Hollywood movies with short intermissions, and the other two movie sessions were composed of short clip compilations of four independent films with short intermissions (see Fig 5.1 for descriptions of movie clips).

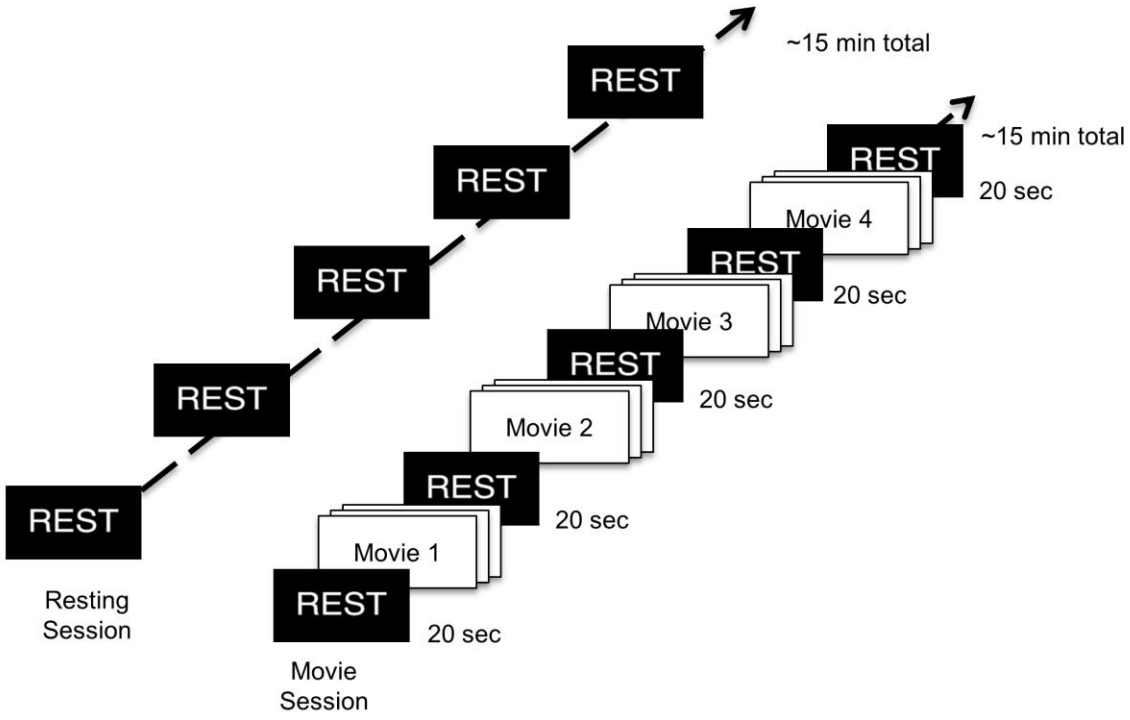

Day 1		Day 2	
Session 1	**Session 2**	**Session 3**	**Session 4**
Two Men (4 min 5 sec)	Inception (3 min 48 sec)	Off the Shelf (3 min 1 sec)	Home Alone (3 min 54 sec)
Welcome to Bridgeville (3 min 41 sec)	Social Network (4 min 20 sec)	1212 (3 min 5 sec)	Erin Brockoviche (3 min 51 sec)
Pockets (3 min 9 sec)	Oceans Eleven (4 min 11 sec)	Mrs. Meyers Clean Day (3 min 25 sec)	Star Wars (4 min 17 sec)
Inside the Human Body (1 min 5 sec)		Northwest Passage (2 min 23 sec)	

Figure 5.1. Human Connectome Project 7T experiment design for resting-state scans and movie scans.

5.3.2 Pre-Processing

Spatial image preprocessing initially followed the HCP minimal preprocessing pipeline, minimizing spatial smoothing and spatial distortion while maximizing alignment across image modalities. The HCP minimal preprocessing pipeline transformed the data from the original resolution to 2 mm resolution into a 91,282 grayordinate space called CIFTI (Glasser et al.

2013). CIFTI grayordinates comprise cortical grey matter surface vertices (both left and right hemisphere, 30k vertices each) and subcortical grey matter voxels (30k voxels). In this study, only cortical grey matter surface vertices of both hemispheres were used.

The BOLD time series then underwent four additional steps. First, the data were normalized by their mean, transforming each timeseries into % BOLD fluctuation, and global signal regression (GSR) was conducted. Second, to minimize the effect of subject motion, BOLD timeseries were censored and corrected using the DVARS measure (temporal derivative of RMS variance), which is highly correlated with frame-wise head-motion displacement (Power et al. 2012). For each subject, approximately 5% of BOLD frames were replaced by interpolating the magnitude values of neighboring BOLD time points.

Third, each subject's BOLD timeseries of cortical grey matter surface vertices (both left and right hemisphere, 30k vertices each) were registered into the Gordon-Laumann parcellation (Gordon et al. 2016), and then averaged across the vertices within a parcel. This procedure resulted in a mean BOLD timeseries for each parcel, reducing 60K timeseries to 324. The 324 Gordon-Laumann parcels are grouped into 13 different resting-state networks (RSN) (see Fig. 5.2): Visual (VIS), Retrosplenial Temporal (RST), Dorsal Attention (DAN), Dorsal Somatomotor (SMd), Somatomotor Mouth (SMv), Auditory (AUD), Cingulo-Operculum (CON), Ventral Attention (VAN), Salience (SAL), Cingulo-parietal (CPN), Fronto-parietal (FPN), Default Mode (DMN), and None. Therefore, use of the mean parcel BOLD time series allowed simple comparisons of the functional topographies between resting state BOLD and movie-watching BOLD while increasing the signal-to-noise ratio of movie-evoked and resting BOLD timeseries.

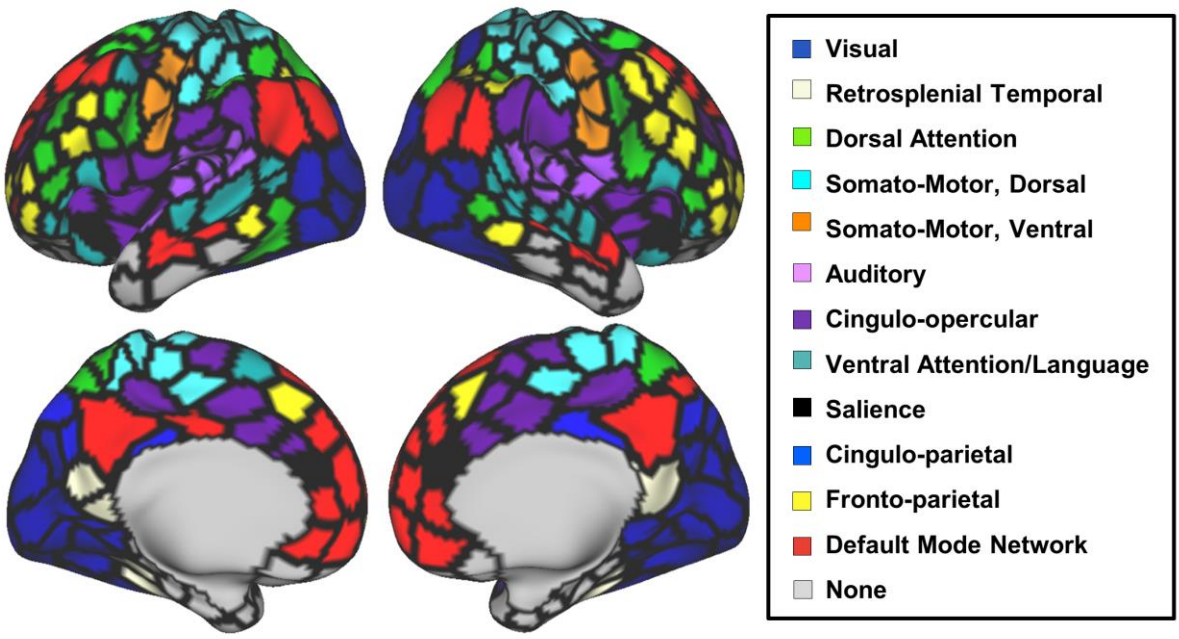

Figure 5.2. Gordon-Laumann Parcellation with 13 resting state networks.

The final processing step was temporal filtering of the mean parcel BOLD timeseries. Since low frequency fluctuations (< 0.1 Hz) account for about 90% of the correlation coefficient between regions, a bandpass filter of 0.008Hz to 0.08 Hz was applied (Cordes et al. 2001). For each movie BOLD time series, the first six seconds from the beginning of each clip within each movie was eliminated to account for hemodynamic lag.

5.3.3 Resting State Functional Connectivity (rs-FC) and Movie Functional Connectivity (m-FC)

BOLD signal time series obtained from different scans were concatenated, and a correlation matrix was computed for each subject by calculating parcel-to-parcel, i.e. pairwise, the temporal correlation (Pearson r) between timeseries. Pearson r-values for individual parcel pairs were converted to Fisher Z-transformed values. A group average resting-state functional

connectivity matrix was obtained by averaging over subjects the individual subject correlation matrices and then transforming the Fisher z-values into Pearson r-values (Fig. 5.3 Left).

5.3.4 Functional Connectivity after temporal averaging: Movie (m-avgFC) and Resting State (rs-avgFC)

Temporal averaging time-locked to specific events is used in neurophysiology to increase signal to noise of stimulus or task evoked activity. Previous work has shown that movie observation leads to highly synchronized signal time series across different subjects, due presumably to consistent phase resets of ongoing spontaneous activity induced by events in the movie (Hasson et al. 2004; Mantini et al. 2012). Therefore, averaging across subjects BOLD time series from a specific parcel prior to computing functional connectivity should lead to suppression of correlations due to intrinsic activity and subject-specific movie-evoked activity, and should enhance the correlation due to movie-evoked activity shared across subjects. We computed parcel-to-parcel FC matrices on group averaged BOLD signal time series in the resting state (rs-avgFC) and during the movie (m-avgFC) (Fig. 5.3 Middle). The prediction is that movie FC should reflect predominantly movie-related activity shared across subjects, whereas resting state FC should show weak or no correlation because intrinsic activity should not be synchronized across subjects.

5.3.5 Inter-subject Functional Correlation (ISFC)

The effectiveness of temporal averaging in removing effects of intrinsic activity on FC was compared to that of a second method, “Inter-Subject Functional Correlation (ISFC)”, which was recently introduced by Simony et al. (2016) (see also Mantini et al. 2012). Subjects were

evenly and randomly split into two groups. For each parcel, the BOLD signal time series were averaged across the subjects within each group. Then a parcel-by-parcel pairwise functional connectivity matrix was computed between groups. The computed FC was not symmetric at this point since the correlation coefficients of paired region A and B were computed as:

ρAB, upper diagonal = correlation between the BOLD(region A, group1) and BOLD(region B, group2).

ρBA, lower diagonal = correlation between the BOLD(region A, group2) and BOLD(region B, group1).

To keep the conventional unidirectional connectivity characteristic of FC, symmetricity in ISFC was imposed by averaging upper diagonal values and lower diagonal values. By randomly permuting 50 times the subjects assigned to each group, 50 FC matrices were obtained. The r-values of the 50 matrices were converted to Fisher Z-transformed values, the 50 matrices were averaged, and the values of the averaged matrix were converted from z-values back to r-values (Fig. 5.3 Right). ISFC matrices were computed for both resting state and movie-evoked timeseries.

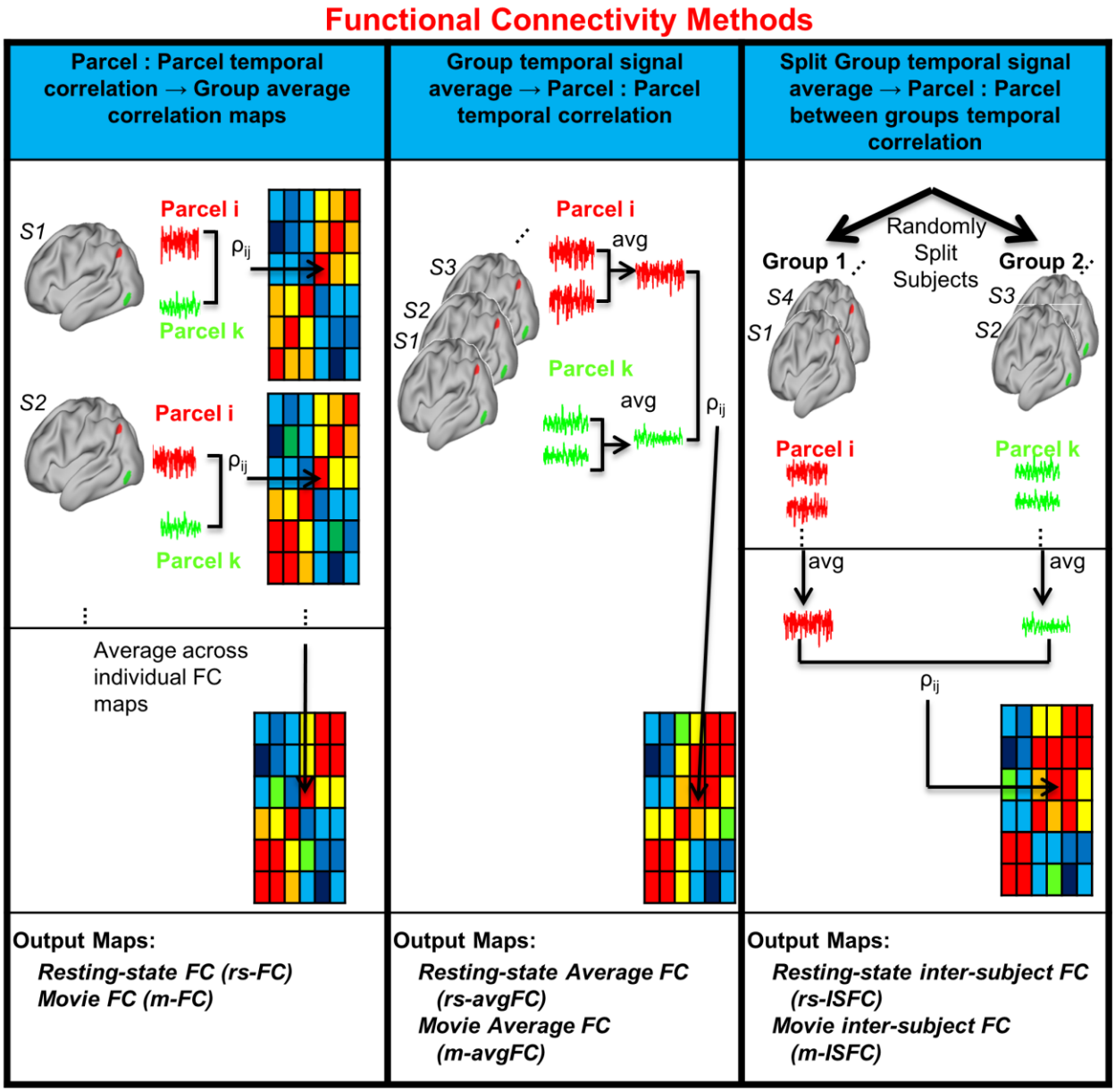

Figure 5.3. **Three methods for computing functional connectivity matrices. Left)** Resting state functional connectivity (rs-FC) and movie FC (m-FC) group correlation matrices were generated by averaging individual correlation matrices that were computed from pairwise, parcel-to-parcel BOLD temporal correlations. **Middle)** For both movie and resting-state conditions, the BOLD time series for each parcel was first temporally averaged across subjects. Then group m-avgFC and rs-avgFC matrices were calculated from pairwise, parcel-to-parcel BOLD temporal correlations. **Right)** In the ISFC method, subjects were randomly split into two groups. Within a group, the BOLD time series for each parcel was first temporally averaged across subjects. Then, a group FC matrix was computed by correlating, for each pair of parcels, the parcel time series from one group with the parcel time series from the other group. This procedure was repeated fifty times with different random groupings of subjects, and the resulting FC matrices were averaged to produce the final group m-ISFC and rs-ISFC matrices

5.3.6 Statistical analysis of time-series correlations

The statistical significance of each observed correlation was accessed by a permutation procedure based on surrogate data (Simony et al. 2016). Phase-randomized surrogate BOLDs time series of equal mean and autocorrelation to the original signal were obtained. The phase-randomization was computed by rotating the phase $\phi(f)$ by an independent random variable $\varphi(f)$ which was uniformly chosen in the range of $[0, 2\pi)$ (Prichard and Theiler 1994).

For the orthogonality test, null distributions of both maximum noise correlation values and minimum noise correlation values were obtained via repeated generations (1,000) of surrogate BOLD signals (Resting state, movie-evoked, and movie-residual). FWER were controlled by a threshold (R*) at the q*100th percentile of the null distribution of maximum values. The thresholds for each condition are given above in each case (all for $q<0.005$), along with the % significant ROI-pairs out of the 52326 possible ROI-pairs.

For each surrogate resting-state BOLD and movie-BOLD, all FC maps (rs-FC, rs-avgFC, rs-ISFC, m-FC, m-avgFC, and m-ISFC) were computed, then the maximum noise correlation values and the minimum noise correlation values for each FC map were obtained. By repeating the above procedure 5,000 times, null distributions of the maximum noise correlation values and the minimum noise correlation values were obtained for each FC map. Family-wise error rate (FWER) was controlled by a threshold (R*) at the q*100th percentile of the null distribution of maximum values ($q = 0.005$). Since separate thresholds were applied for positive and negative values, the FWER was 0.01, two-tailed.

5.3.7 Data-driven FC network reorganization

The Resting state (rs-FC) and movie-evoked (m-ISFC) FC matrices generated above were organized in terms of the pre-defined RSNs. To analyze the network organization of the resting state and movie-evoked state, three different unsupervised, data-driven analyses were conducted.

First, hierarchical clustering methods were implemented. Resting state (rs-FC) and movie-evoked (m-ISFC) FC matrices were converted to dissimilarity matrices by calculating a dissimilarity index (1 – Pearson's r for paired parcels). A hierarchical clustering analysis, applied to each matrix, yielded an FC dendrogram (Connolly et al. 2012; Cauda et al. 2013; Riedel et al. 2015). The number of clusters (detected communities) were determined by the Davies-Bouldin index (DBI), which determines the optimal number of clusters (Davies and Bouldin 1979). FC matrices were then re-ordered based on the hierarchical clustering results.

Second, resting state FC (rs-FC) and movie-evoked FC (m-ISFC) were reorganized into communities by implementing the Louvain community detection algorithm (Blondel et al. 2008) from the Brain Connectivity Toolbox (Rubinov and Sporns 2010) for varying threshold edge densities (4~20%). Due to the randomized initialization procedure, each run of algorithm resulted variations in detected communities. To account these variations, 10,000 runs of Louvain algorithms were conducted for each FC maps. For each parcel, the most frequently assigned community throughout the entire iterations was chosen. For the network modularity measurement, the average modularity across runs of algorithm was used. To evaluate the stability of communities, Newman's Q modularity (Newman 2004) was evaluated based on both newly detected communities (unsupervised) and pre-defined RSNs (supervised). The values of modularity ranges between 0 (community is no better than random connection) and 1 (strong

community structure) while the modularity of typical networks with a strong modular structure ranges from 0.3 to 0.7 (Newman and Girvan 2004). Since movie-evoked FC (m-ISFC) was an averaged map of 50 different permutations of split subjects, the modularity scores were assessed for each permutation. Similarly, the modularity scores of resting state FC (rs-FC) were assessed from 50 different permutations of rs-FC generated from 35 randomly chosen subjects. To test for a difference in mean modularity scores between rs-FC and m-ISFC, a cluster-based nonparametric test with a p-value of 0.0001 was performed (Maris and Oostenveld 2007) as follows:

1) Collect trials of the two experimental conditions (the modularity scores of rs-FC and m-ISFC in all permutations).

2) Draw a combined dataset that had two subsets of randomly assigned modularity scores.

3) Calculate the difference in mean modularity scores between subsets.

4) Repeat above steps 2 and 3 1,000,000 times to construct a histogram of the difference in mean modularity scores.

5) Calculate a p-value based on the proportion of random partitions that resulted in a larger test statistic than the observed one.

Finally, resting state FC (rs-FC) and movie-evoked FC (m-ISFC) were visualized with spring embedded models that were computed using a 4% threshold edge density. Similarly, communities defined from hierarchical clustering and Louvain community detection algorithms were visualized with spring embedded models.

5.4 Results

5.4.1 Orthogonality of movie-evoked and resting BOLD signals

We first checked that group-averaged BOLD signals evoked by the movie were orthogonal to intrinsic signals, since otherwise removing one signal would partly remove the other.

Two different methods were used to test orthogonality. In the first, we averaged the movie BOLD timeseries from 35 subjects (group 1) to get a stable estimate of the movie-evoked BOLD timeseries. We then correlated this group 1 timeseries with the resting-state timeseries of each subject from a different group of 35 subjects (group 2). The correlation between the Group 1 (average) and Group 2 (single subject) timeseries was on average, essentially zero with a small standard deviation across group 2 subjects (correlation coefficient: μ = -6.32e-4 and σ = 0.041). A non-parametric permutation test with family error wise correction for the significance of the computed FC (Simony et al. 2016) indicated no significant ROI-pairs (threshold R* = -0.289 and 0.288).

In a second analysis, we again averaged the movie BOLD timeseries from 35 subjects (group 1) to get a stable estimate of the movie-evoked BOLD timeseries. For each subject in a different group of 35 subjects (group 2), we subtracted the group 1 timeseries from the movie timeseries for that group 2 subject to yield a residual timeseries. The residual timeseries contained subject-specific movie-evoked BOLD signals and intrinsic signals, with at most a small contribution from movie-evoked signals. We then correlated the residual timeseries for that group 2 subject with the group 1 average movie-evoked timeseries. The correlation between the two timeseries was on average, essentially zero with a small standard deviation across group 2

subjects (correlation coefficient: μ = -0.003 and σ = 0.057). A total of 0.31% of significant ROI-pairs were found (threshold R* = -0.282 and 0.282).

The above analyses show that the group movie-evoked BOLD signal is orthogonal to the resting state and movie-residual BOLD signals. We also conducted two tests of the orthogonality of different resting-state timeseries. In the first analysis, we correlated the resting BOLD timeseries across runs within a subject. The correlation between two timeseries was on average, essentially zero with a small standard deviation across subjects (correlation coefficient: μ = -0.001 and σ = 0.060), and no significant ROI pairs were found (threshold R* = -0.292 and 0.291). In a second analysis, we correlated the resting-state BOLD timeseries from different subjects for a given run. Again, the correlation between the two timeseries was on average, essentially zero with a small standard deviation across subjects (correlation coefficient: μ = -4.16e-4 and σ = 0.041). No significant ROI-pairs were found (threshold R* = -0.217 and 0.221).

5.4.2 The influence of intrinsic activity on network synchronization during natural vision

Because the BOLD signal measured during movie viewing includes both intrinsic fluctuations and movie-evoked fluctuations (Fox et al. 2006; Becker et al. 2011), pure movie-evoked patterns of inter-regional signal synchronization can only be isolated after removing the fluctuations due to intrinsic activity. We tested two procedures for accomplishing this.

Figure 5.4a shows the group resting FC matrix (rs-FC), which was computed by averaging across subjects the single-subject FC matrices formed from the correlations between BOLD timeseries for all pairs of parcels from the Gordon-Laumann parcellation (see Fig. 5.3, left panel). The rs-FC matrix shows the characteristic block structure along the diagonal that

highlights different resting state networks (RSNs). A nonparametric test (FWER p=.01, two-tailed) indicated that 84.7% of ROI-pairs in the rs-FC matrix were significant. Figure 5.4d shows the group movie FC matrix (m-FC), similarly computed by averaging of single-subject FC matrices computed from the BOLD timeseries during movie viewing. A nonparametric test (FWER p=.01, two-tailed) showed that 82.0% of ROI-pairs in the m-FC matrix were significant. The spatial correlation between the resting and movie FC matrices was very high, 0.87, replicating the correspondence between task and rest FC previously reported (Cole et al. 2014). However, this correspondence may have reflected the common influence of intrinsic activity. To compute pure movie-evoked FC, we averaged the BOLD time series from different parcels over subjects before computing the FC between parcels (see Fig. 5.3 middle panel). Since fluctuations of intrinsic activity vary in time from subject to subject, inter-subject averaging of BOLD time series should reduce the magnitude of intrinsic BOLD variation to near zero, leaving only the components that are time-locked to events in the movie. The movie-evoked FC after inter-subject averaging (m-avgFC) is shown in Figure 5.4e. A nonparametric test (FWER p=.01, two-tailed) showed that 38.2% of ROI-pairs in the m-avgFC matrix were significant. The spatial correlation between resting and movie-evoked matrices was only 0.63, much less than the previous correlation (0.87), consistent with a reduction of the large contribution of intrinsic activity.

To test whether the inter-subject averaging procedure completely removed the effect of intrinsic activity on FC, we applied the same procedure to the resting state data. After inter-subject averaging, each parcel's BOLD timeseries showed only small variations around zero, as expected (not shown). Nevertheless, as shown in Figure 5.4b, the resulting FC matrix (rs-avgFC) was almost identical to the original resting FC matrix, with a spatial correlation of 0.95. Therefore, the influence of intrinsic activity on the topography of movie-evoked FC was not

fully removed by inter-subject averaging of parcel BOLD time series. This result is consistent with a recent report that averaging of BOLD time series during natural image viewing is insufficient to remove intrinsic fluctuations (Henriksson et al. 2015). A nonparametric test (FWER p=.01, two-tailed) showed that 13.6% of ROI-pairs in the rs-avgFC matrix were significant.

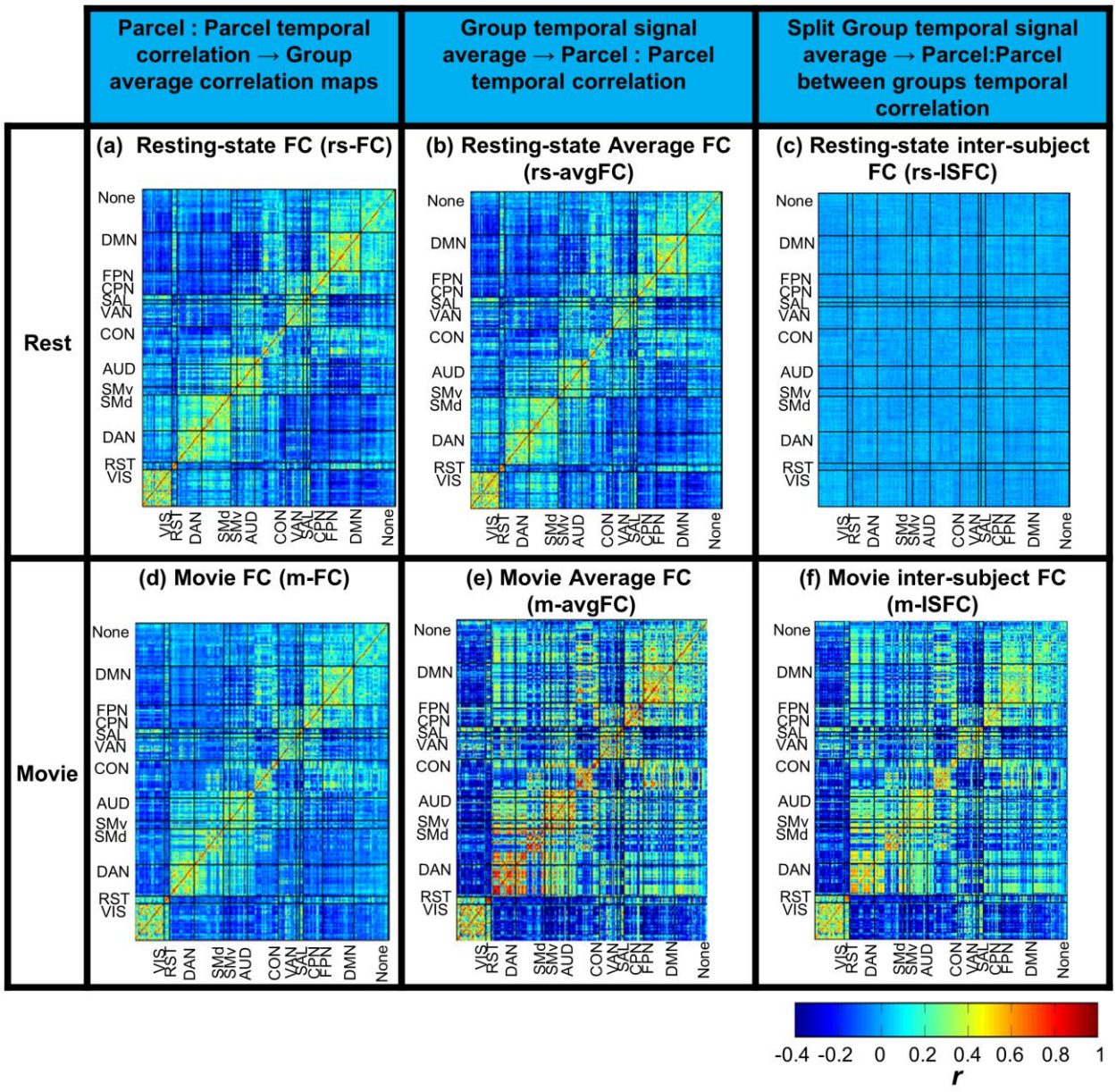

Figure 5.4. Functional connectivity matrices for rest and natural vision generated by three methods. FC matrices for both resting state BOLD and movie-watching BOLD were computed using the methods

shown in Figure 5.3. **(a)** Resting-state FC (rs-FC), **(b)** Resting-state average FC (rs-avgFC), **(c)** Resting-state inter-subject functional correlation (rs-ISFC), **(d)** Movie FC (m-FC), **(e)** Movie average FC (m-avgFC), and **(f)** Movie inter-subject functional correlation (m-ISFC).

5.4.3 Inter-subject functional correlation effectively removes the influence of intrinsic activity

We tested a second procedure for removing intrinsic activity called "Inter-Subject Functional Correlation" (ISFC) (see Fig. 5.3 right panel), which was recently introduced by Simony et al. (2016). Briefly, the method involves the same assumption as the first method, namely that intrinsic activities are uncorrelated across subjects. However, intrinsic activity is removed by correlating the BOLD time series for two parcels across two groups of subjects rather than within the same group. First, subjects were randomly split into two groups. Then, the BOLD time series for each parcel was averaged within each group, similar to the inter-subject averaging procedure of the first method, resulting in a relatively stable estimate of the movie activity for each parcel. Note, however, that since data from only half of the subjects were used to compute the average timeseries in a group, the parcel timeseries for the ISFC method had lower signal-to-noise than the timeseries computed using the inter-subject averaging method. In the final step of the ISFC method, we computed the FC between two parcels by correlating the averaged time series for the first parcel from one group with the averaged time series for the other parcel from the other group. This correlation step was repeated for all pairs of parcels to derive a complete FC matrix. The same procedure was then repeated over many iterations using different assignments of subjects to the two groups. A final ISFC matrix was computed by averaging the matrices generated from each iteration.

The FC matrix computed by applying the ISFC procedure to the resting-state scans (rs-ISFC) is shown in Figure 5.4c. No structure is evident, with the correlations tightly grouped around zero (mean correlation ρ = 3.57e-4, σ = 0.03, max ρ = 0.12, min ρ = -0.13). A nonparametric test (FWER p=.01, two-tailed) showed that no ROI-pairs in the rs-ISFC matrix were significant. Moreover, the spatial correlation between the rs-ISFC matrix and the original resting-state matrix (rs-FC) was only 0.10. These results indicate that the effects of intrinsic activity on FC were more fully removed by the ISFC than inter-subject averaging procedure.

Finally, we computed movie-evoked FC using the ISFC procedure (Fig. 5.4f, m-ISFC), allowing us to determine pure movie-evoked FC free of any influence from intrinsic activity. The overall topography of the m-ISFC matrix was very similar to that of the m-avgFC matrix. A nonparametric test (FWER p=.01, two-tailed) showed that 61.2% of ROI-pairs in the m-ISFC matrix were significant. Correspondingly, the correlation between the m-ISFC and rs-FC matrices was 0.60, only slightly less than the correlation (0.63) between the m-avgFC and rs-FC matrices. Therefore, the ISFC and inter-subject averaging methods produced very similar movie-evoked FC matrices, even though they produced very different resting FC matrices. The reasons for this discrepancy are considered in the discussion.

5.4.4 Inter-subject averaging was more contaminated by intrinsic activity when FC was computed from fewer subjects

The preceding section demonstrated that the ISFC method more fully removed the influence of intrinsic activity during movie-watching than the inter-subject averaging method. We next determined the effectiveness of each method as a function of the number of subjects

used to compute the FC matrices, since as a practical matter, large datasets may not be routinely available.

Spatial correlations between different FC matrices as a function of the number of subjects are illustrated in Figure 5.5. The effectiveness of the ISFC procedure in removing intrinsic activity is depicted in Figure 5.5a. Regardless of sample size, the spatial similarity of the rs-FC and rs-ISFC matrices was quite low (Fig. 5.5a, green), indicating that the rs-ISFC matrix contained no resting network structure. Conversely, the spatial similarity of the rs-FC and rs-avgFC matrices was quite high for all sample sizes (Fig 5.5a, blue), indicating that resting network structure was preserved in spite of the averaging of resting timeseries across subjects.

Figure 5.5b compares the similarity of the topography of intrinsic activity during rest (rs-FC) with the topographies during movie-watching in which intrinsic activity was left in (m-FC), was putatively removed by averaging timeseries over subjects (m-avgFC), or was putatively removed by computing FC between subjects (m-ISFC). Regardless of sample size, resting FC was highly correlated with movie FC when intrinsic activity was not removed (Fig. 5.5b, blue). Averaging of timeseries across subjects reduced rest-movie correlations (Fig. 5.5b, green), with an effect that increased signal-to-noise (movie-evoked activity to intrinsic activity) ratio at larger sample sizes, as expected. However, even at the largest sample size, the correlation of resting and movie FC was lowest with the ISFC procedure (Fig. 5.5b, red). The slight increase in the spatial similarity of the rs-FC and m-ISFC matrices (Fig. 5.5b, red) with sample size likely reflected a corresponding increase in the SNR for each parcel timeseries, as discussed above. Because this effect appeared to asymptote by the largest sample size, however, it likely does not explain the residual difference between the correlations of rs-FC with m-avgFC vs. m-ISFC. Overall, the ISFC procedure was the most effective at removing intrinsic activity and performed

well at all sample sizes. For large sample sizes, the averaging and ISFC methods yielded similar results for movie-evoked FC, but not resting FC.

The spatial similarity of the movie FC matrices computed using the three methods of Figure 5.3 was evaluated in Figure 5.5c. The high spatial correlation values between m-ISFC and m-avgFC showed that the overall topography of m-ISFC was very similar to that of m-avgFC, particularly when a sufficient number of subjects were sampled (Fig. 5.5c, red). Finally, the reliability of the ISFC procedure is shown in Figure 5.5d. The spatial correlation between m-ISFC from only 10 random subjects and m-ISFC from all 70 subjects was high (Fig. 5.5d, red), indicating that the topography of pure movie-evoked FC was captured with small samples.

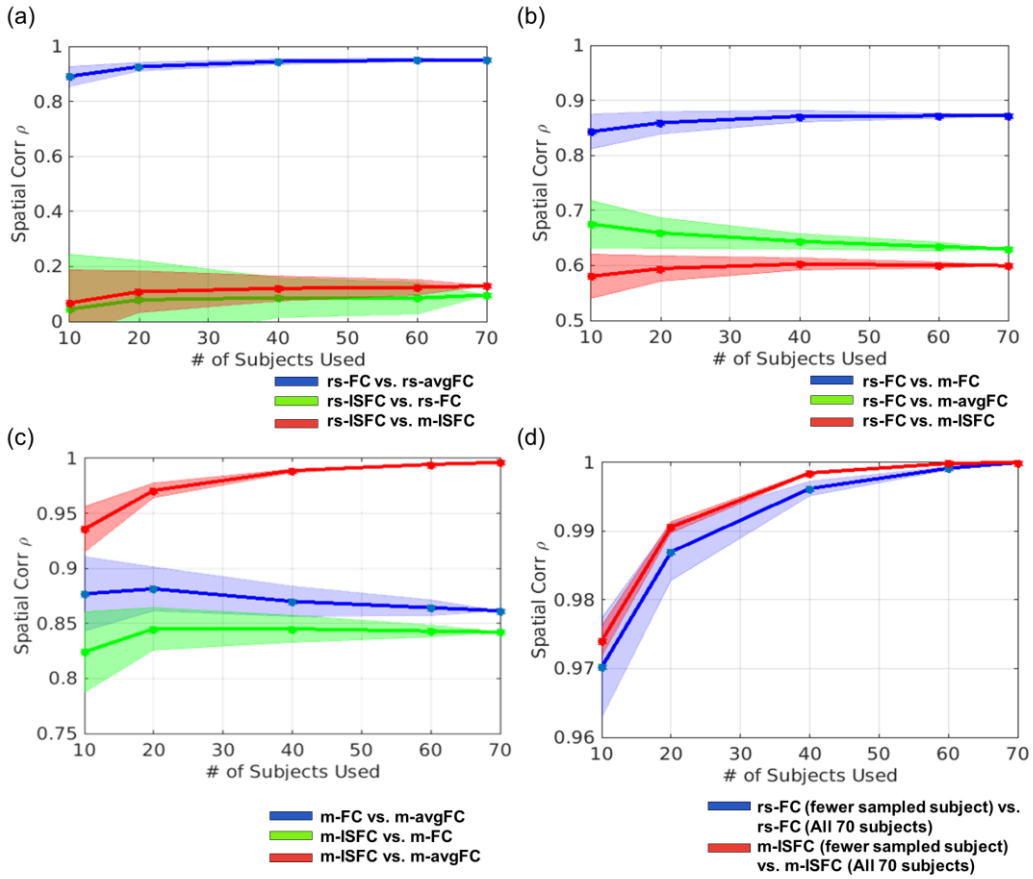

Figure 5.5. Spatial correlation of FC matrices as a function of sample size. (a) Correlation of resting-state FC (rs-FC) with resting-state average FC (blue) and resting-state inter-subject FC (green), and

correlation of rest and movie inter-subject FC (red), with 95% confidence intervals. **(b)** Correlation of resting-state FC (rs-FC) with movie FC (m-FC, blue) movie average FC (m-avgFC, green) and movie inter-subject FC (m-ISFC, red) , with 95% confidence intervals. **(c)** Correlation of movie FC matrices that were computed using the three methods of Figure 5.3, with 95% confidence intervals. **(d)** FC matrices based on all 70 subjects were compared to matrices of the same type computed from fewer subjects (rs-FC, Blue; m-ISFC, red), with 95% confidence intervals.

5.4.5 Effect of number of BOLD MR frames on the similarity of rest and movie FC matrices

Resting and movie FC matrices are more accurately estimated as more BOLD frames are analyzed (Laumann et al. 2015). We evaluated how the spatial correlation between rs-FC and movie FC matrices depended on epoch length (number of BOLD frames) (Fig. 5.6). For example, we analyzed 5 independent BOLD data sets (both movie and rest), each consisting of 500 BOLD frames, yielding 5 rs-FC, 5 m-FC, 5 m-avgFC, and 5 m-ISFC matrices. The spatial correlation among the rs-FC and movie FC matrices was computed for each of the 25 possible combinations and then averaged. Figure 5.6 shows the correlation coefficient between resting and movie FC matrices as a function of the epoch length. For all movie FC matrices, the correlation with the rest FC matrix increased with epoch length, consistent with previous work (Laumann et al. 2015).

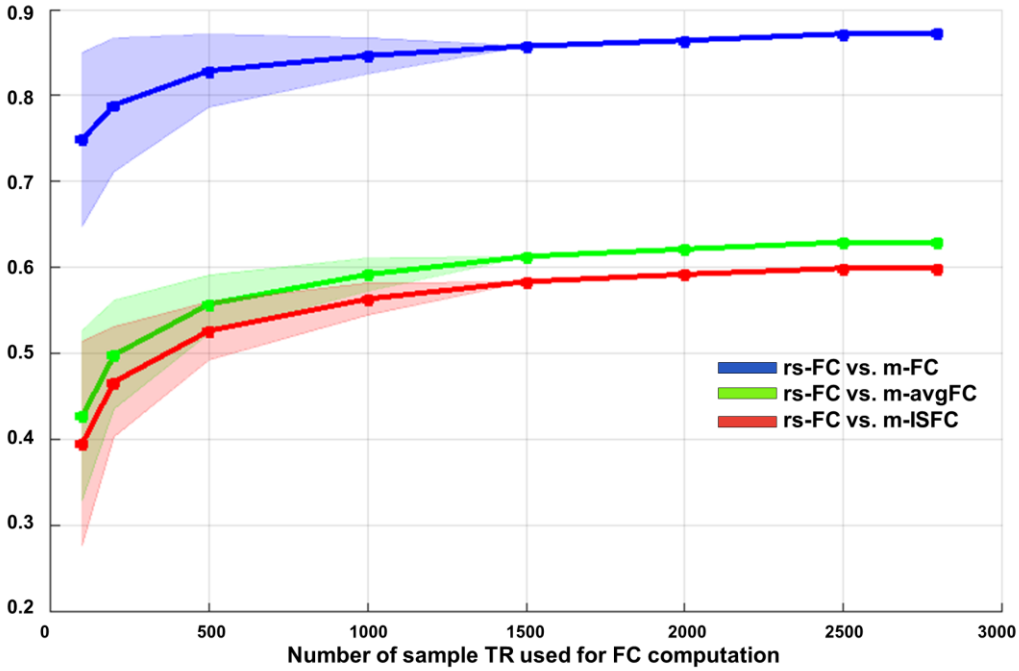

Figure 5.6. Correlation coefficient between resting and 3 movie FC matrices as a function of the epoch length.

5.4.6 Consistency of reductions in task-rest similarity across movies

The similarity of task-evoked and resting FC matrices was substantially reduced when the effects of intrinsic activity on movie FC were eliminated using the ISFC procedure. We next determined whether this reduction was consistent across the movies in the HCP dataset, which differed widely in content (including Hollywood movies, documentaries, commercials, and independent movies (Figure 5.1). Consistency would suggest that the reduction in similarity did not depend on the details of the cognitive processes engaged by each movie.

Movie FC matrices (m-FC and m-ISFC) were computed for each of twelve movies that lasted at least 3 minutes (see Figure 5.1). The spatial correlation of each movie matrix with the resting FC matrix (rs-FC) was then measured (see Table 5.1). The similarity of individual m-FC matrices to the resting FC matrices varied over a small range ($\mu = 0.80$, $\sigma = 0.032$), as did the

similarity of m-ISFC matrices ($\mu = 0.48$, $\sigma = 0.028$). The lower spatial correlation value of each individual movie matrix to the resting matrix relative to the original aggregate analysis, reflected the smaller number of BOLD frames that were analyzed for each movie (e.g. for the individual m-ISFC matrices the mean correlation was 0.48 while in the aggregate analysis the correlations was 0.60; see previous section, Effect of number of BOLD MR frames on the similarity of rest and movie FC matrices) Importantly, all twelve movies showed a substantial reduction in task-rest similarity when intrinsic activity was removed (see bottom row, Table 5.1). Therefore, the large decreases in task-rest similarity after the removal of intrinsic activity generalized over the individual movies within the HCP dataset, indicating that the reduction did not depend on the detailed content of the movies.

Table 5.1. Spatial correlations of individual clip m-FC between rs-FC, spatial correlations of individual clip m-ISFC between rs-FC, and its differences.

	Clip1	Clip2	Clip3	Clip4	Clip5	Clip6	Clip7	Clip8	Clip9	Clip10	Clip11	Clip12	μ	σ
m-FC	0.79	0.85	0.84	0.73	0.80	0.83	0.82	0.77	0.80	0.80	0.79	0.81	0.80	0.032
m-ISFC	0.46	0.52	0.47	0.50	0.46	0.48	0.49	0.48	0.43	0.53	0.48	0.49	0.48	0.028
Difference	0.33	0.33	0.37	0.23	0.34	0.35	0.33	0.29	0.37	0.27	0.31	0.32	0.32	0.040

The movie FCs (m-FC and m-ISFC) were computed for each of twelve movies that lasted at least 3 minutes (see Figure 5.1 and below list), then measured its spatial correlations to the rs-FC. The mean and standard deviation of task-rest similarity across movies, as well as the reduction in task-rest similarity following the removal of intrinsic activity were measured.

Clip 1: Two Men
Clip 2: Welcome to Bridgeville
Clip 3: Pockets
Clip 4: Inception
Clip 5: Social Network
Clip 6: Oceans Eleven
Clip 7: Off the Shelf
Clip 8: 1212
Clip 9: Mrs. Meyers Clean Day
Clip 10: Home Alone

Clip 11: Erin Brockoviche
Clip 12: Star Wars

5.4.7 Different patterns of functional interactions during rest and natural vision

Since the ISFC procedure effectively removed the influence of intrinsic activity on FC, we next considered the relationship between FC during rest and natural vision. The spatial correlation between the m-ISFC and rs-FC matrices was 0.60, lower than the 0.87 correlation between the m-FC and rs-FC matrices. Because the influence of intrinsic activity was removed, however, this residual similarity reflected signals generated from entirely different sources, i.e. intrinsic vs movie-evoked activity.

During movie-watching (Fig. 5.4f) the functional connectivity of individual regions, relative to rest, was selectively increased or decreased with other regions in the same network, and particularly with other regions in different networks, resulting in a heterogeneous m-ISFC matrix. We statistically evaluated these within-network and between-network FC changes from rest to natural vision by measuring the mean and variance of the FC of region pairs within and across the standard resting networks. In Figure 5.7a (movie) and Figure 5.7b (resting), the diagonal and off-diagonal cells show, respectively, the mean FC of parcel pairs within each network and between each pair of networks. Figure 5.7c indicates the difference in mean FC between movie and rest, with cells showing a significant difference in mean FC displayed in color. Statistical significance was determined by t-tests over the different inter-regional FC values within a network or across networks, with a p-value of 0.05 after Bonferroni correction for multiple comparisons (a total of 78 comparisons, comprising the diagonal and upper-diagonal

cells of the FC matrix and excluding the ’none’ category). Figures 5.7d, 5.7e, and 5.7f show the analogous matrices for the variance of FC, with significance determined by F-tests.

Not counting the cells involving the ‘none’ category, 60.3% of the cells (47/78) showed significant differences between rest and movie in mean FC, including both increases (e.g. DAN FC) and decreases (e.g. DAN-VIS FC) in FC from rest to movie. Significant mean effects were observed in 33.3% (4/12) of within-network and 65.2% (43/66) of between-network cells. Significant differences in variance were more common overall, occurring in 79.5% (62/78) of cells, and in all cases reflected increased variance during the movie. Non-significant effects often involved networks that contained relatively small numbers of regions (e.g. CPN, SAL). Significant variance effects were observed in 66.7% (8/12) of within-network cells and 81.8% (54/66) of between-network cells. Therefore, significant differences in both mean FC and variance occurred in a higher percentage of between-network than within-network cells.

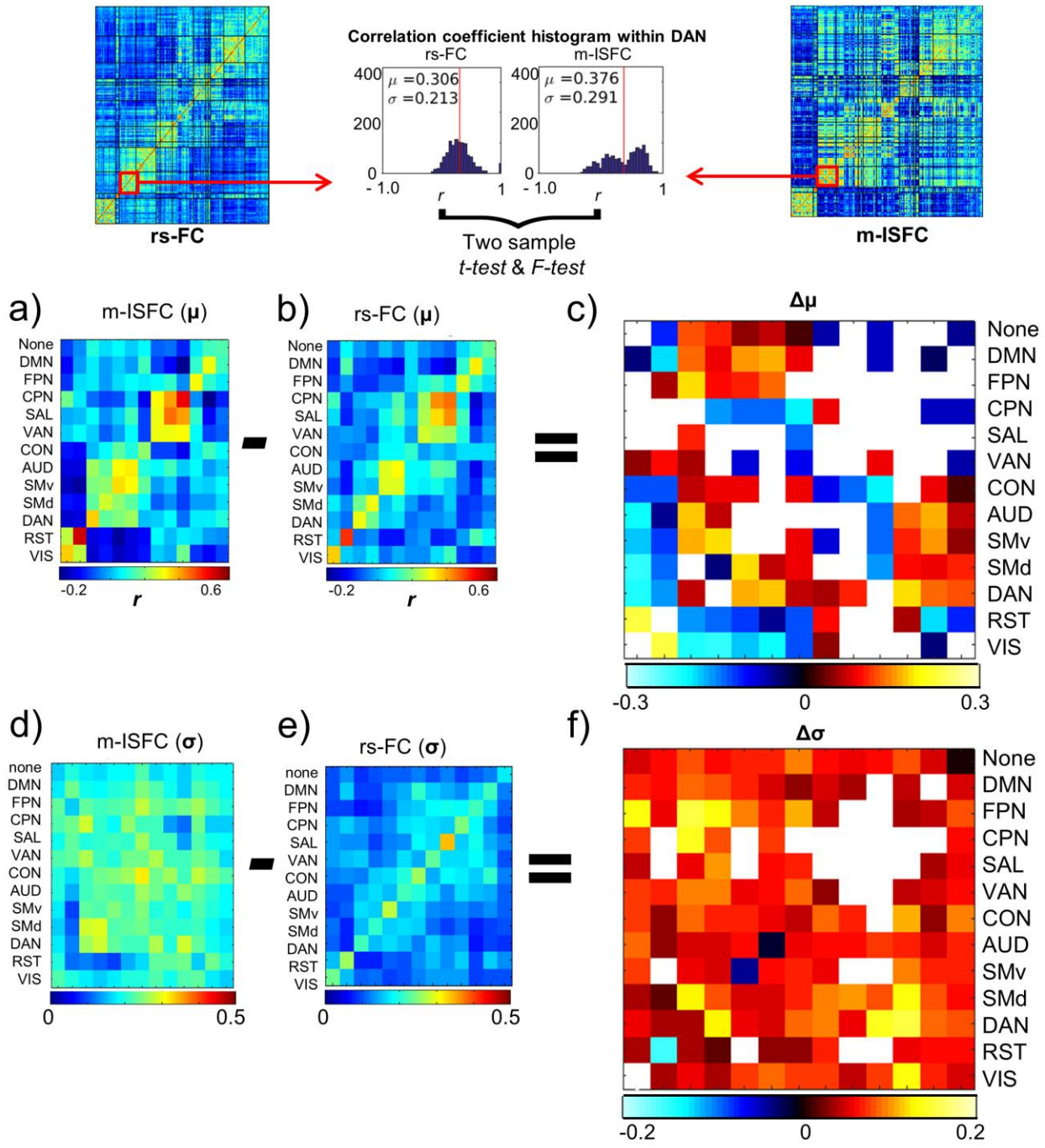

Figure 5.7. Statistical analysis of changes in network organization between rest and natural vision. Mean functional connectivity of region pairs within and across RSNs were computed for movie-evoked (m-ISFC, **a**) and resting state (rs-FC, **b**) FC. The mean difference matrix (**c**, m-ISFC minus rs-FC) is depicted with cells of only significant difference in the mean of FC (as determined by t-tests with a p-value of 0.05 after Bonferroni correction for multiple comparisons, total 78 comparisons of diagonal and upper-diagonal values only, excluding the 'none' category).

Variance of the functional connectivity of region pairs within and across the RSNs were computed for both movie-evoked (m-ISFC, **d**) and resting state (rs-FC, **e**) FCs. The variance difference

matrix (f, m-ISFC minus rs-FC) is depicted with cells of only significant difference in the variance of FC (as determined by F-tests with a p-value of 0.05 after Bonferroni correction for multiple comparisons, total 78 comparisons of diagonal and upper-diagonal values only, excluding the 'none' category).

5.4.8 A new set of networks during natural vision

The statistical analysis of the FC matrices for rest and natural vision indicated that natural vision involved a large-scale reorganization of BOLD resting network structure. This reorganization could have involved the formation of a new set of networks that were just as modular as those observed during rest, or a less modular structure in which most regions broadly interacted with many other regions. To objectively identify the BOLD network organizations for intrinsic and movie-evoked FC, we conducted both hierarchical clustering analyses and graph theory analyses of modularity and community structure on the rs-FC and m-ISFC matrices.

In order to conduct the hierarchical clustering analysis, the Pearson correlation coefficients within each FC matrix were transformed to dissimilarity indices ($d_{ij} = 1 - \rho_{ij}$ || ij = Pair of parcelsi and parcelsj). The optimal number of clusters for each FC matrix ($N_{clust,rs\text{-}FC} = 2$ and $N_{clust,m\text{-}ISFC} = 7$) was determined by the Davies-Bouldin Index (DBI) (Davies and Bouldin 1979), as shown in Figures 5.8a and 5.8d. The ordering of parcels in the rs-FC matrix was rearranged to match the dendrogram generated by the clustering analysis and is displayed in Figure 5.8b. The color assignments in the dendrogram were based on the same color assignments as the predefined networks from the Gordon-Laumann parcellation (Fig. 5.1). Figure 5.8b shows that the color arrangements within the rs-FC dendrogram were mostly, although not always, homogeneous, indicating that the clustering algorithm largely replicated the apriori network structure. Moreover, the two clusters at the top-level of the hierarchy were consistent with previous demonstrations of a large-scale distinction between externally and internally directed networks (Fox et al. 2005; Golland et al. 2008). Cluster one (Fig. 5.8c) included most/all parcels

belonging to the RST, CON, FPN, and DMN networks, corresponding to an internal network grouping, and the second cluster included most/all parcels belong to the VIS, SMd SMv, AUD, VAN, and DAN networks, corresponding to an external network grouping. Figure 5.8g left panel shows the topography of the external and internal clusters.

The ordering of parcels in the m-ISFC matrix was also rearranged in line with the clustering analysis and is displayed in Figure 5.8e. Figure 5.8f shows the composition of five of the seven clusters at the top level of the hierarchy (the other two clusters contained only 1 and 2 parcels, and are not shown). Several results stand out. The m-ISFC matrix (Fig. 5.8e) showed a clear block structure along the main diagonal, reflecting a modular, network organization. However, this modular organization departed from the apriori network structure. Some apriori networks were combined largely intact to form new groupings adaptive for natural vision. Cluster #5 (Fig. 5.8f) merged a largely intact visual network with an intact RST network, which is involved in navigation, scene perception, and scene memory, along with some parcels from the fronto-parietal network. However, many apriori networks were split up and distributed across different clusters (Fig. 5.8f). For example, the DAN was split between clusters #3 and #4. Interestingly, the large-scale division between internal and external networks was not respected, with clusters including parcels from networks of both types. For example, the largest cluster in the m-ISFC matrix, cluster #3, included parcels from both external networks (e.g. SMd, AUD, DAN) and internal networks (e.g. CON, FPN, DMN). Similarly, the Davies-Bouldin index for natural vision did not show a minimum at two clusters (Fig. 5.8d), unlike the index values for the resting-state (Fig. 5.8a). The topography of the five clusters is shown in Figure 5.8g, right. We defer a description of the possible functions associated with these clusters until further analyses are presented.

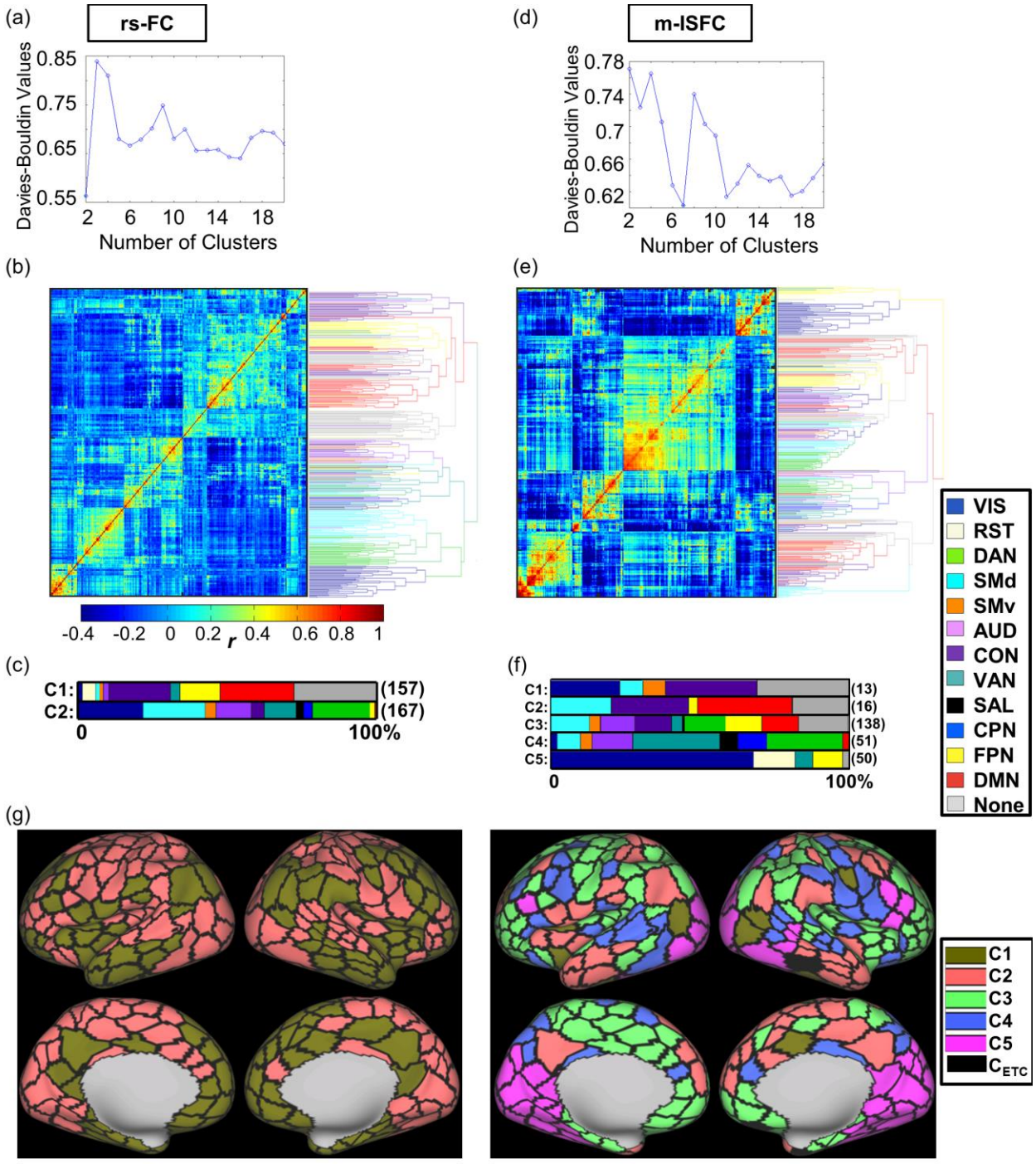

Figure 5.8. Hierarchical clustering analysis reveals distinctive network organizations for rest and natural vision. a) and d) Davies-Bouldin Index (DBI) values as a function of the number of clusters for rs-FC (a, minimum DBI = 2) and m-ISFC (d**,** minimum DBI = 7). **b) and e**) Region labels along the x- and y-axes of the resting-state FC matrix (b**)** and m-ISFC matrix (e**)** were re-ordered in accordance with the dendrogram from the hierarchical clustering algorithm. The dendrogram was colored according to the predefined network assignments from the Gordon-Laumann (GL) parcellation (Fig. 5.2). **c) and f)** Percentage distribution of predefined GL RSNs for each cluster (e.g. C1) defined from the hierarchical

clustering algorithm for rs-FC (c) and m-ISFC (f). The number by each bar indicates the total number of parcels contained in the cluster. Two clusters containing less than three parcels are not shown. **(g)** Clusters for rs-FC (**Left**) and m-ISFC (**Right**) were projected onto the cortical surface.

One general conclusion from the clustering analysis is that during natural vision, regions from the resting networks were re-distributed into a new set of BOLD networks. This re-distribution should have reduced the modularity of the m-ISFC graph computed using the apriori networks. Figure 5.9a, left panel confirms this prediction, with much lower modularity scores during natural vision than rest. However, when modularity was computed without assuming a pre-defined network structure by using the Louvain algorithm, modularity scores during rest and natural vision were roughly similar at moderate and low edge densities (Fig. 5.9a, right panel). Therefore, natural vision produced a new network organization that was roughly as modular as the organization during rest. This is consistent with the clear network organization shown in the m-ISFC matrix that was ordered by the dendrogram from the clustering analysis (Fig. 5.8d).

As in the clustering analysis, one community for m-ISFC (#1 in Fig. 5.9c) merged the visual network and the RST network involved in navigation, scene perception and scene memory (see Fig. 5.9b for the topography of each Louvain community). Similarly, the DAN was again split between two communities (i.e. the green blocks within clusters #5 and #6 in Figure 5.9c, right column).

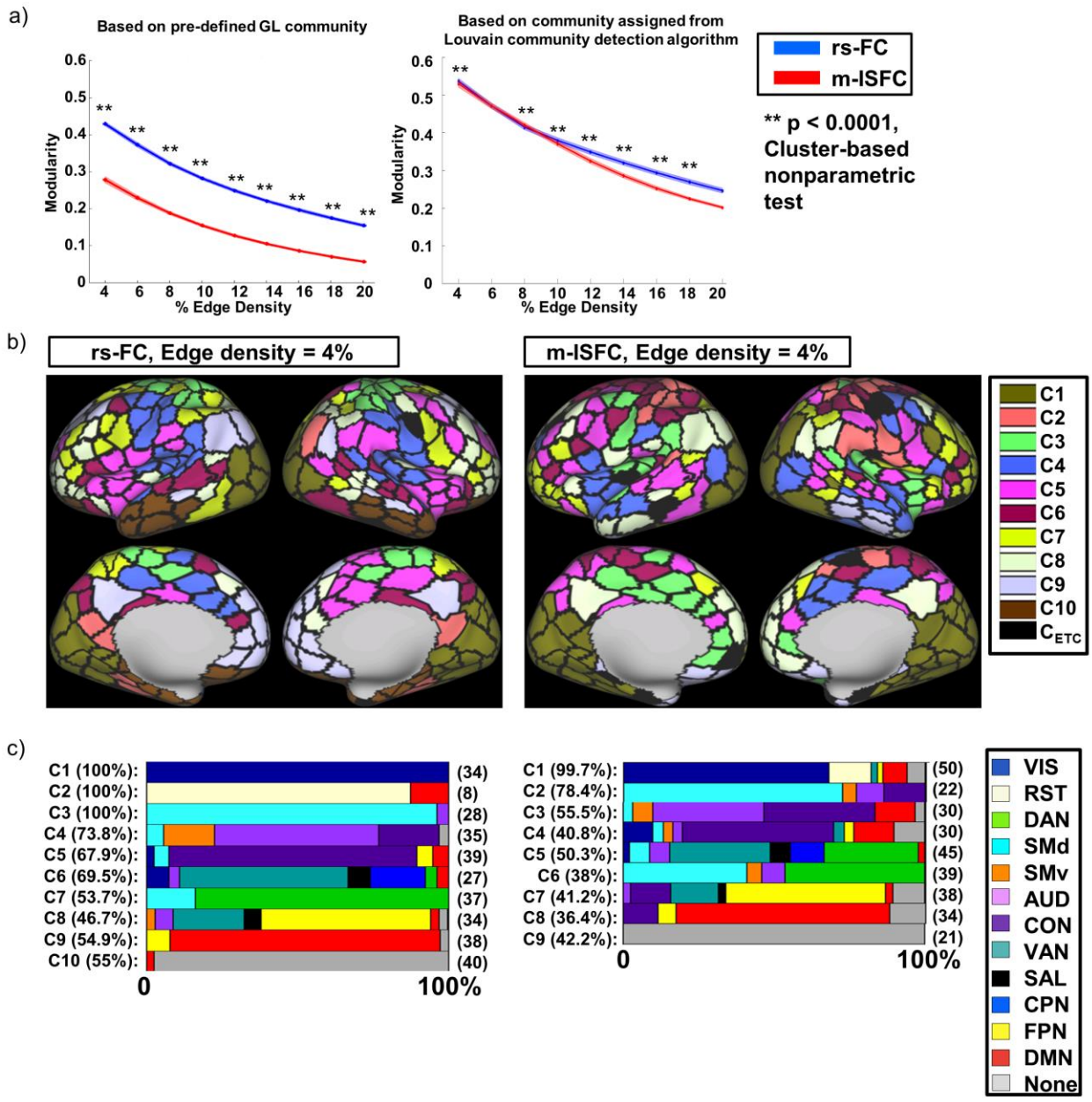

Figure 5.9. Analysis of community structure and modularity during rest and natural vision. (a) Modularity of rs-FC (blue) and m-ISFC (red) matrices was computed using the pre-defined Gordon-Laumann communities (left graph), or without assuming a pre-existing community structure by using the Louvain algorithm (right graph). A cluster-based nonparametric test with a p-value of 0.0001 was performed to test for a difference in mean modularity between rs-FC and m-ISFC. **(b)** Communities identified using the Louvain algorithm (C1 to C10) for rs-FC (**Left**) and m-ISFC (**Right**) were projected onto the cortical surface. The percentage distribution of predefined RSNs for the communities identified by the Louvain algorithm for **(c)** rs-FC and m-ISFC. The number on the right of the each bar indicates the total number of parcels contained in the community. The number on the left of the each bar indicates the frequency of community assignments from 10,000 iterations of the Louvain Algorithm. Communities containing fewer than five parcels are not shown.

5.4.9 Visualization of the network organization during rest and natural vision

To illustrate the functional groupings identified by the clustering and graph analyses and to provide more insight into their functions, resting state FC (rs-FC) and movie-evoked FC (m-ISFC) matrices were visualized via spring embedded models (Fig. 5.10). The colors of the nodes in the models in Figures 5.10a and 5.10d were based on the apriori Gordon-Laumann networks, those in Figures 5.10b and 5.10e on the communities from the unsupervised Louvain algorithm, and those in Figures 5.10c and 5.10f on the top-level clusters from the hierarchical clustering analysis.

Under resting conditions, the spring-embedded model of the apriori Gordon-Laumann networks (Fig. 5.10a) was very similar to the model of the Louvain communities (Fig. 5.10b), with nodes of similar colors (i.e. nodes from similar apriori networks or Louvain communities) grouped together. Therefore, the data-driven resting network structure from the current study matched that observed in previous studies. Additionally, the spring embedded model of rs-FC showed a similar arrangement to the spring embedded resting-state model reported in a previous study (Power et al. 2011). Finally, the top-level grouping from the cluster analysis (Fig. 5.10c) showed a clear separation that corresponded to the distinction between internally-directed and externally-directed networks, again consistent with previous work (Fox et al. 2005; Golland et al. 2008).

In contrast, under natural vision the apriori Gordon-Laumann networks (Fig. 5.10d) did not match the new BOLD network structure, with intermingling of differently colored nodes to form new functional groupings. These groupings, presumably adaptive for natural vision, are evident in Figures 5.10e and 5.10f, which display respectively the Louvain communities and the

top-level clusters from the clustering analysis. The Visual and RST network were merged into a single vision/scene analysis community (community #1, Fig. 5.10e; also cluster #5, Fig. 5.10f), as noted earlier, which was adjacent to a community (#5, Fig. 5.10e; also cluster #4, Fig. 5.10f) that combined more visually-related parcels from the DAN and VAN/language parcels (see Fig. 5.10d). The DAN/VAN component of this multi-community grouping might be involved in controlling attention to the display. The remaining parcels of the DAN were integrated with many dorsal somato-motor parcels (Fig. 5.10d) into Community #6, which was adjacent to a community (#3, Fig. 5.10e) containing many parcels from the auditory network (Fig. 5.10d). This DAN/SMd/AUD grouping could reflect attention to/interpretation of action as well as sound, perhaps including dialog. Community #7 (Fig. 5.10e) was possibly the most centrally located in the model and primarily contained parcels from the FPN, along with small contributions from the VAN and CON. The central location of this 'cognitive control' community was consistent with the critical role of the FPN in task-dependent processing (Dosenbach et al. 2008; Cole et al. 2013).

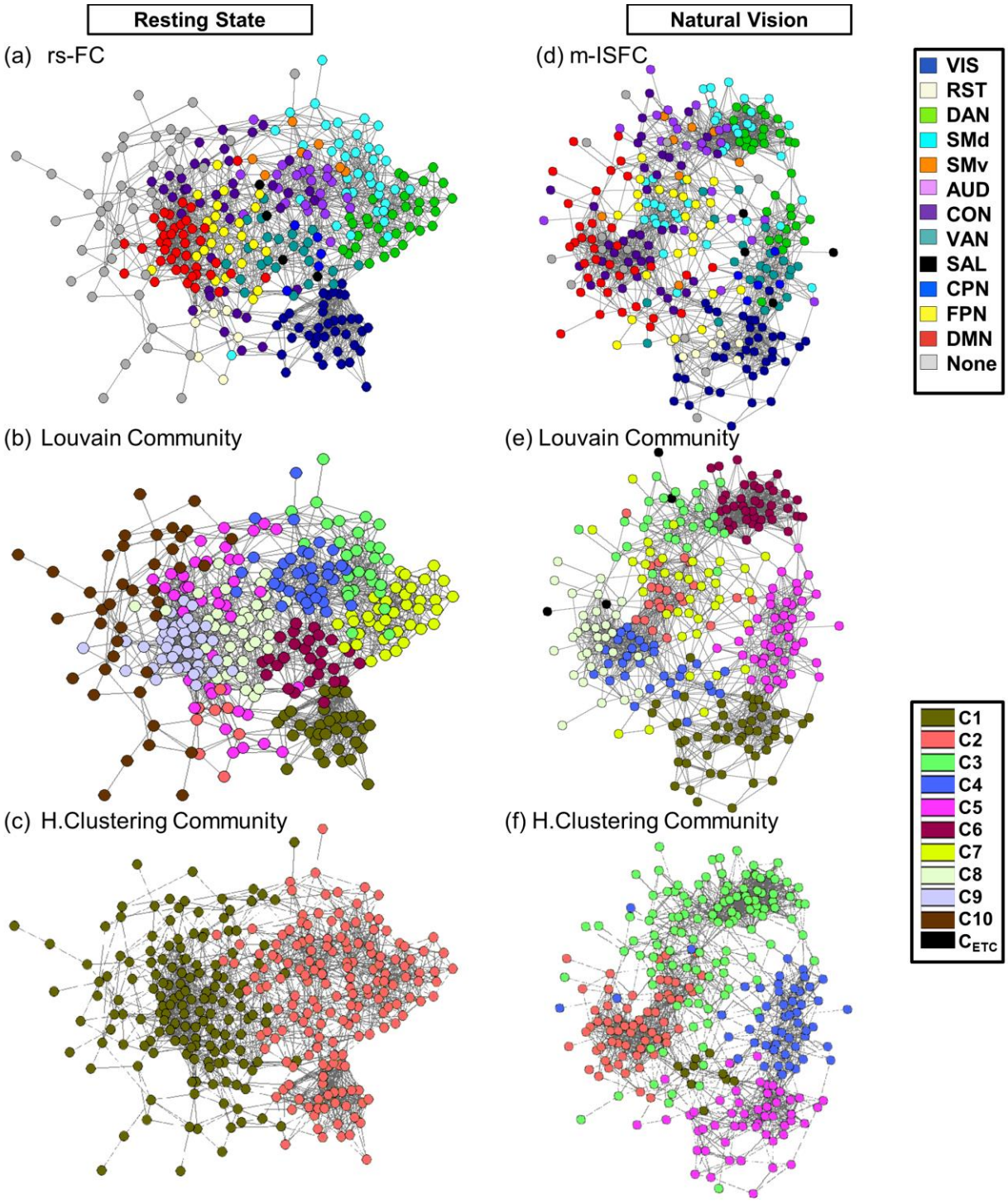

Figure 5.10. Spring embedded models reveal different network organizations for rest and natural vision. Spring embedded models were generated for Resting-state FC (rs-FC) and Movie-evoked FC (m-ISFC) matrices of 4% edge density. Nodes were colored by the predefined network assignment from the Gordon-Laumann parcellation (a & d), by Louvain community assignment (b & e), and by Hierarchical-clustering (c & f). See Figures 5.8c, 5.8f, and 5.9c for the percentage distribution of pre-defined RSNs for each cluster and community.

5.5 Discussion

Natural vision produced substantial modifications in the functional connectivity (FC) observed at rest, resulting in a new BOLD network structure that was roughly as modular as the resting structure. During natural vision, RSNs were split into components that re-combined with components from other RSNs to form new communities, or remained intact but merged with other RSNs to form larger communities. As discussed below, the formation of these communities was consistent with the cognitive demands imposed by natural vision. Interestingly, these groupings did not necessarily respect the large-scale internal/external distinction that governs resting state structure, indicating a fundamental change from the resting structure. All of the above results were supported by both hierarchical clustering and graph-based analyses and indicate that the BOLD network structure evoked by natural vision was only partly constrained by the resting structure.

5.5.1 BOLD network organization during natural vision and rest

Movie viewing changed the network structure observed during rest to produce new functional groupings in line with the demands of natural vision. The visual network merged with the network for navigation, scene perception and scene memory, along with parcels from the FPN to form a community adaptive for analyzing the visual content of the movie. The dorsal attention network was split into two parts that may have reflected the multi-modal/multi-dimensional nature of the movie. Parcels from the DAN and VAN, along with some from the salience and cingulo-parietal networks, were combined into a single community that was adjacent to the visual/scene community described above. This larger DAN/VAN/VIS/Scene

grouping may have been involved in controlling attention to the display. The remaining DAN parcels were integrated with dorsal somato-motor parcels into a community adjacent to another community that included large contributions from the auditory network. The resulting DAN/SMd/AUD grouping may have been involved in attention to/interpretation of action and perhaps attention to sound and dialog. Although these assignments of function are speculative, the reorganization of the dorsal attention network into two separate communities/clusters was evident both in the Louvain community analyses and in the cluster analysis. Finally, internally- and externally-directed processes interacted more strongly during natural vision than rest. The Davies-Bouldin index for resting FC showed a minimum at two clusters, and the composition of those clusters matched the internal/external distinction. In contrast, the smallest local minimum value of the Davies-Bouldin index for natural vision occurred at seven clusters, and the largest cluster found combined parcels from several internal and external networks. Similarly, Louvain communities combined CON parcels with those from the auditory network and dorsal somato-motor network.

The observed changes in BOLD network structure were consistent with prior observations of differences in functional connectivity during resting and task states. Spadone et al reported increased functional connectivity between visual and dorsal attention regions during an attention-shifting paradigm (Spadone et al. 2015). Betti et al. reported with fMRI and MEG a decrease in the correlation within networks of alpha/beta band limited power (BLP, especially visual and auditory), and an increase in the correlation between networks (e.g. visual and language networks) of theta, beta, and gamma BLP (Betti et al. 2013). Both Spadone et al. and Betti et al reported that the overall topographies of FC during rest and natural vision were very similar, as did a subsequent fMRI paper by Cole et al. (2014), but their methodologies did not

remove the effects of intrinsic activity during movie viewing (see below, relation to previous studies).

5.5.2 Implications for the function of resting state activity

The introduction noted two different conceptions of the relationship between intrinsic and task-evoked activity, i.e. a task state is selected from a broad repertoire of resting states or is independently generated from a default resting state through unknown mechanisms. The new BOLD network organization observed during natural vision seems more consistent with the latter viewpoint, a conclusion similar to that of Betti et al. (Betti et al. 2013). Our results indicate that resting state organization does not fully constrain the large-scale functional connectivity of brain areas that is adaptive for natural vision. More generally, we suggest that the brain can change its network structure to meet the demands of a task even if that structure departs substantially from the resting structure. The view that network structure can change to meet the current task demand is in line with previous views (Miller and Cohen 2001; Heinzle et al 2012).

5.5.3 Sources of the residual shared structure between rest and task

Although the spatial correlation between rest and movie, $r = 0.60$, was smaller than the rest-task correlations previously reported, it was nonetheless significant. This result is, consistent with recent studies indicating that task activation can be predicted from resting FC (Cole et al. 2016; Tavor et al. 2016). Importantly, since the ISFC procedure completely removed the effects of intrinsic activity from the FC matrix, the shared FC topography did not reflect a common source of signals, i.e. intrinsic activity, but instead represented a correspondence between the resting network structure and the evoked structure observed during natural vision. A

focus on this residual correspondence may allow a better understanding of how resting-state FC constrains task-evoked signals and FC.

This correspondence may have resulted from several factors. First, a common structural connectivity matrix promotes rest-task correspondence (Vincent et al. 2006; Greicius et al. 2009; Hasson et al. 2009; Honey et al. 2009). Barttfeld et al studied the variability of FC whole brain patterns in different behavioral conditions (awake, drowsy, anesthesia) in monkeys (Barttfeld et al. 2015). They reported that the variability of FC patterns increased with arousal/wakefulness, and that FC patterns under anesthesia were closely related to the structural connectivity organization. The latter, structurally-driven component of FC should be common to task and rest.

In addition, experience driven by natural vision may include some modal or highly frequent FC patterns that through repetition and Hebbian mechanisms become part of the tonic, resting FC structure. Consistent with this idea several studies have reported modifications of resting FC patterns after learning (Albert et al. 2009; Lewis et al. 2009; Tambini et al. 2010; Harmelech and Malach 2013). Recent work has also suggested long-term, experience-dependent influences on FC in visual cortex. FC between different visual areas is increased in ROIs that have overlapping receptive fields (Heinzle et al. 2011; Raemaekers et al. 2014; Wilf et al. 2017) or represent similar eccentricities (Arcaro et al. 2015). Wilf et al. (2017) additionally reported that the FC of visual cortex from movie viewing, after removal of intrinsic activity, was more similar to resting FC than the FC from iso-eccentricity stimulation, iso-polar stimulation, or predictions based on retinotopic, polar angle or eccentricity distance. Therefore, a component of the residual shared structure between rest and natural vision likely reflects frequently experienced patterns of inter-regional, evoked activity. Conversely, the FC in visual cortex

evoked by stimulation can differ from resting FC, with larger differences for non-naturalistic stimulation.

Finally, FC on average is greater between nearby brain regions both during task and rest, an effect that largely reflects stronger structural and functional interactions between neighboring regions, but may also partly result from method-related factors such as smoothing.

5.5.4 Relation to previous studies

The conclusion that natural vision produced large changes in the resting network structure does not conflict with the previous results of Cole et al. who reported very similar FC matrices for resting and task conditions, since the latter authors did not remove the effects of intrinsic activity from their task FC matrices (Cole et al. 2014). Interestingly, Cole et al. also reported that regressing the mean task activity from the BOLD timeseries only slightly increased the correlation of rest and task FC matrices from 0.86 to 0.90 (results taken from the HCP 'seven-task' dataset, n=118). The large effect of removing intrinsic activity on the movie FC matrix, coupled with the much smaller effect of removing mean task activity on the task FC matrix (Cole et al. 2014), suggests that intrinsic fluctuations are larger in magnitude than task/movie-evoked fluctuations. On this view, the resting FC matrix matched the non-regressed task FC matrix in Cole et al. and the movie FC matrix (m-FC) in the present study because during the task/movie the sum of the intrinsic modulations and the (very different) task/movie-evoked modulations was dominated by the same intrinsic modulations that were present at rest.

The same factor, in conjunction with the insensitivity of correlation to overall changes in magnitude, explains why the inter-subject averaging and ISFC procedures produced very similar movie FC matrices but very different resting FC matrices. Inter-subject averaging of intrinsic

fluctuations greatly reduced their magnitude. As a result, the sum of these signals with the movie-evoked signals was dominated by the latter, producing similar m-avg and m-ISFC matrices. However, during rest the intrinsic signals were not summed with signals from a different source. Therefore, smaller amplitude intrinsic signals were sufficient to produce the same FC matrix as the resting matrix measured without inter-subject averaging. Larger amplitudes of intrinsic than movie-evoked activity might partly reflect the fact that the power of the local field potential is on average greater and more synchronized at rest than during tasks (Pfurtscheller and Lopes Da Silva 1999; Betti et al. 2013).

5.5.5 Group FC vs. subject-specific FC

The ISFC procedure (Simony et al. 2016) is a powerful technique for eliminating the influence of intrinsic activity on the FC measured during a task. It produces stable estimates of functional connectivity, uncontaminated by intrinsic activity, over a wide range of sample sizes. In contrast, the temporal averaging procedure requires a large sample size to achieve a similar result. It is important to note, however, that the ISFC procedure as well as temporal averaging also eliminates task-evoked FC that is specific to an individual rather than common across a group.

Wilf et al. (Wilf et al. 2017) have reported a procedure that eliminates the effects of intrinsic signals on FC while retaining both group and subject-specific, movie-evoked FC. Their subjects viewed the same movie twice, allowing within-subject FC to be computed from the correlation between the two viewings (see Henrikksen et al. for a related approach in which representational dissimilarity matrices were computed within vs. across trials, and Hasson et al. for earlier work on inter-subject synchronization during movie viewing). However, this

procedure only preserved group and individual FC patterns that were invariant over repeated viewings, which could skew the observed FC. For example, on a second viewing, subjects likely could better predict the spatio-temporal content of the movie.

5.5.6 Limitations

Because eye-movements are not controlled in the natural vision paradigm each subject may have received different retinal inputs during the movie, depending on their fixation patterns. As noted above, subject-specific FC was not assessed by the ISFC technique. However, the free-viewing paradigm has been used in many previous fMRI studies of natural vision (Hasson et al. 2004; Bartels and Zeki 2005; Golland et al. 2007; Huth et al. 2012; Mantini et al. 2012; Betti et al. 2013; Stansbury et al. 2013) and has consistently shown strong inter-subject correlations in visual cortex as well as many other brain regions (Hasson et al. 2004, 2010). Responses in visual cortex are sufficiently consistent that a reverse inference procedure can be conducted in which the brain response in a region such as the fusiform gyrus during individual frames of the movie can be used to predict the regions' selectivity (Hasson et al. 2004). In the current paper, the m-ISFC matrix showed high correlations between visual regions. Therefore, movie-viewing evokes a consistent BOLD response across many brain regions, despite the fact that eye movements are not controlled. In this paper, we studied the network organization over the entire brain of these consistent responses.

Because the present work was based on the BOLD signal, our conclusions only apply to low-frequency activity. Although the relationship between FC networks during task and rest has been measured at higher frequencies (Betti et al. 2015), intrinsic signals were not removed from task FC.

m-ISFC reflects an unknown mixture of inter-regional interactions and independent co-activations. Although Cole et al. (2014) removed the mean BOLD activation from task timeseries through regression, an analogous procedure was not possible here since the movie did not involve repeated 'trials', i.e. each time segment of the movie was different.

The ISFC procedure eliminates interactions between task-evoked signals and intrinsic signals, treating these signals as additive. Some prior studies reporting high task-rest similarity used procedures that also likely minimized or attenuated interaction effects, suggesting that these effects do not explain the reduction of task-rest similarity when intrinsic activity is removed. The high correspondence reported by Smith et al. (2009), for example, was not caused by interactions, since time-locked activations have no consistent phase relationship with intrinsic activity. Cole et al. (2014) compared the similarity of group-averaged task-evoked FC matrices with group-averaged resting FC matrices rather than calculating task-rest similarity in individuals. Group-averaging would have minimized interaction effects that differed across subjects. Moreover, the effects of interactions on the similarity of task-evoked and resting FC may depend on the detailed nature and consistency of the interactions across regions, and therefore may be difficult to predict. However, we acknowledge that interactions between task-evoked signals and intrinsic activity may well affect task-rest similarity and consequently the degree to which reductions are observed when intrinsic activity is removed.

The reduction in movie-rest similarity after the effects of intrinsic activity were removed was highly robust and consistent across individual movies. One question, however, is whether similar reductions will be found for other kinds of tasks. The seven tasks from the Human Connectome dataset tested by Cole et al. (2014), Emotional, Gambling, Language, Motor, Relational, Social, and N-back, showed correlation coefficients between rest and task FC

matrices that were very similar to those between rest and m-FC matrices (i.e. matrices in which the effects of intrinsic activity were not removed), with only modest variation across the seven tasks ($\mu = 0.83$ $\sigma = 0.037$). However, despite the similarity of rest-task correspondences across movies and tasks when intrinsic activity was left in, it is still possible that the magnitude of reductions in similarity when intrinsic activity is removed will differ for some tasks.

Finally, although the relationship between resting and task-evoked activity has usually been conceptualized in terms of the correspondence between resting and task networks defined by inter-regional correlations or between resting networks and patterns of task co-activation, it also can be conceptualized in terms of the similarity of the information carried by patterns of neural activity during task and rest (Fiser et al. 2010). Numerous studies have shown that multivoxel patterns of local activity during tasks carry information about specific stimuli, classes of stimuli, or even task operations (Haxby et al. 2001; Kamitani and Tong 2005; Haynes and Rees 2006; Kriegeskorte et al. 2008; Connolly et al. 2012; Guntupalli et al. 2016), and can be modulated by learning and attention. The current study, however, did not test whether intrinsic activity influences or constrains the information carried by task-evoked activity since activity was averaged over a parcel and was not analyzed using multi-voxel techniques.

5.6 Mathematical derivation of intrinsic and extrinsic activity effect in various FC computations

It has been known that each individual has variations in its resting state functional connectivity structures while the population-level of resting state functional connectivity is rather stable. To understand the increasing spatial correlation between rs-FC and rs-avgFC with the

increasing sample size, we revisited how the rs-FC and rs-avgFC was computed mathematically. The below derivations had same or modified notations to Simony et al. 2016 (Simony et al. 2016).

5.6.1 Derivation of rs-FC

Based on the given individual FC variations and stable group-level FC, the individual BOLD signal (denoted *Y*) of a region can be decomposed as below:

BOLD of region A [Y_A] = Population-wise correlated intrinsic BOLD [$I1_A$] + subject-specific correlated intrinsic BOLD *[$I2_A$] + Noise signal [N_A]*

So that, subject-wise functional connectivity of two regions (*A* and *B*) of subject *X* would be

$E_X[Y_A, Y_b] = E_X[I1_A, I1_B] + E_X[I2_A, I2_B] + E_X[N_A, N_B]$

The population/group-level rs-FC of two regions (*A* and *B*) with sample size *n* was computed as

rs-FC $[Y_A, Y_b] = \tanh((\sum_{X=1}^{n} \operatorname{atanh}(E_X[Y_A, Y_B])/n))$

$\approx (\sum_{X=1}^{n} E_X[Y_A, Y_B])/n$ *** Let's simplify the computation by ignoring fisher-z transformation

$\approx (\sum_{X=1}^{n} E_X[I1_A, I1_B])/n + (\sum_{X=1}^{n} E_X[I2_A, I2_B])/n + (\sum_{X=1}^{n} E_X[N_A, N_B])/n$

i1 *i2* *i3*

*** Let's simplify the computation by linearly expending the correlation coefficient terms.

a) Since the $E_X[I1_A, I1_B]$ is originated from population-wise correlated intrinsic BOLD signals,

$(\sum_{X=1}^{n} E_X[I1_A, I1_B])/n == E[I1_A, I1_B]$ regardless the size of n

b) Since $E_X[I2_A, I2_B]$ is originated from subject-specific correlated intrinsic BOLD signals,

$(\sum_{X=1}^{n} E_X[I1_A, I1_B])/n \rightarrow 0$, as n increases.

c) Since $E_X[N_A, N_B]$ is originated from noise signals,

$(\sum_{X=1}^{n} E_X[N_A, N_B])/n \rightarrow 0$, as n increases.

d) Therefore, when rs-FC is computed with enough sample subjects, the rs-FC can be expressed as

rs-FC [Y_A, Y_b] ≈ $(\sum_{X=1}^{n} E_X[I1_A, I1_B])/n$

5.6.2 Derivation of rs-avg FC

By using the same notation as above,

BOLD of region A [Y_A] = Population-wise correlated intrinsic BOLD [$I1_A$] + subject-specific correlated intrinsic BOLD *[$I2_A$] + Noise signal [N_A]*

The rs-avgFC of two regions (*A* and *B*) with sample size *n* was computed as

rs-avgFC [Y_A, Y_b] = $E[\frac{(\sum_{X=1}^{n} Y_{A,X})}{n}, \frac{(\sum_{X=1}^{n} Y_{B,X})}{n}]$

$\approx E[\frac{(\sum_{X=1}^{n} I1_{A,X})}{n}, \frac{(\sum_{X=1}^{n} I1_{B,X})}{n}] + E[\frac{(\sum_{X=1}^{n} I2_{A,X})}{n}, \frac{(\sum_{X=1}^{n} I2_{B,X})}{n}] + E[\frac{(\sum_{X=1}^{n} N_{A,X})}{n}, \frac{(\sum_{X=1}^{n} N_{B,X})}{n}]$

i4 *i5* *i6*

Since *I1* is population-wise correlated intrinsic BOLD, the correlation coefficients of its mean signal will be constant across varying size of *n*. On the other hand, *I2* and *N* is subject-specific signal; therefore, the correlation coefficients of its mean signal will be converged into 0 as *n* increases.

Therefore, above mathematical derivations in **5.6.1** and **5.6.2** explain how increasing sample size helps both rs-FC and rs-avgFC converging into ‘true’ population-wise correlation coefficients. The increasing spatial correlation between rs-FC and rs-avgFC in terms of increasing sample

subject number is effectively due to both FCs becomes close to *i1* and *i4* terms only. It is important to note that the above computations were highly simplified inducing discrepancies to the real computation outputs. For example, the spatial correlation between rs-FC and rs-avgFC in Figure 5.4.a was converged around 0.94 indicating both rs-FC and rs-avgFC cannot be simplified by *i3* and *i4* terms only

5.6.3 Derivation of m-FC

The movie BOLD can be decomposed as population-wise shared movie BOLD, subject-specific movie BOLD, population-wise correlated intrinsic BOLD, subject-specific correlated intrinsic BOLD, and Noise.

The individual movie BOLD signal (denoted *Y*) of a region can be decomposed as below:

BOLD of region A [Y_A] = Population-wise shared movie BOLD [M1] + subject-specific movie BOLD [M2] + Population-wise correlated intrinsic BOLD [I1] + subject-specific correlated intrinsic BOLD [I2] + Noise [N]

The m-FC of two regions (*A* and *B*) with sample size *n* was computed as

m-FC [Y_A, Y_b] = tanh($(\sum_{X=1}^{n} \text{atanh}(E_X[Y_A, Y_B])/n)$)

$\approx (\sum_{X=1}^{n} E_X[Y_A, Y_B])/n$ *** Let's simplify the computation by ignoring fisher-z transformation

$\approx (\sum_{X=1}^{n} E_X[M1_A, M1_B])/n + (\sum_{X=1}^{n} E_X[M2_A, M2_B])/n +$

$(\sum_{X=1}^{n} E_X[I1_A, I1_B])/n + (\sum_{X=1}^{n} E_X[I2_A, I2_B])/n + (\sum_{X=1}^{n} E_X[N_A, N_B])/n$

a) Since M2, I2, and N is subject-specific terms,

$(\sum_{X=1}^{n} E_X[M2_A, M2_B])/ n + (\sum_{X=1}^{n} E_X[I2_A, I2_B])/n + (\sum_{X=1}^{n} E_X[N_A, N_B])/n \rightarrow 0$, as n increases.

b) Since the $E_X[I1_A, I1_B]$ is originated from population-wise correlated intrinsic BOLD signals,

$(\sum_{X=1}^{n} E_X[I1_A, I1_B])$/n == $E[I1_A, I1_B]$ regardless the size of n

c) Since M1is population-wise shared movie BOLD,

$(\sum_{X=1}^{n} E_X[M1_A, M1_B])$/n == $E[M1_A, M1_B]$ regardless the size of n

Therefore, m-FC could be effectively expressed as,

m-FC [Y_A, Y_b] ≈ $(\sum_{X=1}^{n} E_X[M1_A, M1_B])$/n + $(\sum_{X=1}^{n} E_X[I1_A, I1_B])$/n

≈ $E[I1_A, I1_B]$+ $E[M1_A, M1_B]$

The population-wise shared movie BOLD accounts less than 50% of BOLD variances for individual movie BOLD (data not shown). This indicates that the mean of individual FC maps (m-FC) is rather a structural expression of resting state functional connectivity than an expression of movie functional connectivity.

5.6.4 Derivation of m-avg FC

The m-avgFC of two regions (*A* and *B*) with sample size *n* was computed as

m-avgFC [Y_A, Y_b] = $E[\frac{(\sum_{X=1}^{n} Y_{A,X})}{n}, \frac{(\sum_{X=1}^{n} Y_{B,X})}{n}]$

≈ $E[\frac{(\sum_{X=1}^{n} M1_{A,X})}{n}, \frac{(\sum_{X=1}^{n} M1_{B,X})}{n}]$ + $E[\frac{(\sum_{X=1}^{n} M2_{A,X})}{n}, \frac{(\sum_{X=1}^{n} M2_{B,X})}{n}]$ + $E[\frac{(\sum_{X=1}^{n} I1_{A,X})}{n}, \frac{(\sum_{X=1}^{n} I1_{B,X})}{n}]$

+ $E[\frac{(\sum_{X=1}^{n} I2_{A,X})}{n}, \frac{(\sum_{X=1}^{n} I2_{B,X})}{n}]$ + $E[\frac{(\sum_{X=1}^{n} N_{A,X})}{n}, \frac{(\sum_{X=1}^{n} N_{B,X})}{n}]$

a) Since the M1 is population-wise shared movie BOLD,

$M1_{A,X} = \frac{(\sum_{X=1}^{n} M1_{A,X})}{n}$, and $E[\frac{(\sum_{X=1}^{n} M1_{A,X})}{n}, \frac{(\sum_{X=1}^{n} M1_{B,X})}{n}] = E[M1_A, M1_B]$, at large size of n

b) Since the M1 is subject-specific movie BOLD,

$E[\frac{(\sum_{X=1}^{n} M2_{A,X})}{n}, \frac{(\sum_{X=1}^{n} M2_{B,X})}{n}] \rightarrow 0$, as n increases.

c) Since I2 is subject-specific correlated intrinsic BOLD signals and N is noise,

$$E\left[\frac{\left(\sum_{X=1}^{n} I2_{A,X}\right)}{n}, \frac{\left(\sum_{X=1}^{n} I2_{B,X}\right)}{n}\right] + E\left[\frac{\left(\sum_{X=1}^{n} N_{A,X}\right)}{n}, \frac{\left(\sum_{X=1}^{n} N_{B,X}\right)}{n}\right] \rightarrow 0, \text{ as n increases.}$$

d) The computation of correlation of I1, population-wise correlated intrinsic BOLD, is where relative amount of variance from movie vs. ongoing fluctuation becomes significant. The population-wise shared movie BOLD [M1] was acquired by averaging 35 subjects' movie BOLD timeseries (equivalent to the number of subjects used in m-ISFC). The ongoing fluctuations is acquired by subtracting the population-wise shared movie BOLD [M1] from the averaged individual movie BOLD time series of n subjects. The ongoing fluctuations of region A, therefore, were equivalent to

$$Y_{\text{Ongoing Fluctuation, A}} = \frac{\left(\sum_{X=1}^{n} M2_{A,X}\right)}{n} + \frac{\left(\sum_{X=1}^{n} I1_{A,X}\right)}{n} + \frac{\left(\sum_{X=1}^{n} I2_{A,X}\right)}{n} + \frac{\left(\sum_{X=1}^{n} N_{A,X}\right)}{n}$$

The amounts of variance from population-wise shared movie BOLD were measured by n = 1 (single subject), 5, 10, 20, and 30. The amount of variance from population-wise shared movie BOLD were less than 50% across all networks (data not shown). By increasing the number of subjects, the amount of variance from population-wise shared movie BOLD was increased near to 100%. This is the expected results since the population-wise shared movie BOLD was the simple average of BOLD timeseries across 35 subjects.

In above demonstrations of spatial similarity between rs-FC and rs-avgFC, it was shown that correlation from I1 was preserved across different number of subjects. This was possible since the relative variances of [I1], [I2], and [N] were preserved while averaging resting state BOLD time series across subjects. The relative variances among [M1], [M2], [I1], [I2], [N] were changed significantly while averaging across subjects, and the correlation coefficients term of I1 would be present but small as number of subject increases.

$E[\frac{(\Sigma_{X=1}^{n} I1_{A,X})}{n}, \frac{(\Sigma_{X=1}^{n} I1_{B,X})}{n}] \rightarrow \epsilon$ (small but present), as n increases.

Therefore, the m-avgFC with many subjects could be effectively described as

$$\text{m-avgFC } [Y_A, Y_b] = E[\frac{(\Sigma_{X=1}^{n} Y_{A,X})}{n}, \frac{(\Sigma_{X=1}^{n} Y_{B,X})}{n}]$$

$$\approx E[\frac{(\Sigma_{X=1}^{n} M1_{A,X})}{n}, \frac{(\Sigma_{X=1}^{n} M1_{B,X})}{n}] + E[\frac{(\Sigma_{X=1}^{n} I1_{A,X})}{n}, \frac{(\Sigma_{X=1}^{n} I1_{B,X})}{n}]$$

$$\approx E[M1_A, M1_B] + \epsilon$$

5.6.5 Derivation of m-ISFC

By using the same notation as above,

$$\text{m-ISFC } [Y_A, Y_b] = E[\frac{(\Sigma_{X=1}^{n} Y_{A,X})}{n}, \frac{(\Sigma_{XX=1}^{n} Y_{B,XX})}{n}]$$

$$\approx E[\frac{(\Sigma_{X=1}^{n} M1_{A,X})}{n}, \frac{(\Sigma_{X=1}^{n} M1_{B,XX})}{n}] + E[\frac{(\Sigma_{X=1}^{n} M2_{A,X})}{n}, \frac{(\Sigma_{X=1}^{n} M2_{B,XX})}{n}] + E[\frac{(\Sigma_{X=1}^{n} I1_{A,X})}{n}, \frac{(\Sigma_{X=1}^{n} I1_{B,XX})}{n}]$$

$$+ E[\frac{(\Sigma_{X=1}^{n} I2_{A,XX})}{n}, \frac{(\Sigma_{X=1}^{n} I2_{B,XX})}{n}] + E[\frac{(\Sigma_{X=1}^{n} N_{A,X})}{n}, \frac{(\Sigma_{X=1}^{n} N_{B,X})}{n}]$$

, while X = 1st sampled group and XX = 2nd sampled group of n subjects.

Since M2, I1, I2, and N are subject-specific terms which doesn't share its time series across subjects,

$$E\left[\frac{(\Sigma_{X=1}^{n} I1_{A,X})}{n}, \frac{(\Sigma_{X=1}^{n} I1_{B,XX})}{n}\right] + E[\frac{(\Sigma_{X=1}^{n} M2_{A,X})}{n}, \frac{(\Sigma_{X=1}^{n} M2_{B,XX})}{n}]$$

$$+ E[\frac{(\Sigma_{X=1}^{n} I2_{A,XX})}{n}, \frac{(\Sigma_{X=1}^{n} I2_{B,XX})}{n}] + E[\frac{(\Sigma_{X=1}^{n} N_{A,X})}{n}, \frac{(\Sigma_{X=1}^{n} N_{B,X})}{n}] \rightarrow 0, \text{ as n increases.}$$

Since M1is population-wise shared movie BOLD,

$M1_{A,X} = \frac{(\Sigma_{X=1}^{n} M1_{A,X})}{n}$, and

$E[\frac{(\Sigma_{X=1}^{n} M1_{A,X})}{n}, \frac{(\Sigma_{X=1}^{n} M1_{B,XX})}{n}] = E[M1_{A,X}, M1_{B,XX}] = E[M1_A, M1_B]$ with large size of n

Therefore, m-ISFC effectively isolates correlation coefficients of population-wise shared movie BOLD only.

5.7 References

Albert NB, Robertson EM, Miall RC. 2009. The resting human brain and motor learning. Curr Biol. 19(12):1023–1027

Arcaro MJ, Honey CJ, Mruczek RE, Kastner S, Hasson U. 2015. Widespread correlation patterns of fMRI signal across visual cortex reflect eccentricity organization. Elife. 19:4

Bartels A, Zeki S. 2005. Brain dynamics during natural viewing conditions--a new guide for mapping connectivity in vivo. Neuroimage. 24(2):339-349.

Barttfeld P, Uhrig L, Sitt JD, Sigman M, Jarraya B, Dehaene S. 2015. Signature of consciousness in the dynamics of resting-state brain activity. Proc Natl Acad Sci. 112(3):887-892

Becker R, Reinacher M, Freyer F, Villringer A, Ritter P. 2011. How ongoing neuronal oscillations account for evoked fMRI variability. J Neurosci. 31(30):11016–11027.

Berkes P, Orban G, Lengyel M, Fiser J. 2011. Spontaneous cortical activity reveals hallmarks of an optimal internal model of the environment. Science. 331(6013):83–87.

Betti V, DellaPenna S, de Pasquale F, Mantini D, Marzetti L, Romani GL, Corbetta M. 2013. Natural scenes viewing alters the dynamics of functional connectivity in the human brain. Neuron. 79(4):782–797.

Biswal B, Yetkin FZ, Haughton VM, Hyde JS. 1995. Functional connectivity in the motor cortex of resting human brain using echo-planar MRI. Magn Reson Med. 34(4):537-41.

Blondel VD, Guillaume JL, Lambiotte R, Lefebvre E. 2008. Fast unfolding of communities in large networks. J Stat Mecha. 2008:1–12.

Brookes MJ, Woolrich M, Luckhoo H, Price D, Hale JR, Stephenson MC, Barnes GR, Smith SM, Morris PG. 2011. Investigating the electrophysiological basis of resting state networks using magnetoencephalography. Proc Natl Acad Sci. 108(40):16783–16788.

Cauda F, Costa T, Diano M, Sacco K, Duca S, Geminiani G, Torta DM. 2014. Massive modulation of brain areas after mechanical pain stimulation: a time-resolved FMRI study.

Cereb Cortex. 24(11):2991–3005.

Cole MW, Reynolds JR, Power JD, Repovs G, Anticevic A, Braver TS. 2013. Multi-task connectivity reveals flexible hubs for adaptive task control. Nat Neurosci. 16(9):1348–1355.

Cole MW, Bassett DS, Power JD, Braver TS, Petersen SE. 2014. Intrinsic and task-evoked network architectures of the human brain. Neuron. 83(1):238–251.

Cole MW, Ito T, Bassett DS, Schultz DH. 2016. Activity flow over resting-state networks shapes cognitive task activations. Nat Neurosci. 19(12):1718-1726

Connolly AC, Guntupalli JS, Gors J, Hanke M, Halchenko YO, Wu YC, Abdi H, Haxby JV. 2012. The representation of biological classes in the human brain. J Neurosci. 32(8):2608–2618.

Cordes D, Haughton VM, Arfanakis K, Carew JD, Turski PA, Moritz CH, Moritz CH, Quigley MA, Meyerand ME. 2001. Frequencies contributing to functional connectivity in the Cereb Cortex. in "resting-state" data. AJNR Am J Neuroradiol. 22(7):1326–1333.

Davies DL, Bouldin DW. 1979. A cluster separation measure. IEEE Trans Pattern Anal Mach Intell. 1(2):224–227.

de Pasquale F, Della Penna S, Snyder AZ, Lewis C, Mantini D, Marzetti L, Belardinelli P, Ciancetta L, Pizzella V, Romani GL, et al. 2010. Temporal dynamics of spontaneous MEG activity in brain networks. Proc Natl Acad Sci. 107(13):6040–6045.

Dosenbach NU, Fair DA, Cohen AL, Schlaggar BL, Petersen SE. 2008. A dual-networks architecture of top-down control. Trends Cogn Sci. 12(3):99–105.

Fiser J, Chiu C, Weliky M. 2004. Small modulation of ongoing cortical dynamics by sensory input during natural vision. Nature. 431(7009):573–578.

Fiser J, Berkes P, Orbán G, Lengyel M. 2010. Statistically optimal perception and learning:from behavior to neural representations. Trends Cogn Sci. 14(3):119–130.

Florin E, Baillet S. 2015. The brain's resting-state activity is shaped by synchronized cross-frequency coupling of oscillatory neural activity. Neuroimage. 111:26–35.

Fox MD, Snyder AZ, Vincent JL, Corbetta M, Van Essen DC, Raichle ME. 2005. The human brain is intrinsically organized into dynamic, anticorrelated functional networks. Proc Natl Acad Sci. 102(27):9673–9678.

Fox MD, Snyder AZ, Zacks JM, Raichle ME. 2006. Coherent spontaneous activity accounts for trial-to-trial variability in human evoked brain responses. Nat Neurosci. 9(1):23–25.

Glasser MF, Sotiropoulos SN, Wilson JA, Coalson TS, Fisch B, Andersson JL, Xu J, Jbabdi S, Webster M, Polimeni JR, et al. 2013. The minimal preprocessing pipelines for the Human Connectome Project. Neuroimage. 80:105–124.

Golland Y, Golland P, Bentin S, Malach R. 2008. Data-driven clustering reveals a fundamental subdivision of the human cortex into two global systems. Neuropsychologia. 46(2):540–553.

Gordon EM, Laumann TO, Adeyemo B, Huckins JF, Kelley WM, Petersen SE. 2016. Generation and Evaluation of a Cortical Area Parcellation from Resting-State Correlations. Cereb Cortex. 26 (1):288-303

Greicius MD, Supekar K, Menon V, Dougherty RF. 2009. Resting-state functional connectivity reflects structural connectivity in the default mode network. Cereb Cortex. 19(1):72–78.

Guntupalli JS, Hanke M, Halchenko YO, Connolly AC, Ramadge PJ, Haxby JV. 2016. A Model of Representational Spaces in Human Cortex. Cereb Cortex. 26(6):2919–2934

Harmelech T, Malach R. 2013. Neurocognitive biases and the patterns of spontaneous correlations in the human cortex. Trends Cogn Sci. 17(12):606–615.

Hasson U, Nir Y, Levy I, Fuhrmann G, Malach R. 2004. Intersubject synchronization of cortical activity during natural vision. Science. 303(5664):1634–1640.

Hasson U, Nusbaum HC, Small SL. 2009. Task-dependent organization of brain regions active during rest. Proc Natl Acad Sci. 106(26):10841–10846.

Hasson U, Malach R, Heeger DJ. 2010. Reliability of cortical activity during natural stimulation. Trends Cogn Sci. 14(1):40–48.

Haxby JV, Gobbini MI, Furey ML, Ishai A, Schouten JL, Pietrini P. 2001. Distributed and overlapping representations of faces and objects in ventral temporal cortex. Science. 293(5539):2425–2430.

Haynes JD, Rees G. 2006. Decoding mental states from brain activity in humans. Nat Rev Neurosci. 7(7):523–534.

He BJ, Snyder AZ, Zempel JM, Smyth MD, Raichle ME. 2008. Electrophysiological correlates of the brain's intrinsic large-scale functional architecture. Proc Natl Acad Sci. 105(41):16039–16044.

Heinzle J, Wenzel MA, Haynes JD. 2012. Visuomotor Functional Network Topology Predicts Upcoming Tasks. J. Neurosci. 32(29), 9960–9968.

Henriksson L, Khaligh-Razavi SM, Kay K, Kriegeskorte N. 2015. Visual representations are

dominated by intrinsic fluctuations correlated between areas. Neuroimage. 114:275–286.

Honey CJ, Sporns O, Cammoun L, Gigandet X, Thiran JP, Meuli R, Hagmann P. 2009. Predicting human resting-state functional connectivity from structural connectivity. Proc Natl Acad Sci. 106(6):2035–2040.

Huth AG, Nishimoto S, Vu AT, Gallant JL. 2012. A continuous semantic space describes the representation of thousands of object and action categories across the human brain. Neuron. 76(6): 1210–1224.

Kamitani Y, Tong F. 2005. Decoding the visual and subjective contents of the human brain. Nat Neurosci. 8(5):679–685.

Kenet T, Bibitchkov D, Tsodyks M, Grinvald A, Arieli A. 2003. Spontaneously emerging cortical representations of visual attributes. Nature. 425(6961):954–956.

Kriegeskorte N, Mur M, Ruff DA, Kiani R, Bodurka J, Esteky H, Tanaka K, Bandettini PA. 2008. Matching Categorical Object Representations in Inferior Temporal Cortex of Man and Monkey. Neuron. 60(6):1126–1141.

Laumann TO, Gordon EM, Adeyemo B, Synder AZ, Joo SJ, Chen MY, Gilmore AW, McDermott KB, Nelson SM, Dosenbach NU, et al. 2015. Functional System and Areal Organization of a Highly Sampled Individual Human Brain. Neuron. 87(3), 657-670.

Lewis CM, Baldassarre A, Committeri G, Romani GL, Corbetta M. 2009. Learning sculpts the spontaneous activity of the resting human brain. Proc Natl Acad Sci. 106(41):17558–17563.

Mantini D, Hasson U, Betti V, Perrucci MG, Romani GL, Corbetta M, Orban GA, Vanduffel W. 2012. Interspecies activity correlations reveal functional correspondence between monkey and human brain areas. Nat Methods. 9(3):277–282.

Maris E, Oostenveld R. 2007. Nonparametric statistical testing of EEG- and MEG-data. J Neurosic Methods. 164(1), 177–190.

Mennes M, Kelly C, Colcombe S, Castellanos FX, Milham MP. 2013. The extrinsic and intrinsic functional architectures of the human brain are not equivalent. Cereb Cortex. 23(1):223–229.

Miller EK, Cohen JD. 2001. An integrative theory of prefrontal cortex function. Annu Rev Neurosci. 24:167-202

Newman ME. 2004. Fast algorithm for detecting community structure in networks. Phys Rev E Stat Nonlin Soft Matter Phys. 69.

Newman ME, Girvan M. 2004. Finding and evaluating community structure in networks. Phys

Rev E Stat Nonlin Soft Matter Phys. 69.

Nir Y, Mukamel R, Dinstein I, Privman E, Harel M, Fisch L, Gelbard-Sagiv H, Kipervasser S, Andelman F, Neufeld MY, et al. 2008. Interhemispheric correlations of slow spontaneous neuronal fluctuations revealed in human sensory cortex. Nat Neurosci. 11(9):1100–1108.

Petersen SE, Sporns O. 2015. Brain Networks and Cognitive Architectures. Neuron. 88(1):207–219.

Pfurtscheller G, Lopes da Silva FH. 1999. Event-related EEG/MEG synchronization and desynchronization:Basic principles. Clin Neurophysiol. 110(11):1842–1857.

Power JD, Cohen AL, Nelson SM, Wig GS, Barnes KA, Church JA, Vogel AC, Laumann TO, Miezin FM, Schlaggar BL, et al. 2011. Functional Network Organization of the Human Brain. Neuron. 72(4):665–678.

Power JD, Barnes KA, Snyder AZ, Schlaggar BL, Petersen SE. 2012. Spurious but systematic correlations in functional connectivity MRI networks arise from subject motion. NeuroImage. 59(3):2142–2154.

Prichard D, Theiler J. 1994. Generating surrogate data for time series with several simultaneously measured variables. Phys Rev Lett. 73(7):951-954.

Raemaekers M, Schellekens W, van Wezel RJ, Petridou N, Kristo G, Ramsey NF. 2014. Patterns of resting state connectivity in human primary visual cortical areas: A 7T fMRI study. Neuroimage. 84:911-921

Raichle ME. 2011. The restless brain. Brain Connect. 1(1):3-12.

Riedel MC, Ray KL, Dick AS, Sutherland MT, Hernandez Z, Fox PM, Eickhoff SB, Fox PT, Laird AR. 2015. Meta-analytic connectivity and behavioral parcellation of the human cerebellum. Neuroimage. 117:327–342.

Rubinov M, Sporns O. 2010. Complex network measures of brain connectivity:Uses and interpretations. NeuroImage. 52(3):1059–1069.

Simony E, Honey CJ, Chen J, Lositsky O, Yeshurun Y, Wiesel A, Hasson U. 2016. Dynamical reconfiguration of the default mode network during narrative comprehension. Nat Commun. 7:12141

Smith SM, Fox PT, Miller KL, Glahn DC, Fox PM, Mackay CE, Filippini N, Watkins KE, Toro R, Laird AR, et al. 2009. Correspondence of the brain's functional architecture during activation and rest. Proc Natl Acad Sci. 106(31):13040–13045.

Spadone S, Della Penna S, Sestieri C, Betti V, Tosoni A, Perrucci MG, Romani GL, Corbetta M.

2015. Dynamic reorganization of human resting-state networks during visuospatial attention. Proc Natl Acad Sci. 112(26):8112–8117.

Stansbury DE, Naselaris T, Gallant JL. 2013. Natural Scene Statistics Account for the Representation of Scene Categories in Human Visual Cortex. Neuron. 79(5):1025–1034.

Tambini A, Ketz N, Davachi L. 2010. Enhanced Brain Correlations during Rest Are Related to Memory for Recent Experiences. Neuron. 65(2):280–290.

Tavor I, Parker Jones O, Mars RB, Smith SM, Behrens TE, Jbabdi S. 2016. Task-free MRI predicts individual differences in brain activity during task performance. Science. 352(6282), 216–220.

Tsodyks M, Kenet T, Grinvald A, Arieli A. 1999. Linking spontaneous activity of single cortical neurons and the underlying functional architecture. Science. 286(5446):1943–1946.

Uğurbil K, Xu J, Auerbach EJ, Moeller S, Vu AT, Duarte-Carvajalino JM, Lenglet C, Wu X, Schmitter S, Van de Moortele PF, et al. 2013. Pushing spatial and temporal resolution for functional and diffusion MRI in the Human Connectome Project. NeuroImage. 80:80–104.

Van Essen DC, Ugurbil K, Auerbach E, Barch D, Behrens TEJ, Bucholz R, Chang A, Chen L, Corbetta M, Curtiss SW, et al. 2012. The Human Connectome Project:A data acquisition perspective. NeuroImage. 62(4):2222–2231.

Varela F, Lachaux JP, Rodriguez E, Martinerie J. 2001. The brainweb:phase synchronization and large-scale integration. Nat Rev Neurosci. 2(4):229–239.

Vincent JL, Snyder AZ, Fox MD, Shannon BJ, Andrews JR, Raichle ME, Buckner RL. 2006. Coherent spontaneous activity identifies a hippocampal-parietal memory network. J Neurophysiol. 96(6):3517–3531.

Wilf M, Strappini F, Golan T, Hahamy A, Harel M, Malach R. 2017. Spontaneously Emerging Patterns in Human Visual Cortex Reflect Responses to Naturalistic Sensory Stimuli. Cereb Cortex. 27(1):750-763.

Chapter 6: Concluding Remarks

Studies of spontaneous activity with fMRI have revealed that the topography of temporal covariance structures across brain regions, so called resting state networks (RSN), are similar to the topography of various cognitive and behavioral task-evoked fMRI responses (Raichle et al. 2001; Greicius et al. 2003; Fox et al. 2005; Nir et al. 2006; Smith et al. 2009; Power et al. 2011; Mennes et al. 2013). A large-scale whole brain comparison of resting state FC and task-evoked FC with 64 tasks across multiple cognitive and behavioral domains showed a very high overall topographic similarity ($\rho = 0.90$) (Cole et al. 2014). In addition to the strong spatial similarity, several studies have shown that resting FC can be changed by learning, i.e. by repeating specific task patterns, in various domains (motor, visual, memory, and neuro-feedback) (Albert et al. 2009; Lewis et al. 2009; Tambini et al. 2010; Harmelech and Malach 2013).

The above observations have led to the idea that spontaneous brain activity is not random, but represent a set of activity sub-states that represent specific task activity patterns convolved over time. A related idea is that intrinsic activity is shaped by task activity in the course of development and in the adult life by individual experiences through a Hebbian learning process. Conversely, task-evoked activity is influenced and constrained by intrinsic activity. The aim of the current thesis was to reveal correspondences between intrinsic activity and task-evoked activity in order to test the hypothesis that spontaneous activity plays a role in coding information states, so called representational hypothesis. We measured in human visual cortex the blood oxygen level dependent (BOLD) signal with fMRI to analyze the multivoxel activity patterns and FC structures of intrinsic activity, and compared them to those evoked by natural and synthetic visual stimuli.

The current work was largely inspired by three experimental strategies from the literature:

a) The successful history of multi-variate pattern experiments measuring task-evoked activity pattern (Haxby et al. 2001 and 2006; Cox and Savoy 2003; Kriegeskorte et al. 2007 and 2008), and their spatiotemporal correlation structure (Coutanche and Thompson-Schill, 2013; Anzellotti et al. 2017 and 2018; Chen et al. 2018) to infer what information is coded in different regions of cortex.

b) The comparisons of intrinsic activity and task-evoked patterns in visual cortex in anesthetized animals (Tsodyks et al. 1999; Kenet et al. 2003; Omer et al. 2018).

c) The paradigm of natural vision (movie watching) that induces strong inter-subject correlation of activity time courses (Hasson et al. 2004; Bartels and Zeki 2005; Golland et al. 2008; Mantini et al. 2012; Betti et al. 2013) in a distributed semantic space (Huth et al. 2012; Stansbury et al. 2013), and that has been shown to be represented in FC patterns (Wilf et al. 2017; Strappini et al. 2018).

By adapting the above strategies, we developed a multivariate-pattern analysis (MVPA) approach to evaluate spatial patterns of intrinsic and task-evoked activity in Chapter 2-4. Then, in Chapter 5, we used a more naturalistic movie-watching paradigm to compare whole-brain FC network structure at rest and during natural vision.

In Chapter 2 and 4, to investigate task-to-rest correspondences, we developed a measure of correlation variability (the U90 value) that measures the spread of correlation coefficient distributions between task-evoked and resting-state activity patterns. Using natural categorical visual object stimuli, we showed in Chapter 2 that the spread of correlation coefficients (positive,

negative) was significantly greater in functionally specialized human visual extra-striate regions for the preferred stimulus categories, or categories whose evoked activity induced similar patterns of activation, as compared to low level control stimuli. In addition, we found that the similarity between task and rest patterns linearly varied across subjects with the strength of selective task activation. In other words, stronger face selective responses corresponded to more frequent face-like matches in the resting state. Conversely, in early visual cortex, which is more responsive to low level features, spontaneous activity patterns represented more commonly phase and position scrambled control stimuli as compared to whole objects.

We interpret these findings by proposing that the spatial pattern of resting activity in a distributed set of regions varies over frames along an axis that is best aligned with the spatial pattern of the regions' preferred stimulus tuning. This is consistent with the hypothesis that resting multivoxel patterns of activity within a brain region code for relevant stimulus features.

The same experimental design was adapted in Chapter 4 to linguistic, pseudo-linguistic, and phase-scrambled control stimuli. Linguistic stimuli, as compared to natural stimuli, are entirely dependent on training, and cannot rely on built-in genetically determined mechanisms, or early development experiences. The results confirmed the results on natural stimuli as the U90 values for linguistic stimuli at rest were higher both in visual regions (word form area) and temporal/frontal language areas, as compared to scrambled stimuli. However, we did not find a selective language effects suggesting that resting activity in these regions is more tuned to high contrast high frequency line like stimuli. Also, we did not observe a significant correlation with task evoked responses. This may be due to the fact that the representation of visual words is acquired relatively late, and is supposed to be 'recycled' from other representations. It is therefore possible that the emergence of a visual word pattern does require a more indirect

mapping with intrinsic activity. Another explanation that a template for words cannot be very specific as a word to be read must be inspected with attention, hence the modulation of task evoked activity may be critical for linguistic differences to emerge in activity.

Overall, the combined findings in Chapter 2 and Chapter 4 supports the idea of a closed loop relationship between intrinsic activity and task-evoked activity. These results are the first demonstration of a correlation between multi-variate rest and task-evoked activity patterns in human visual cortex (see Omer et al. 2019 for a similar study in monkey cortex).

It is noteworthy that the experimental design is simple and universal enough to be applied to other cognitive-behavioral task across different domains (e.g. auditory sensory task, memory task, and motor-task). Also, the experimental design can be adopted to other recording modalities, such as ECoG or high-density EEG, for data with higher spatiotemporal resolution.

In Chapter 3, we generated pattern-based FC based on inter-regional temporal correlation computed from multivoxel similarity timeseries for body-, scene-, and preferred-templates. The pattern-based FC showed a high degree of similarity to regular resting state FC (ρ=0.78). This indicates that activity patterns in the functionally related regions of cortex fluctuated coherently. It was also shown that body and the scene representations fluctuate independently in different regions. The idea of sub-state of resting-state FC as replaying subset information states coding for different stimuli or task patterns is novel and was confirmed. The use of pattern-based FC might inform studies of resting-state organization by fractionating existing resting-state networks, and identifying the functional factors associated with that fractionation. Dynamic functional connectivity methods (Hutchison et al. 2013) and graph theory associated analysis methods (see a review of Sporns and Betzel, 2016) can also be adapted into the pattern-based FC analysis for a

better understanding in temporal developments and modular brain organizations of resting-state FC in terms of the specific task-representations.

In Chapter 5, to overcome the limitation of static visual stimuli, we used movie-watching, and compared whole-brain FC network structure during movie-watching vs. resting-state. We examined the BOLD network structure of natural vision using procedures that minimized the contribution of spontaneous activity, and found that the correlation between resting and movie-evoked FC ($\rho = 0.60$) was lower than previously reported (up to $\rho = 0.90$). Also, natural vision induces a modular network re-organization as shown by hierarchical clustering and graph-based analyses. Overall, we demonstrated that the whole-brain FC structure evoked by movie-watching is partly constrained by the resting network structure. The current work of task-rest correspondences during natural vision is limited to static FC spatial similarity measures. More dynamic analyses will be possible, especially if integrated with dynamic semantic analyses as in (Huth et al. 2012; Stansbury et al. 2013).

The relationship between spontaneous and task-evoked brain activity is an increasingly important topic in neuroscience. Throughout the analyses and results discussed in this dissertation, we provided evidences of a closed cycle relationship between intrinsic activity and task-evoked activity across regions in human brain, and a representational role for intrinsic patterns. Intrinsic activity, in contrast to the traditional notion of being just random noise, appears to encode meaningful information in time. Future studies will focus on understanding the dimensionality and dynamics of these sub-states in different cognitive and behavioral task domains.

References

Albert NB, Robertson EM, Miall RC. 2009. The resting human brain and motor learning. Curr Biol. 19(12):1023–1027

Anzellotti S, Caramazza A, Saxe R. 2017. Multivariate pattern dependence. PLoS Comput Biol. 13(11):e1005799

Anzellotti S, Coutanche MN. 2018. Beyond Functional Connectivity: Investigating Networks of Multivariate Representations. 22(3):258-269

Bartels A, Zeki S. 2005. Brain dynamics during natural viewing conditions--a new guide for mapping connectivity in vivo. Neuroimage. 24(2):339-349.

Betti V, DellaPenna S, de Pasquale F, Mantini D, Marzetti L, Romani GL, Corbetta M. 2013. Natural scenes viewing alters the dynamics of functional connectivity in the human brain. Neuron. 79(4):782–797.

Chen RH, Ito T, Kulkarni KR, Cole MW. 2018. The Human Brain Traverses a Common Activation-Pattern State Space Across Task and Rest. Brain Connect.

Cole MW, Bassett DS, Power JD, Braver TS, Petersen SE. 2014. Intrinsic and task-evoked network architectures of the human brain. Neuron. 83(1):238–251.

Coutanche MN, Thompson-Schill SL. 2013. Informational connectivity: identifying synchronized discriminability of multi-voxel patterns across the brain. Front Hum Neurosci. 7:15

Cox DD, Savoy RL. 2003. Functional magnetic resonance imaging (fMRI) "brain reading": Detecting and classifying distributed patterns of fMRI activity in human visual cortex. Neuroimage. 19(2 Pt 1):261-70.

Fox MD, Snyder AZ, Vincent JL, Corbetta M, Van Essen DC, Raichle ME. 2005. The human brain is intrinsically organized into dynamic, anticorrelated functional networks. Proc Natl Acad Sci USA. 102:9673-9678.

Golland Y, Golland P, Bentin S, Malach R. 2008. Data-driven clustering reveals a fundamental subdivision of the human cortex into two global systems. Neuropsychologia. 46(2):540–553.

Greicius MD, Krasnow B, Reiss AL, Menon V. 2003. Functional connectivity in the resting brain: a network analysis of the default mode hypothesis. Proc Natl Acad Sci USA. 100:253-258.

Harmelech T, Malach R. 2013. Neurocognitive biases and the patterns of spontaneous correlations in the human cortex. Trends Cogn Sci. 17(12):606–615.

Hasson U, Nir Y, Levy I, Fuhrmann G, Malach R. 2004. Intersubject synchronization of cortical activity during natural vision. Science. 303(5664):1634–1640.

Haxby JV, Gobbini MI, Furey ML, Ishai A, Schouten JL, Pietrini P. 2001. Distributed and overlapping representations of faces and objects in ventral temporal cortex. Science. 293:2425-2430.

Haxby JV, Bryan R, Gobbini MI. 2006. The representation of mammalian faces in human cortex. Journal of Vision. 6(86)

Hutchison RM, Womelsdorf T, Allen EA, Bandettini PA, Calhoun VD, Corbetta M, Della Penna S, Duyn JH, Glover GH, et al. 2013. Dynamic functional connectivity: Promise, issues, and interpretations. Neuroimage.80:360-78

Huth AG, Nishimoto S, Vu AT, Gallant JL. 2012. A continuous semantic space describes the representation of thousands of object and action categories across the human brain. Neuron. 76(6): 1210–1224.

Kenet T, Bibitchkov D, Tsodyks M, Grinvald A, Arieli A. 2003. Spontaneously emerging cortical representations of visual attributes. Nature. 425(6961):954-956.

Kriegeskorte N, Formisano E, Sorger B, Goebel R. 2007. Individual faces elicit distinct response patterns in human anterior temporal cortex. Proc Natl Acad Sci U S A. 104:20600-20605.

Kriegeskorte N, Mur M, Ruff DA, Kiani R, Bodurka J, Esteky H, Tanaka K, Bandettini PA. 2008. Matching categorical object representations in inferior temporal cortex of man and monkey. Neuron. 60:1126-1141.

Mantini D, Hasson U, Betti V, Perrucci MG, Romani GL, Corbetta M, Orban GA, Vanduffel W. 2012. Interspecies activity correlations reveal functional correspondence between monkey and human brain areas. Nat Methods. 9(3):277–282.

Mennes M, Kelly C, Colcombe S, Castellanos FX, Milham MP. 2013. The extrinsic and intrinsic functional architectures of the human brain are not equivalent. Cereb Cortex. 23(1):223–229.

Nir Y, Hasson U, Levy I, Yeshurun Y, Malach R. 2006. Widespread functional connectivity and fMRI fluctuations in human visual cortex in the absence of visual stimulation. Neuroimage. 30:1313-1324.

Omer DB, Fekete T, Ulchin Y, Hildesheim R, Grinvald A. 2018. Dynamic Patterns of Spontaneous Ongoing Activity in the Visual Cortex of Anesthetized and Awake Monkeys are Different. Cereb Cortex.

Power JD, Cohen AL, Nelson SM, Wig GS, Barnes KA, Church JA, Vogel AC, Laumann TO, Miezin FM, Schlaggar BL, Petersen SE. 2011. Functional network organization of the human brain. Neuron. 72:665-678.

Raichle ME, MacLeod AM, Snyder AZ, Powers WJ, Gusnard DA, Shulman GL. 2001. A default mode of brain function. Proc Natl Acad Sci USA, 98(2):676–682

Smith SM, Fox PT, Miller KL, Glahn DC, Fox PM, Mackay CE, Filippini N, Watkins KE, Toro R, Laird AR, Beckmann CF. 2009. Correspondence of the brain's functional architecture during activation and rest. Proc Natl Acad Sci U S A. 106:13040-13045.

Sporns O, Betzel RF. 2016. Modular Brain Networks. Annu Rev Psychol.67:613-40.

Stansbury DE, Naselaris T, Gallant JL. 2013. Natural Scene Statistics Account for the Representation of Scene Categories in Human Visual Cortex. Neuron. 79(5):1025–1034.

Strappini F, Wilf M, Karp O, Goldberg H, Harel M, Furman-Haran E, Golan T, Malach R. 2018. Resting-State Activity in High-Order Visual Areas as a Window into Natural Human Brain Activations. Cereb Cortex.

Tambini A, Ketz N, Davachi L. 2010. Enhanced brain correlations during rest are related to memory for recent experiences. Neuron. 65:280-290.

Tsodyks M, Kenet T, Grinvald A, Arieli A. 1999. Linking spontaneous activity of single cortical neurons and the underlying functional architecture. Science. 286:1943-1946.

Wilf M, Strappini F, Golan T, Hahamy A, Harel M, Malach R. 2017. Spontaneously Emerging Patterns in Human Visual Cortex Reflect Responses to Naturalistic Sensory Stimuli. Cereb Cortex. 27(1):750-763.